

# THEORY AND DESIGN OF VARIABLE CONDUCTANCE HEAT PIPES: STEADY STATE AND TRANSIENT PERFORMANCE

RESEARCH REPORT NO. 3

DECEMBER 1972

PREPARED BY  
D. K. EDWARDS  
G. L. FLEISCHMAN  
B. D. MARCUS

Contract No. NAS 2-5503

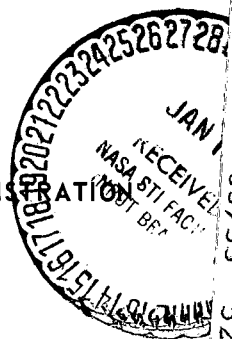
Prepared for  
AMES RESEARCH CENTER  
NATIONAL AERONAUTICS AND SPACE ADMINISTRATION  
Moffett Field, California 93405

PRICES SUBJECT TO CHANGE

Reproduced by  
NATIONAL TECHNICAL  
INFORMATION SERVICE  
US Department of Commerce  
Springfield, VA. 22151

**TRW**  
SYSTEMS GROUP

(NASA-CR-114530) THEORY AND DESIGN OF  
VARIABLE CONDUCTANCE HEAT PIPES: STEADY  
STATE AND TRANSIENT PERFORMANCE (TRM  
Systems Group) 116 p HC CSDL 20M



63/13  
52802  
Unclass

N73-15957

116 p.p.

## FOREWORD

The work described in this report was performed under NASA Contract NAS-2-5503, "Design, Fabrication and Testing of a Variable Conductance Constant Temperature Heat Pipe." The contract is administered by Ames Research Center, Moffett Field, California, under the technical direction of Mr. J. P. Kirkpatrick.

The program is being conducted by TRW Systems Group of TRW, Inc., Redondo Beach, California, with Dr. Bruce D. Marcus serving as Program Manager. Major contributors to the effort, in addition to the authors, include Messrs. C. Salts, D. Opper and V. Reineking.

## TABLE OF CONTENTS

	<u>Page</u>
1.0 INTRODUCTION . . . . .	1
2.0 EXPERIMENTAL VERIFICATION OF THE TRW GASPIPE COMPUTER PROGRAM: TEMPERATURE PROFILES AND HEAT TRANSFER CHARACTERISTICS . . . . .	3
2.1 Experimental Approach . . . . .	3
2.2 Results and Discussion . . . . .	6
3.0 EXPERIMENTAL VERIFICATION OF THE TRW GASPIPE COMPUTER PROGRAM: DIFFUSION FREEZEOUT RATES . . . . .	15
3.1 Experimental Approach . . . . .	17
3.2 Results . . . . .	29
3.3 Discussion . . . . .	35
4.0 GAS-AIDED START-UP FROM THE FROZEN STATE . . . . .	42
4.1 Assumptions and Simplifications in the Model . . . . .	42
4.2 Formulation of Equations . . . . .	44
4.3 Discussion . . . . .	47
5.0 TRANSIENT BEHAVIOR OF HOT RESERVOIR HEAT PIPES: THE TRANPIPE PROGRAM . . . . .	50
5.1 Analytical Model . . . . .	50
5.2 Discussion . . . . .	68
6.0 TRANSIENT BEHAVIOR OF HOT RESERVOIR HEAT PIPES: EXPERIMENTS . . . . .	70
6.1 Test Apparatus . . . . .	70
6.2 Procedure . . . . .	78

	<u>Page</u>
6.3 Results . . . . .	79
6.4 Conclusions and Recommendations . . . . .	91
7.0 REFERENCES . . . . .	96
8.0 NOMENCLATURE . . . . .	97
9.0 APPENDIX A: DRAWINGS, EXPERIMENTAL HOT RESERVOIR HEAT PIPE . . . . .	101

## FIGURES

	<u>Page</u>
2-1. Schematic Diagram of Experimental Heat Pipe System . . . . .	4
2-2. Comparison of Measured and Predicted Temperature Profiles . . . . .	8
2-3. Comparison of Measured and Predicted Temperature Profiles . . . . .	9
2-4. Comparison of Measured and Predicted Temperature Profiles . . . . .	10
2-5. Comparison of Measured and Predicted Heat Rejection Versus Evaporator Temperature . . . . .	14
3-1. Schematic Diagram and Temperature Distribution of a Gas-Loaded Heat Pipe in which Diffusion Freeze-out Occurs . . . . .	16
3-2. Schematic Drawing of Diffusion Freezeout Experiment Heat Pipe . . . . .	18
3-3. Photograph of Experimental Heat Pipe . . . . .	21
3-4. Photograph of Experimental Apparatus . . . . .	21
3-5. Schematic Diagram of Diffusion Freezeout Experiment Apparatus . . . . .	22
3-6. Diffusion Freezeout Experiment Model . . . . .	27
3-7. Temperature Profile for High Sink Conductance . . . . .	31
3-8. Temperature Profile for Low Sink Conductance . . . . .	32

	<u>Page</u>
3-9. Balance Weight Versus Time During Diffusion Freezeout . . . . .	33
3-10. Balance Weight Versus Time During Diffusion Freezeout . . . . .	34
5-1. Flow Chart for Main Program . . . . .	64
5-2. Flow Chart for Subroutine Delta . . . . .	65
a) $\dot{m}_{\text{gas, res}} < \dot{m}_{\text{gas}}$	
5-3. Flow Chart for Subroutine Delta . . . . .	66
b) $\dot{m}_{\text{gas, res}} \geq \dot{m}_{\text{gas}}$	
6-1. Schematic Drawing of Experimental Apparatus for Hot Reservoir Heat Pipe Transient Studies . . . . .	71
6-2. Experimental Hot Reservoir Heat Pipe . . . . .	75
6-3. Test Installation . . . . .	75
6-4. Schematic Diagram of Test Setup . . . . .	76
6-5. Thermocouple Locations . . . . .	77
6-6. Input Power and Sink Temperature Test Profile . . . . .	80
6-7. Experimental Results for Start-up with Liquid in the Reservoir . . . . .	83
6-8. Transient Performance (Without Thermal Mass) . . . . .	88
6-9. Transient Performance (With Thermal Mass Attached) . . . . .	89

	<u>Page</u>
6-10. Transient Performance (Nitrogen Cooled) . . . . .	90
6-11. Transient Performance (Helium Control Gas) . . . . .	92
6-12. Transient Performance (1/4 Inch Feedtube) . . . . .	93
A-1. Tube and Wick Assembly . . . . .	102
A-2. Gas Reservoir . . . . .	103
A-3. Feedtube . . . . .	104
A-4. Saddle . . . . .	105
A-5. Thermal Mass and Backplate . . . . .	106
A-6. Cooling Jacket . . . . .	107

## TABLES

	<u>Page</u>
2-1. Experimental Heat Pipe Design Details . . . . .	5
2-2. Summary of Experimental Measurements . . . . .	7
2-3. Calculated Values of the Molar Gas Inventory . . . . .	12
2-4. Comparison of Predicted and Measured Heat Rejection Rates for $\dot{m} = 1.008 \times 10^{-4}$ lb-moles . . . . .	13
3-1. Heat Pipe Design Details . . . . .	19
3-2. Comparison of Measured and Predicted Rates of Balance Weight Per Unit Time . . . . .	30
3-3. Comparison of Measured and Predicted Diffusion Freezeout Rates . . . . .	36
6-1. Test Schedule - TRANPIPE . . . . .	81
6-2. Start-up with Liquid in the Reservoir . . . . .	85

## 1.0 INTRODUCTION

TRW Systems Group, under contract to NASA-ARC, is performing a comprehensive review, analysis and experimental development program dealing with all aspects of heat pipe technology pertinent to the design and application of self-controlled, variable conductance heat pipes for spacecraft thermal control.

Several previous publications [1, 2, 3, 4, 5]\* reported on theoretical and design developments accomplished earlier in the program. Hardware development and application efforts based on this technology were also documented [6, 7, 8], as was a computer program for designing and predicting performance of such systems [9].

This report deals with further fundamental analytical and experimental efforts which were undertaken to 1) provide additional confidence in existing design tools, 2) generate new design tools, and 3) develop superior variable conductance heat pipe designs. It presents the results of five investigations, as follows:

- o A series of experiments to test the ability of the TRW Gaspipes Computer Program to predict temperature profiles and heat transfer characteristics of gas-controlled heat pipes (Section 2).
- o A series of experiments to test the ability of the TRW Gaspipes Computer Program to predict diffusion freeze-out rates under conditions wherein the gas blocked portion of the condenser falls below the freezing point of the working fluid (Section 3).
- o An analysis of gas aided heat pipe start-up from the frozen state, leading to a closed form solution useful in design (Section 4).

---

\* Numbers in brackets refer to references tabulated in Section 7.0.

- o An analysis of the transient behavior of hot reservoir heat pipes leading to a computer program for predicting both thermally and diffusion dominated transients (Section 5).
- o The development of an improved design for hot reservoir heat pipes and an experimental program to test the validity of the transient analysis and computer program (Section 6).

## 2.0 EXPERIMENTAL VERIFICATION OF THE TRW GASPIPE COMPUTER PROGRAM: TEMPERATURE PROFILES AND HEAT TRANSFER CHARACTERISTICS

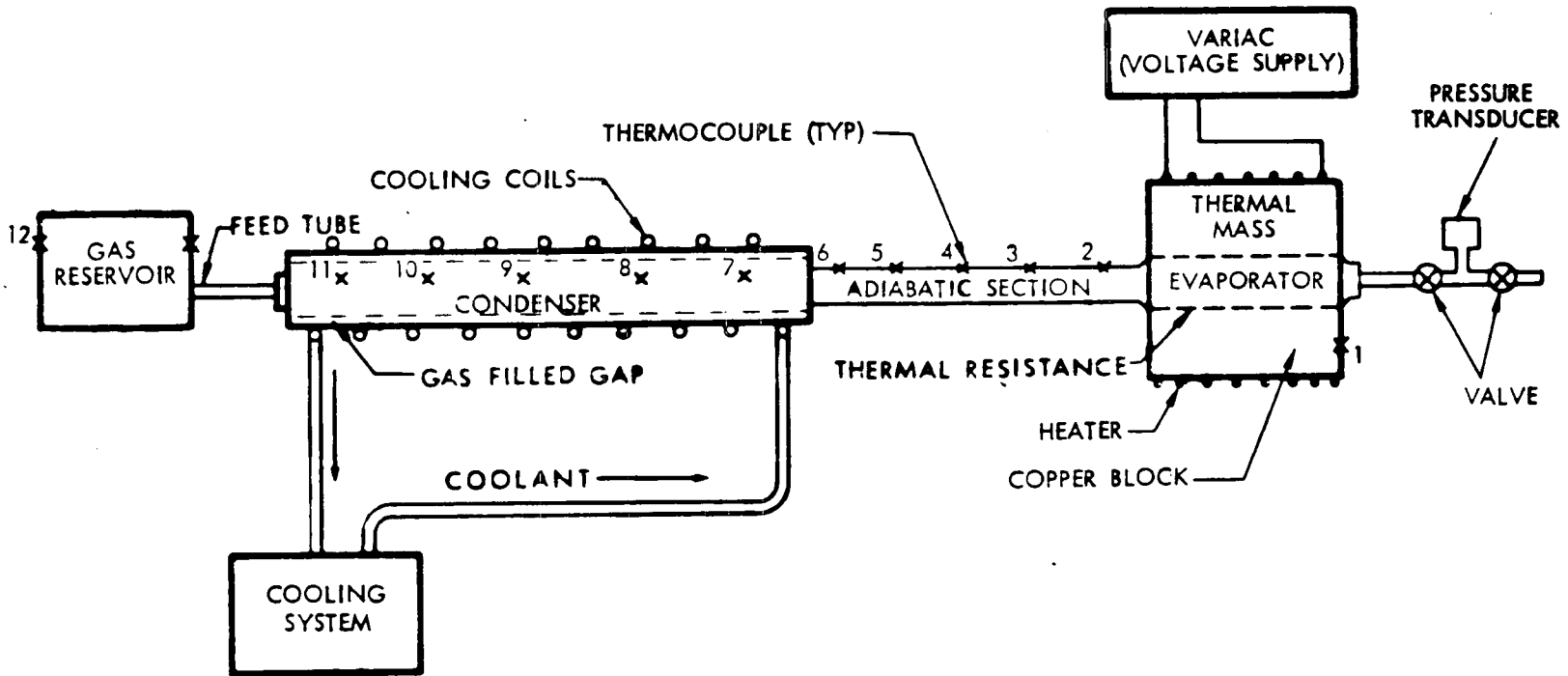
The TRW Gaspipe Computer Program for calculating the heat and mass transfer characteristics of gas-loaded heat pipes has been discussed in several earlier reports and publications [2, 3, 5, 9]. As originally written, the program was limited to treating a heat pipe with a single condenser section exposed to uniform sink conditions. A series of experiments, performed to verify the program at this point, were documented in references [2, 3, and 5].

Subsequent modifications to the computer program extended its capability to deal with two condenser sections with a step change in the condenser/fin properties or the environment. With these modifications the program can accommodate cold traps or adiabatic sections in addition to the primary condenser. Following these modifications, a more extensive series of experiments were undertaken to test the program for various operating conditions including step changes in axial conductance and sink temperature.

### 2.1 Experimental Approach

As shown on Figure 2-1, the experimental system consisted of an aluminum-ammonia-neon heat pipe with a wicked external reservoir. Electrical heat was supplied to a large thermal mass (copper block) mounted on the evaporator. Condenser heat rejection was by conduction, convection and radiation through a thin gas layer between the condenser wall and a cooled copper sleeve. By varying the sleeve temperature or the gas composition in the gas layer, the effects of sink temperature and condenser-to-sink coupling could be independently studied.

The design details of the heat pipe are presented in Table 2-1. Note that there exists a step change in wall thickness from 0.100 to 0.025 inches in passing from the condenser to the adiabatic section. This provides a step change in axial conductance of the heat pipe wall, allowing a test of the program's ability to deal with such situations.



4

FIGURE 2-1. Schematic Diagram of Experimental Heat Pipe System

TABLE 2-1

## Experimental Heat Pipe Design Details

Working Fluid: Ammonia

Inert Gas: Neon ( $1.028 \times 10^{-4}$  +5% lb-moles)

Pipe:

Material	= 6061 (T6) Aluminum
Inside Diameter	= 0.50 in.
Evaporator O.D.	= 0.727 in.
Adiabatic O.D.	= 0.55 in.
Condenser O.D.	= 0.70 in.
Overall Length	= 40.0 in.
Evaporator Length	= 5.0 in.
Adiabatic Length	= 10.0 in.
Condenser Length	= 25.0 in.

Reservoir (wicked):

Material	= Aluminum
Internal Volume	= 11.4 in <sup>3</sup>
Feedtube	= 2.1 in. X 0.25 in. O.D. X 0.02 in. wall

Wick Structure:

Material:	Stainless Steel Screen Mesh
Description:	Two layers of 150 mesh on inside surface of heat pipe and reservoir. One-half of condenser and adiabatic section filled with 70 mesh screen.

Three series of measurements were made with this system. The first utilized a constant sink temperature and air in the gas gap. Four steady-state temperature profiles were recorded for four power settings which caused the gas front to traverse the condenser and adiabatic section.

The second series of measurements was similar to the first except that helium was substituted for air in the gas gap. This increased the condenser-to-sink coupling by about a factor of five. The last series of measurements were again made with helium in the gas gap, but the sink temperature was varied.

## 2.2 Results and Discussion

The measured data for the total of ten runs are presented in Table 2-2 and Figures 2-2, 2-3 and 2-4. In Table 2-2, the evaporator, sink and reservoir temperatures were direct measurements. The heat rejection -  $\dot{Q}$  represents the input power corrected for evaporator insulation losses. The molar gas inventory was calculated from pressure and temperature measurements on the system at ambient temperature and zero input power. Accuracy limitations on the temperature and pressure measurements limit the accuracy on the molar gas inventory to about  $\pm 5\%$  when calculated in this way. Finally, the condenser coefficient of heat transfer -  $h_{\text{cond}}$  was determined using Newton's cooling law,  $q'' = h\Delta T$ , in conjunction with the measured power, temperature profiles, and insulation leakage in the adiabatic section. The measured temperature profiles are shown as the data points on Figures 2-2, 2-3 and 2-4.

The TRW Gaspipe Program was then used to produce temperature profile and  $\dot{Q}$  vs.  $T_{\text{ev}}$  predictions for comparison with the measured data. Because it was anticipated that the position of the gas front would be very sensitive to the pipe's gas inventory, and that the  $\pm 5\%$  accuracy on this measurement might not be sufficient, the computer predictions were performed in two steps. First, the program was used for each run operating on the  $\dot{Q}$  option. This more or less forced the predicted profiles into the proper axial position, allowing a clear comparison of

TABLE 2-2

## Summary of Experimental Measurements

Run	Gas in Pipe	$T_{ev}$ (°R)	$T_s$ (°R)	$T_R$ (°R)	$\dot{Q}$ (BTU/HR)	$h_{cond}$ BTU/HR- FT <sup>2</sup> -°R
A	Air	545.5	491.7	517.4	4.8	2.40
B	Air	547.0	491.7	517.8	15.7	3.15
C	Air	549.6	491.7	519.3	32.9	3.21
D	Air	559.7	491.7	529.2	72.8	3.24
E	Helium	544.7	491.7	516.6	4.9	7.60
F	Helium	544.8	491.7	515.9	17.6	10.40
G	Helium	548.1	491.7	516.5	133.6	14.50
H	Helium	558.1	496.7	527.0	290.4	15.30
I	Helium	554.4	510.2	525.1	117.0	15.7
J	Helium	563.6	536.7	536.6	70.8	17.8

Gas Inventory - =  $1.028 \times 10^{-4}$  lb-moles

$T_{ev}$  - Evaporator temperature

$T_s$  - Sink temperature

$T_R$  - Reservoir temperature

$\dot{Q}$  - Total heat rejection

$h_{cond}$  - Condenser coefficient of heat transfer

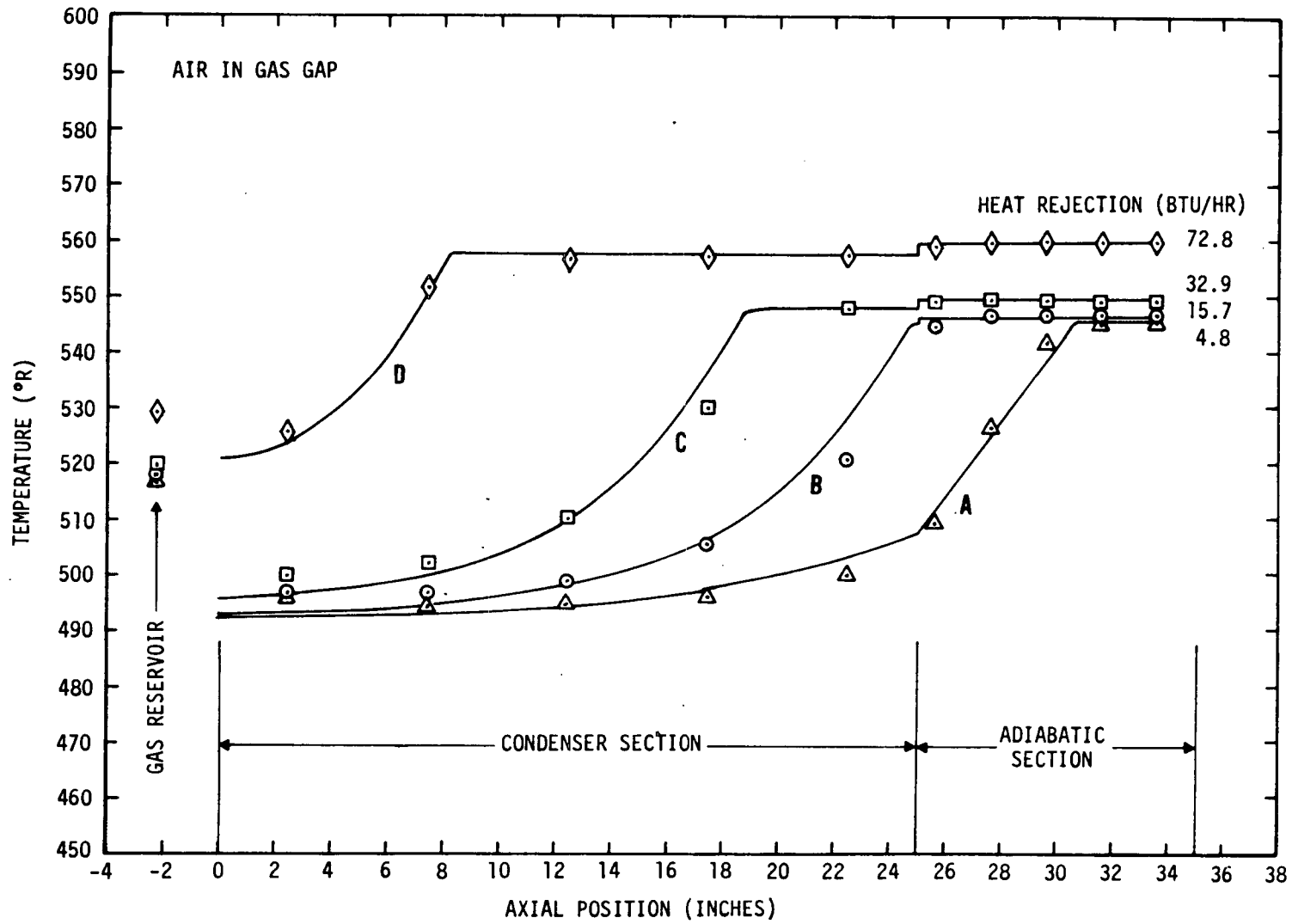


FIGURE 2-2. Comparison of Measured and Predicted Temperature Profiles

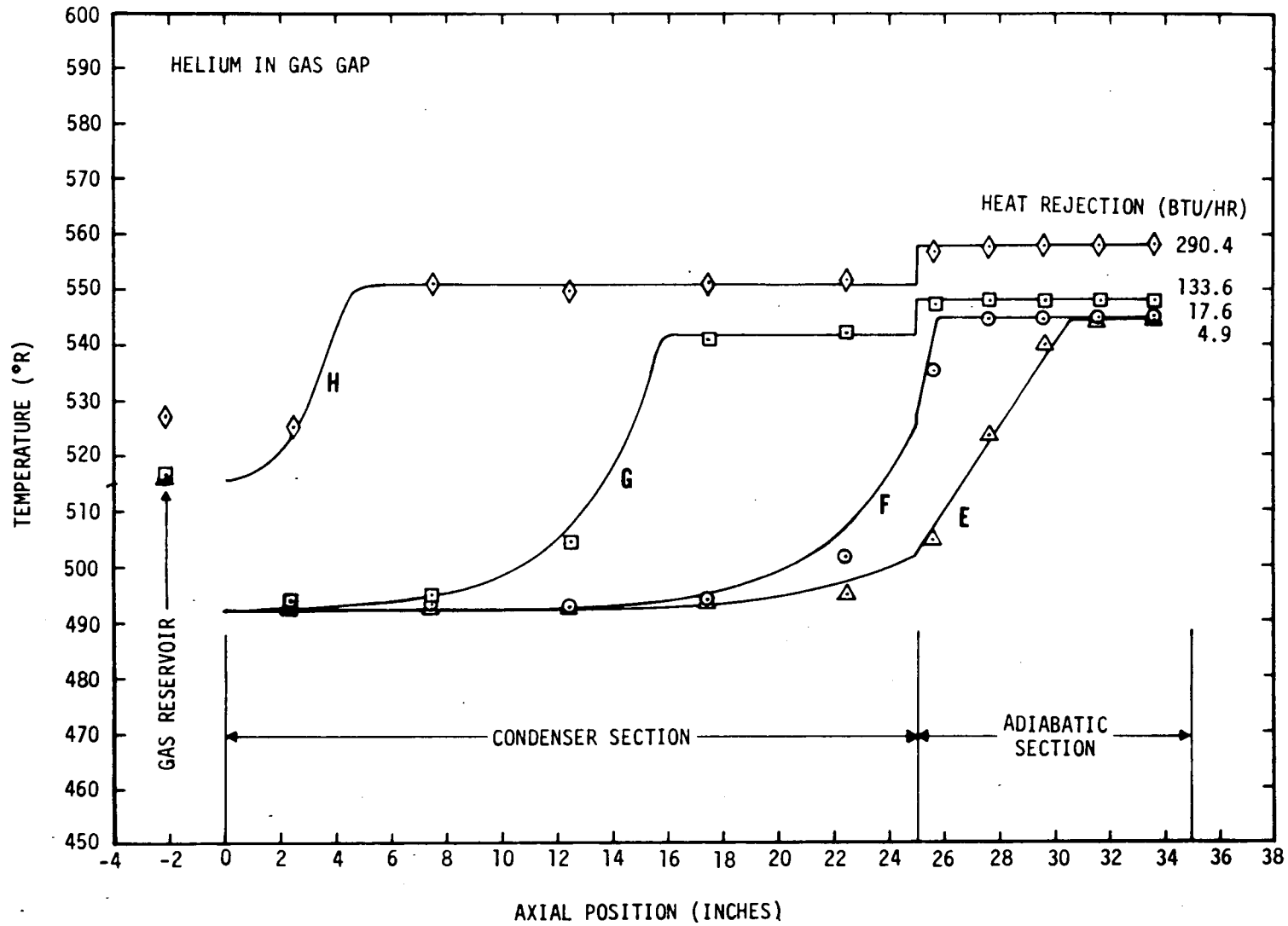


FIGURE 2-3. Comparison of Measured and Predicted Temperature Profiles

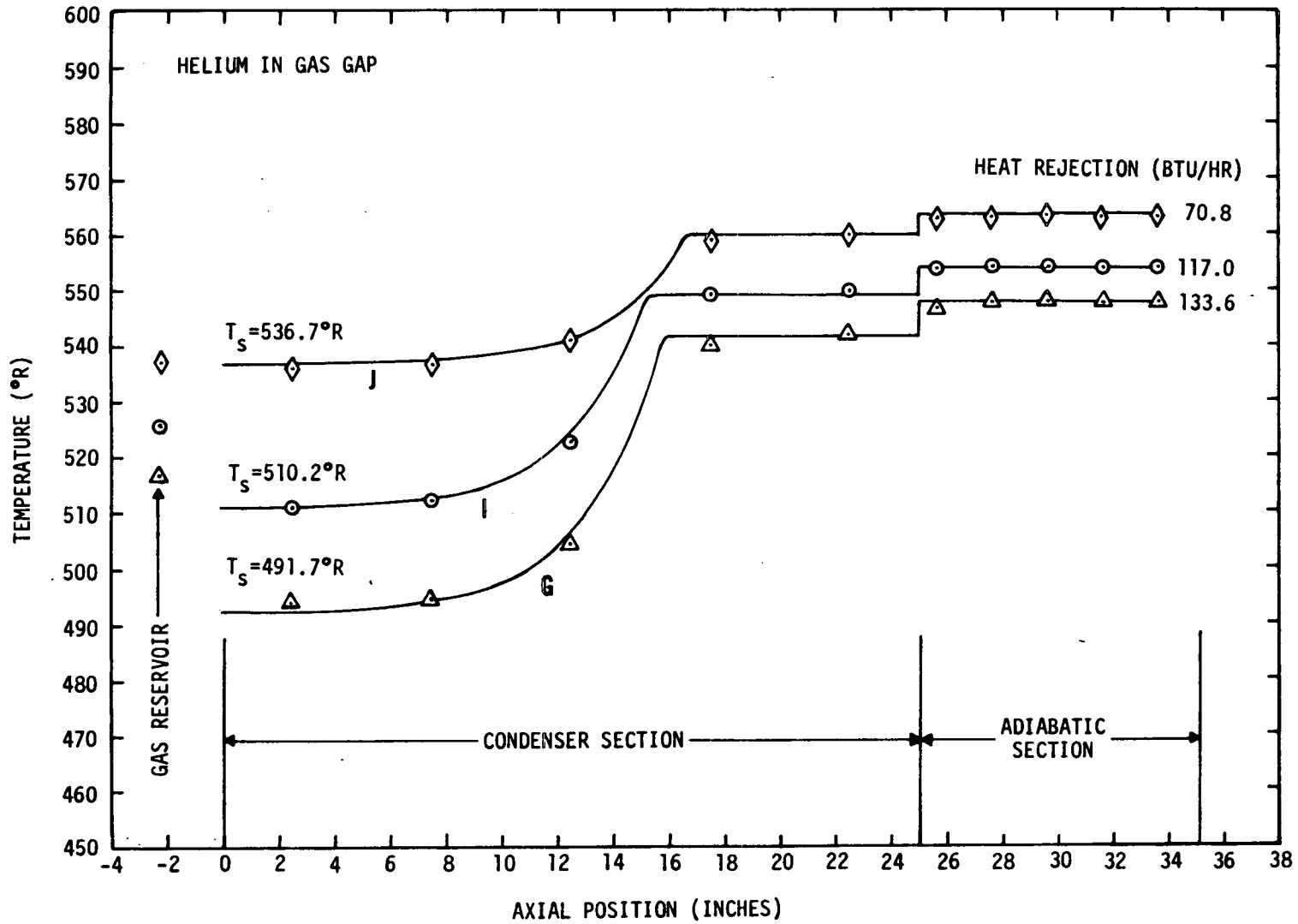


FIGURE 2-4. Comparison of Measured and Predicted Temperature Profiles

predicted and measured profile shapes.

The temperature profiles predicted in this way are presented in Figures 2-2, 2-3 and 2-4 as the solid lines. Figure 2-2 shows the results for constant sink temperature and air in the gas gap. Figure 2-3 shows similar results for helium in the gas gap, and Figure 2-4 shows the results for varying sink temperature with helium in the gas gap.

In general, the program does an excellent job of predicting the measured temperature profiles. It correctly accounts for the effect of condenser-sink coupling, predicting the appreciably sharper fronts for helium in the gas gap than for air. It correctly predicts a nearly linear distribution when the front is within the adiabatic section (Runs A, E, F) as is expected for axial wall conduction. It also accounts properly for the case where the front crosses the step change in axial wall conductance at the condenser/adiabatic section transition (Runs A, E, F), predicting a discontinuity in wall temperature gradient.

The program does, however, have several deficiencies. First, in all cases it predicts a step change in wall temperature\* at the transition between the adiabatic section and condenser, rather than the continuous profile which actually occurs. This is due to the approximate method by which the program handles radial wick resistance (see analysis in User's Manual [9]). For high conductance wicks (e.g., circumferential grooves) or low radial heat flux (compare runs C and D with G and H), this approximation becomes less significant.

A second limitation is that the program is written assuming all heat transfer along the condenser is uni-directional (from evaporator to condenser). It does not account for heat transfer to or from the gas reservoir. For all runs in Figures 2-2 and 2-3, the condenser sink was below ambient and, in spite of a great deal of insulation, heat leakage caused the gas reservoir to run hotter than the condenser.

---

\*It is too small to see in Runs A and E.

Consequent conduction along the feed tube caused the end of the condenser to rise above sink temperature, and this could not be predicted by the Gaspipe Program. The effect is most clearly seen in Runs A, B and C for air in the gas gap. With helium (Runs E, F and G), the higher condenser-to-sink coupling reduced the magnitude of the condenser temperature rise.

This effect is also seen on Figure 2-4 which shows the predicted and measured results from variations in sink temperature. At the low sink temperature (Run G), the reservoir ran significantly higher than the sink causing the end of the condenser to operate slightly above  $T_S$ . As the sink temperature was raised towards ambient, the differential between  $T_R$  and  $T_S$  was reduced and this effect disappeared.

In addition to yielding the temperature profiles of Figures 2-2, 2-3 and 2-4, the Q-option computer runs also yielded calculated molar gas inventories for each case. The calculated values are presented in Table 2-3.

TABLE 2-3

## Calculated Values of the Molar Gas Inventory

Run	A	B	C	D	E	F	G	H	I	J
$M \times 10^4$ lb-moles	1.005	1.021	1.023	1.010	1.010	0.998	1.017	1.004	1.001	1.001

All of the calculated gas inventories fall within  $0.998 \times 10^{-4}$  and  $1.023 \times 10^{-4}$  lb-moles; a total variation of only 2.5%. This is extremely close, and the average of the values in Table 2-3 ( $1.008 \times 10^{-4}$  lb-moles) is probably a more accurate value of the gas inventory than the measured value of  $1.028 \times 10^{-4}$  lb-moles. It deviates from the measurement by only 2% which is well within the estimated +5% measurement accuracy.

Thus, the second step in the computer predictions was to operate the program in the  $m$ -mode, using  $1.008 \times 10^{-4}$  lb-moles as the gas inventory, in order to obtain predicted heat transfer rates vs. evaporator temperature. The results of these computations are presented in Table 2-4.\*

TABLE 2-4  
Comparison of Predicted and Measured Heat Rejection  
Rates for  $m = 1.008 \times 10^{-4}$  lb-moles

Run	A	B	C	D	E	F	G	H
$T_{ev}$ ( $^{\circ}R$ )	545.5	547.0	549.6	559.7	544.7	544.8	548.1	558.1
$\dot{Q}_{pred}$ (BTU/HR)	4.4	15.0	33.7	75.7	5.1	11.7	143.0	287.1
$\dot{Q}_{meas}$ (BTU/HR)	4.8	15.7	32.9	72.8	4.9	17.6	133.6	290.4

The predicted heat rejection rates obtained in this way are in excellent agreement with the measured data, especially in view of the heat pipes sensitivity to evaporator temperature. Small errors in measurement of the evaporator temperature can lead to large prediction errors in locating the gas front and calculating  $\dot{Q}$ . This is clearly shown on Figure 2-5, which presents the data in Table 2-4.

In Figure 2-5, the solid lines are simply curves faired through the predicted points (circles). The shaded bands were then drawn to represent a  $\pm 1^{\circ}R$  variation in  $T_{ev}$ . All of the measured data (squares) for both air and helium in the gas gap fall within the  $\pm 1^{\circ}R$  bands, which is the estimated experimental accuracy for this measurement.

\*Only Runs A through H were treated in this way since these involved relatively constant sink temperatures.

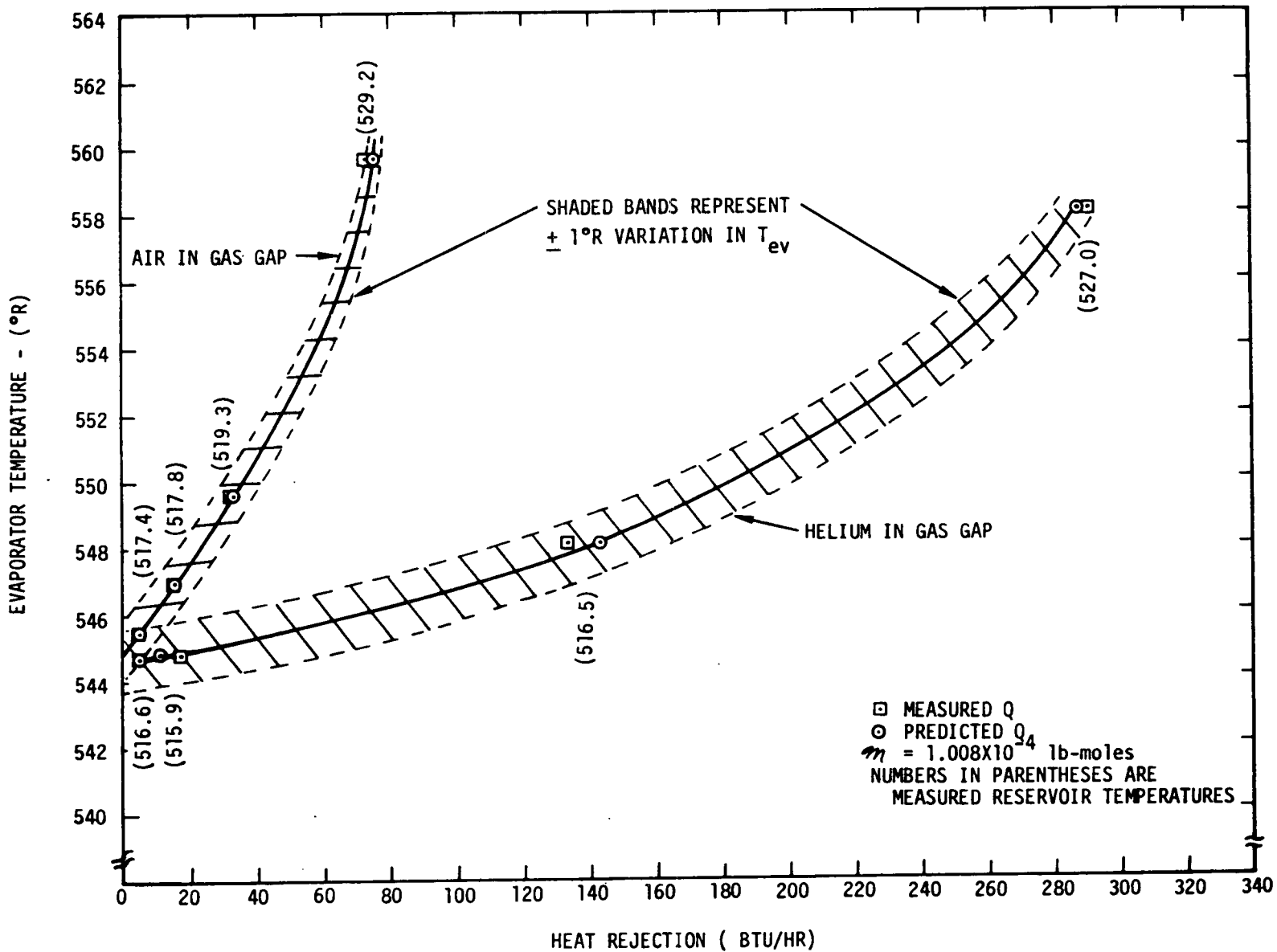


FIGURE 2-5. Comparison of Measured and Predicted Heat Rejection vs. Evaporator Temperature

### 3.0 EXPERIMENTAL VERIFICATION OF THE TRW GASPIPE COMPUTER PROGRAM: DIFFUSION FREEZEOUT RATES

The results presented in the previous section and in reference [3] serve to establish the validity of the analysis and Gaspipes Computer Program insofar as its predictions for temperature profiles and condenser heat rejection characteristics. However, it was also shown in reference [3] that, for heat pipes with materials, dimensions and operating conditions like those used in these experiments (typical of spacecraft thermal control devices), axial heat transport by vapor flow is minimal in the gas blocked region and axial conduction in the wall, fin and wick dominates. Thus, correctly predicting condenser heat rejection rates and wall temperature profiles does not imply that the program also correctly predicts the internal vapor-gas dynamics.

During operation of gas-loaded heat pipes, vapor continually diffuses into the gas blocked region of the condenser and condenses on the wick lined walls to be pumped back to the evaporator. However, in cases where a low sink temperature causes a portion of the gas blocked zone to operate below the freezing point of the working fluid, the vapor diffusing into this region condenses and freezes on the wick (Figure 3-1).

This diffusion freezeout phenomenon can lead to two failure mechanisms for gas-controlled heat pipes. First, because the frozen fluid cannot be pumped back to the evaporator, the fluid inventory in the active portion of the pipe is continually depleted, which can ultimately lead to dryout of the evaporator wick. Second, the freezing fluid builds up a plug of solid material which can eventually completely block the vapor core and cut off communication between the pipe and the gas reservoir, thus seriously degrading the pipe's temperature control capability when the heat load is changed.

Thus, although axial mass transport does not appear to significantly effect the wall temperature profile in the gas blocked region, it is both finite and important in that it is the mechanism behind the

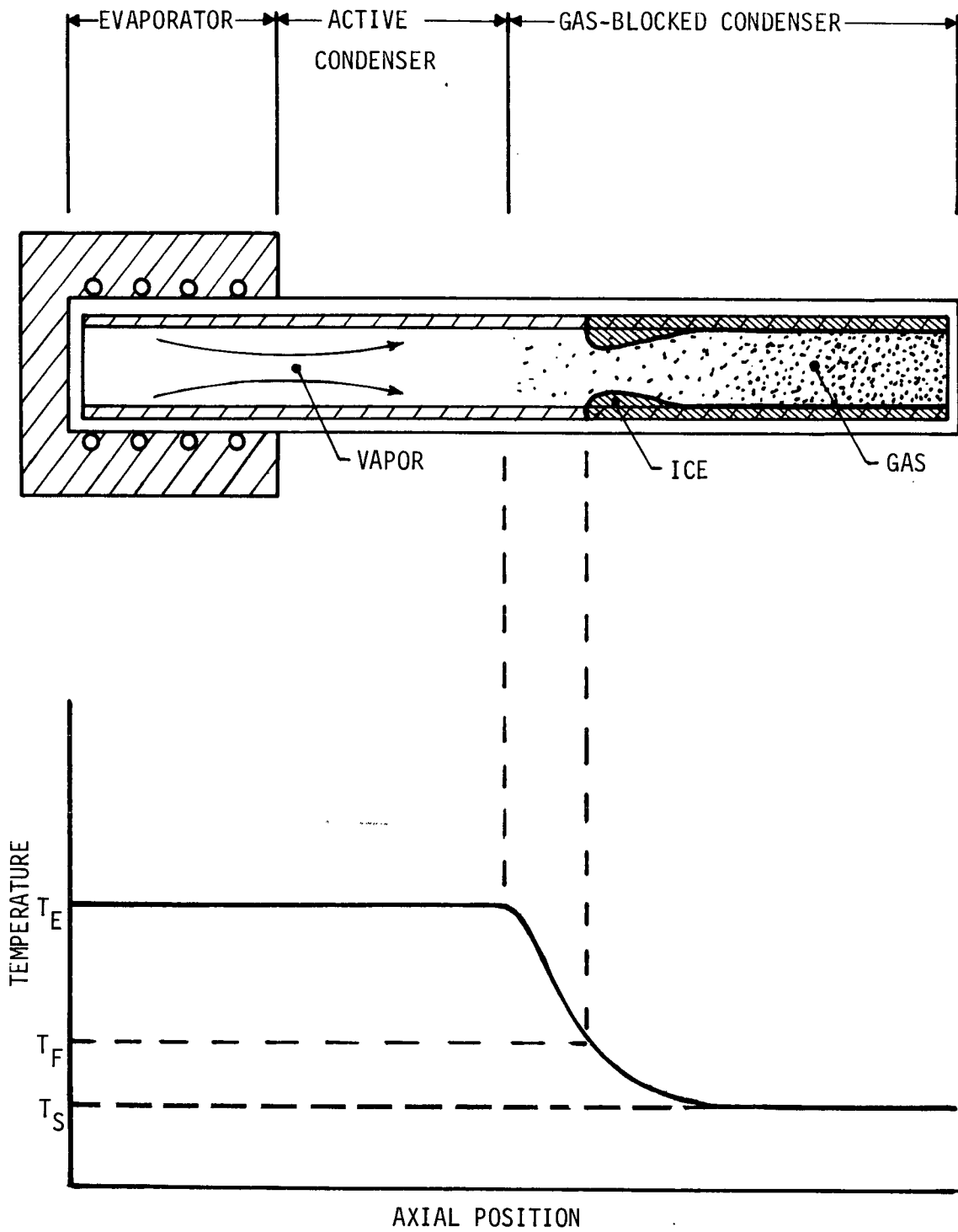


FIGURE 3-1. Schematic Diagram and Temperature Distribution of a Gas Loaded Heat Pipe in which Diffusion Freezeout Occurs.

diffusion freezeout phenomenon.\* Also, since the wall temperature profile is fairly independent of axial mass transfer, a thorough test of the analysis and Gaspipe Computer Program requires a direct measurement of the diffusion freezeout rate itself. This section discusses a series of such experiments and compares the measured diffusion freezeout rates with analytical predictions.

### 3.1 Experimental Approach

To make the measurements, a heat pipe was pivoted on knife-edges, and an analytical balance used to detect changes in the moment about the knife edge axis caused by mass migration within the pipe. The heat pipe design included a capillary excess fluid reservoir so that the initial center of mass of the migrating fluid was known. The center of mass following diffusion freezeout was calculated with the TRW Gaspipe Program. Knowing the dimensional change in the center of mass for the migrating fluid, the diffusion freezeout mass transfer rate was deduced from the rate of change in moment about the knife edges as measured with the analytical balance.

#### 3.1.1 Apparatus

The experimental heat pipe is shown schematically in Figure 3-2, and design details are presented in Table 3-1. Water was selected as the working fluid because of its relatively high freezing point, which facilitated the task of providing sub-freezing sink temperatures. The pipe and screen wicks were manufactured from monel and nickel, materials which can be made chemically compatible with water, so as to avoid the generation of any non-condensable gas over and above that which was purposefully introduced. The latter was chosen to be neon so that the molecular weights of the gas and vapor would be closely matched. However, dissolved nitrogen in the water caused the inert gas composition

---

\*A recent publication by Rohani and Tien [10] suggests there may be some situations of interest wherein diffusion does significantly influence the wall temperature profile.

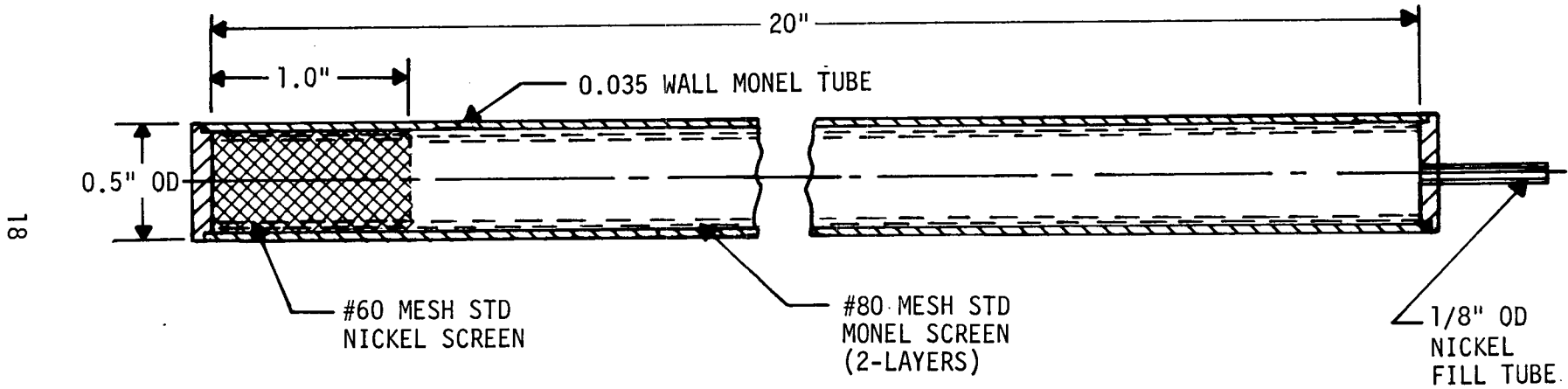


FIGURE 3-2. Schematic Drawing of Diffusion Freezeout Experiment Heat Pipe

TABLE 3-1

## Heat Pipe Design Details

## MATERIALS:

Tube: Monel 400. 1/2 in. O.D. X 0.035 wall

End Caps: Monel 400. 1/2 in. rod

Fill Tube: Nickel 200. 1/8 O.D. X .028 wall

Wicking: 80 mesh monel primary wick  
60 mesh nickel excess fluid reservoir

Working Fluid: water, 6.67 gms.

Control Gas: 53% neon, 47% nitrogen;  $4.3 \times 10^{-8}$  lb-moles

## DIMENSIONS:

Length: 20 1/8 inches (excluding fill tube)

Wick Thickness: 0.022 inches (two layers)

Excess Fluid Reservoir Length: 1.0 inch

Diameter: 0.5 inches

to be 53% neon, 47% nitrogen. The total gas inventory, and hence the amount of nitrogen in the pipe, was determined from the temperature profile obtained in a calibration run. This profile was matched by iteration using the ZGAS option of the Gaspipe Program [9].

The pipe wick structure included a 1.0 inch excess fluid reservoir located at the upstream end of the evaporator. An excess fluid reservoir is a capillary structure placed within the heat pipe to act as a "sponge." By properly sizing the pores of the reservoir, it will serve to store any liquid in the pipe which the primary wicks cannot hold. However, the primary wicks will draw liquid from the reservoir as needed to maintain their proper saturation level. Hence, the excess fluid reservoir served as a source of liquid which re-supplied the primary wick as fluid solidified and accumulated in the sub-freezing portion of the condenser. The reservoir thus established the initial location of the frozen fluid accumulated by the diffusion freezeout process. A more complete discussion of excess fluid reservoirs and how to design them can be found in reference [3].

The heat pipe was instrumented with nine bare wire (0.003 in. diameter) chromel-constantan thermocouples along its length. An electrical heater for the evaporator was fabricated by close winding glass-insulated nichrome wire directly over a three inch length of the pipe surface. The entire unheated portion of the pipe was wrapped with two layers of 0.002 in. thick aluminized mylar tape (one on each side of the thermocouple wires) which served both to make the pipe emissivity uniform and to insulate the bare thermocouple wires from each other and the pipe wall. The heater wires were wrapped with Teflon tape to hold them in place. A photograph of the heat pipe, with its heater and fine wire thermocouples is shown in Figure 3-3.

The test cell is shown pictorially in Figure 3-4, and schematically in Figure 3-5. It consisted of a controlled atmosphere chamber within which the heat pipe was horizontally mounted in a cradle pivoted on one of two sets of knife edges. A tubular phenolic beam was connected to the evaporator end of the heat pipe, extending out of the test cell

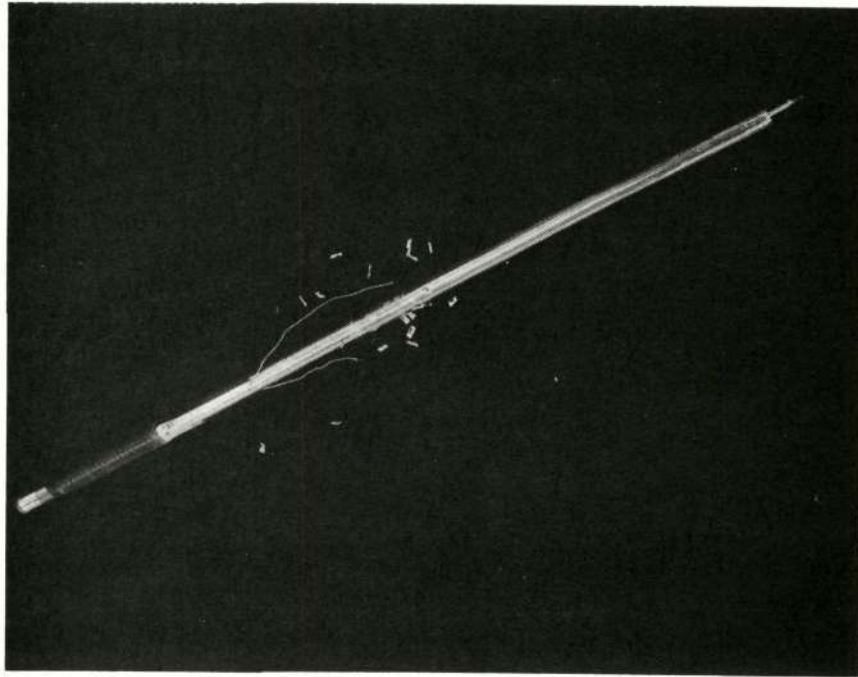


FIGURE 3-3. Photograph of Experimental Heat Pipe

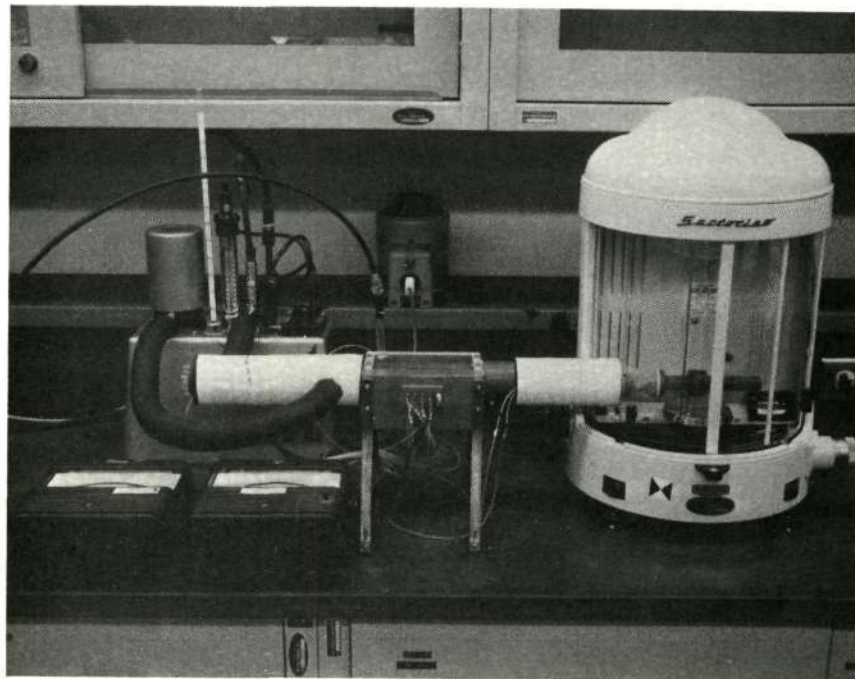


FIGURE 3-4. Photograph of Experimental Apparatus

C

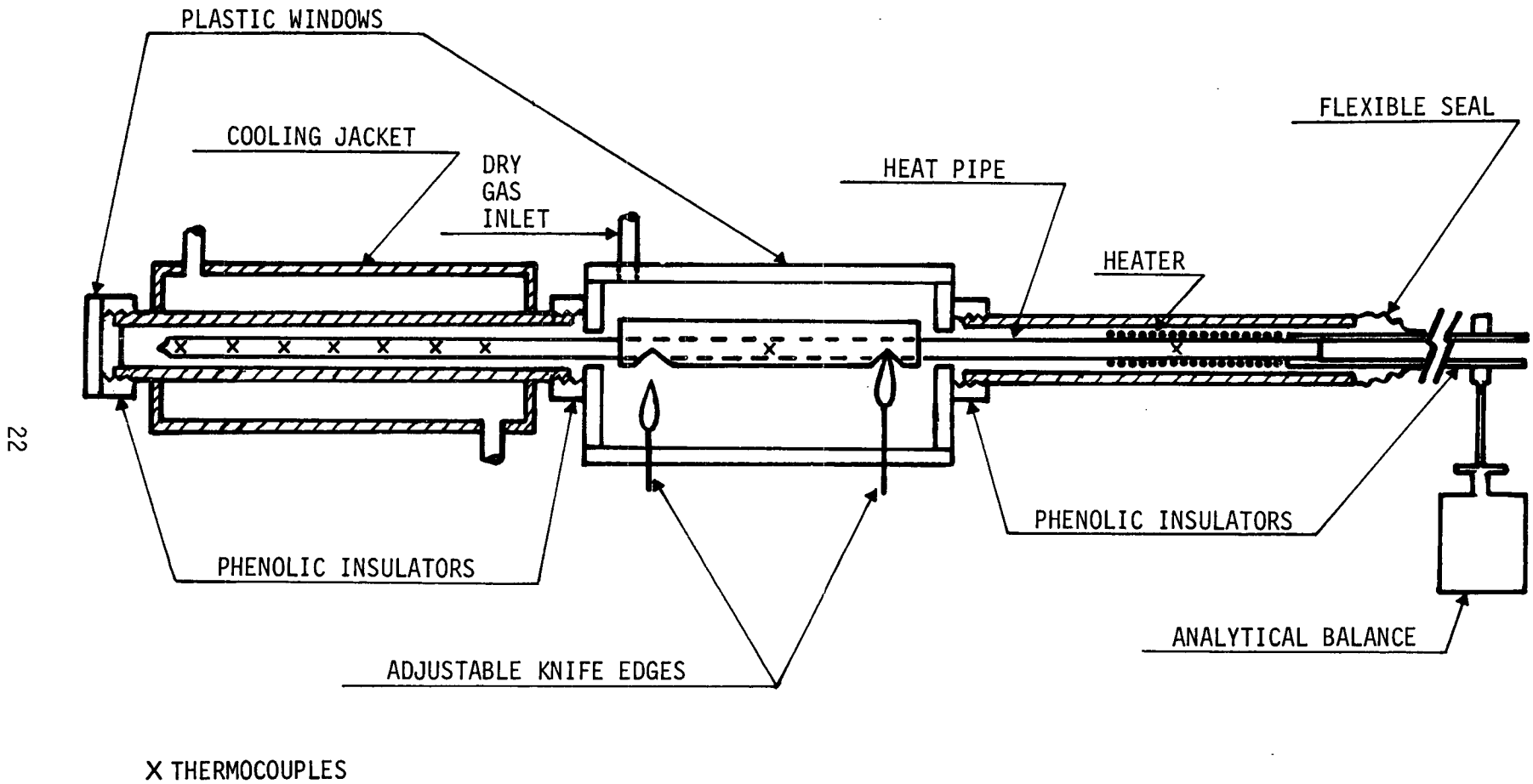


FIGURE 3-5. Schematic Diagram of Diffusion Freezeout Experiment Apparatus

through a flexible seal where an attached "foot" contacted the balance pan.

The test cell consisted of three metallic sections thermally isolated from each other with phenolic bushings. The evaporator and condenser sections were made of brass. The evaporator section was insulated with urethane foam, and the condenser section was surrounded by a similarly insulated cooling jacket maintained at sub-freezing temperatures with a constant temperature circulator using refrigerated ethanol. Cooling of the condenser was primarily by conduction, augmented slightly by convection and radiation, from the pipe surface to the cooled test cell wall through a 0.06 in. annular gas gap.

The third section of the test cell, which contained the knife edges, was also the location of all electrical feed throughs. All of the thermocouple leads were routed along the pipe to the vicinity of the knife edge pivots where a large radius of curvature loop was made in the fine wires before soldering them to chromel-constantan feed throughs in the test cell wall. In this way torques from these contacts between the pipe and chamber were minimized. For the same reason, multi-turn coils of 0.003 inch copper wire were used to connect the nichrome heater leads to the power feed throughs near the knife edges, and a very thin flexible rubber membrane was used for the seal where the phenolic beam extension emerged from the evaporator section of the test cell. To further eliminate friction effects, the experiment was operated on a null basis; i.e., mass was continually added or removed from the balance to compensate for changes in the pipe weight so as to maintain the reading on the balance (and hence the pipe position) constant. Calibration of this system with precision weights showed it could detect a mass migration within the pipe of two hundred milligrams with better than two percent accuracy.

The test chamber was maintained at a slight over pressure with dry gas to prevent condensation on the outside of the pipe and the inside wall of the cooling jacket. Also, by alternatively using nitrogen or helium as the test cell gas, it was possible to experiment with

both low and high values for the condenser-to-sink thermal coupling.

The test cell was also provided with two clear plastic windows to permit visual inspection of the alignment, clearances, and surface conditions.

Additional experimental equipment included a constant voltage transformer, an autotransformer, and precision ammeter and voltmeter in the power circuit; a twelve-channel millivolt recorder and precision portable potentiometer for temperature measurement; and a cathetometer for initially leveling the system.

### 3.1.2 Procedure

The four legs of the test cell were equipped with leveling screws to permit height and level adjustments. To initially align the system, the test cell position and knife edges were adjusted such that 1) the heat pipe was level, 2) the heat pipe condenser and evaporator were concentric with the cylindrical cooling jacket and evaporator housing, respectively, and 3) there was a net weight on the balance pan of approximately 15 grams, including a number of 5 milligram weights which could later be removed. To run an experiment the following procedure was employed:

1. The test cell was purged with the selected dry gas (nitrogen or helium) at a high flow rate for one hour to assure the absence of air or moisture. The gas flow rate was then reduced to a slight bleed in order to minimize convection effects while maintaining a slight gage pressure in the cell.
2. A tare reading was taken on the balance establishing the null point for the experiment.
3. The thermocouple recording potentiometer and the circulating cooling system (at ambient temperature) were turned on.

4. Refrigeration (liquid nitrogen) was supplied to the cooling system, and its control point was set to yield the desired condenser sink temperature.
5. Power was supplied to the heater and, by monitoring all temperatures during the cooling transient, continually adjusted so that the vapor-gas front was completely developed within the primary condenser zone at steady-state conditions. Power was then held constant throughout the rest of the experiment.
6. After the initial transient, five-milligram weights, as required, were added to the balance pan every 5 or 10 minutes so as to maintain the balance reading at its initial null point.
7. The duration of the experiment varied between 2 and 6 hours depending on the diffusion freezeout rate.

Recorded data included the time, mass additions or subtractions from the balance, heater voltage and current, ambient temperature, and the thermocouple readings. In addition to the nine thermocouples on the heat pipe, thermocouples were also placed on the wall of the cooling jacket (to measure the sink temperature) and the wall of the evaporator housing. All eleven thermocouples were monitored on the recorder. However, for improved accuracy, the thermocouples measuring the sink temperature and the pipe temperature in the vicinity of the knife edges (away from the condenser and evaporator) were also measured with a precision hand balanced potentiometer. These temperatures were required inputs to the computer program for predicting the diffusion freezeout rates.

### 3.1.3 Data Reduction

The transient response of the heat pipe to the application of condenser refrigeration and heater power involved internal mass distribution changes in addition to that associated with diffusion freezeout. As the condenser cooled below the freezing point, the water in the condenser wick froze and expanded. Also, as the wick was placed under load, liquid was added to the condenser wicking, and meniscus recession occurred in the evaporator. The net result of these redistributions of mass was to cause the excess fluid reservoir inventory to initially increase which increased the pipe weight on the balance and required mass removal from the balance to maintain its null position. During this transient period, it was not possible to deduce diffusion freezeout rates from the data. However, once steady-state temperature conditions were established, the only mass migration within the pipe was that due to diffusion freezeout. Diffusion resulted in a continuous transfer of mass from the excess fluid reservoir to the sub-freezing portion of the condenser. This mass movement reduced the weight of the pipe on the balance. By compensating for this reduction through the periodic addition of 5 milligram weights to the balance pan, a measure of the diffusion freezeout rate was obtained.

A schematic diagram defining the model for data reduction is shown in Figure 3-6. The following assumptions are made:

1. Changes in torque due to friction at the knife edges, thermocouple and heater wires, and the flexible membrane seal on the balance beam were negligible. Calibration showed this assumption to be true within 2 percent for mass transfer on the order of 200 milligrams.
2. At quasi-steady-state conditions, changes in pipe weight on the balance were due solely to the transfer of mass from the excess fluid reservoir to the sub-freezing portion of the condenser by diffusion freezeout.

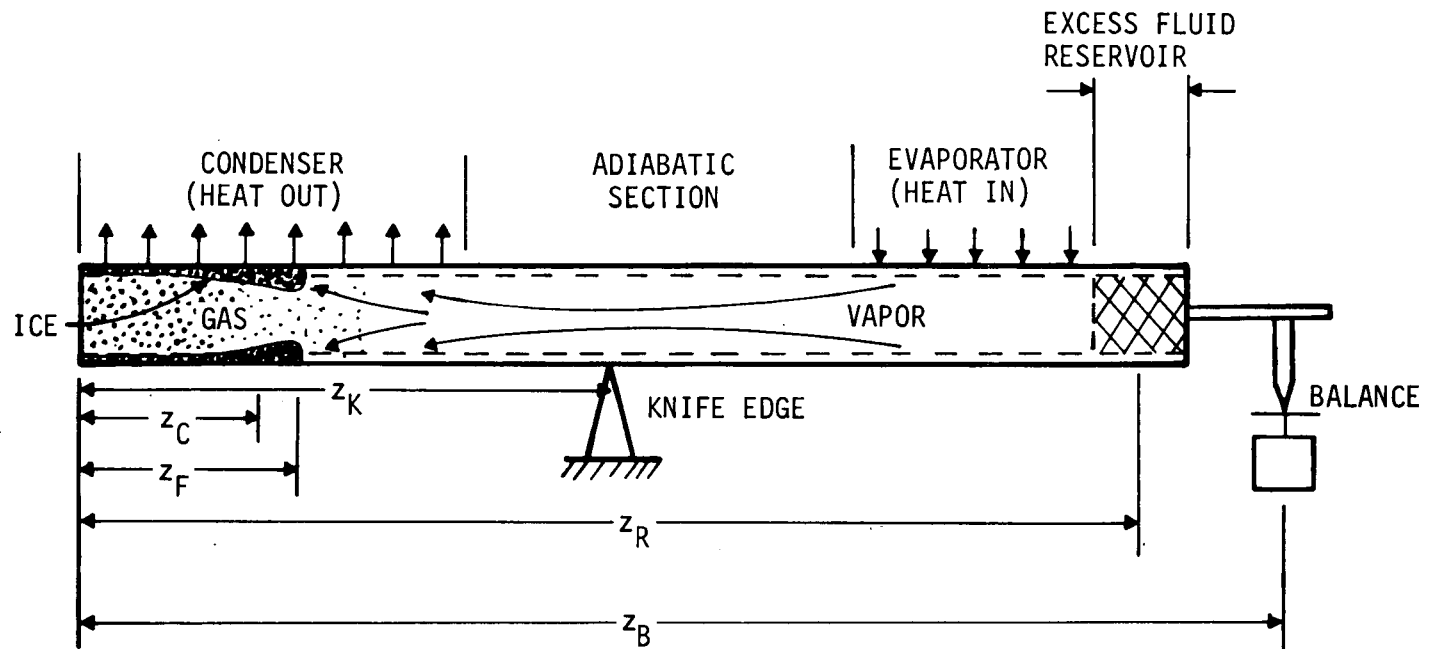


FIGURE 3-6. Diffusion Freezeout Experiment Model

3. All vapor which diffuses past the point on the condenser where the wick surface falls below the freezing point freezes upon condensing and remains stationary; the vapor flow provides the sublimation flux induced by the axial temperature gradient.

With these assumptions, a moment balance about the knife edge yields the following expressions for the rate of mass addition on the balance pan to maintain a null reading:

$$\dot{m}_B = \frac{(z_R - z_C) \dot{m}_V \Big|_{z = z_F}}{z_B - z_K} \quad (3-1)$$

$$(z_R - z_C) \dot{m}_V \Big|_{z = z_F} = \int_0^{z_F} \frac{d\dot{m}_V}{dz} (z_R - z) dz \quad (3-2)$$

where:

- $\dot{m}_B$  - rate of mass addition to the balance
- $\dot{m}_V$  - axial vapor flow rate
- $\frac{d\dot{m}_V}{dz}$  - local condensation and freezing rate
- $z$  - distance from the end of the condenser to any point along the pipe
- $z_C$  - position of the center of mass of the frozen condensate contributed by diffusion freezeout
- $z_F$  - position at which the wick surface reaches the freezing point
- $z_R$  - distance to the mid-point of the excess fluid reservoir

- $z_K$  - distance to the knife edge
- $z_B$  - distance to the point of beam contact with the balance pan

To obtain analytical predictions for  $\dot{m}_B$ , the TRW Gaspipe Computer Program was used to calculate values of the integral in Eq. (3-2). Two of the program outputs are profiles of the wick surface temperature and the local axial mass flow rate of vapor in the heat pipe condenser,  $\dot{m}_V$ . Axial variation of  $\dot{m}_V$  within the condenser represents condensation on the wick surface. Thus, the temperature profile established the location of the freezing point,  $z_F$ , and the vapor mass flow rate profile both established the value of  $\dot{m}_V \Big|_{z = z_F}$  directly and allowed the calculation of the local condensation and freezing rate in the region  $0 \leq z \leq z_F$ ; i.e.,  $\frac{d\dot{m}_V}{dz}$ .

Analytical predictions of  $\dot{m}_B$  obtained in this manner were compared directly with the experimentally measured results.

### 3.2 Results

Table 3-2 presents a summary of the experimental measurements. The rate of mass addition to the balance  $\dot{m}_B$  is compared with the computer predicted value. The measured results are seen to range from 64 percent to 99 percent of the computed values.

Figures 3-7 and 3-8 show two typical temperature profiles, one for a high sink conductance (helium cooled condenser) and the other for a low sink conductance (nitrogen cooled condenser). Also shown are the computer predictions based upon the precision potentiometer readings for evaporator and sink temperatures.

Figures 3-9 and 3-10 show the balance mass additions versus time for the runs corresponding to Figures 3-7 and 3-8. One can see that  $\dot{m}_B$  versus time is essentially a straight line for the first 150 mg or

TABLE 3-2  
COMPARISON OF MEASURED AND PREDICTED  
RATES OF BALANCE WEIGHT PER UNIT TIME

RUN	CONDENSER COEFFICIENT OF HEAT TRANSFER	EVAP. TEMP.	SINK TEMP.	$z_B - z_K$	$z_R - z_C$	$z_F$	$\dot{m}_{B,meas.}$	$\dot{m}_{B, pred.}$	$\frac{\dot{m}_{B,meas.}}{\dot{m}_{B,pred.}}$
	Btu/hrft <sup>2</sup> F	°R	°R	in.	in.	in.	mg/hr	mg/hr	
5	18.5 (He)	553.2	458.1	15.38	15.95	3.75	55	70.6	.78
6	3.2 (N <sub>2</sub> )	550.1	459.7	15.38	16.28	3.80	20	31.2	.64
7	3.2 (N <sub>2</sub> )	550.6	456.8	11.38	16.28	3.80	30	44.5	.67
8	18.5 (He)	558.5	457.1	11.38	16.57	3.12	65	82.6	.79
9	18.5 (He)	540.9	403.2	11.38	14.36	5.25	340	343.4	.99
10	18.5 (He)	550.9	418.0	11.38	15.78	3.87	127	138.4	.92
11	3.2 (N <sub>2</sub> )	546.2	421.4	11.38	15.36	4.45	76	98.0	.78

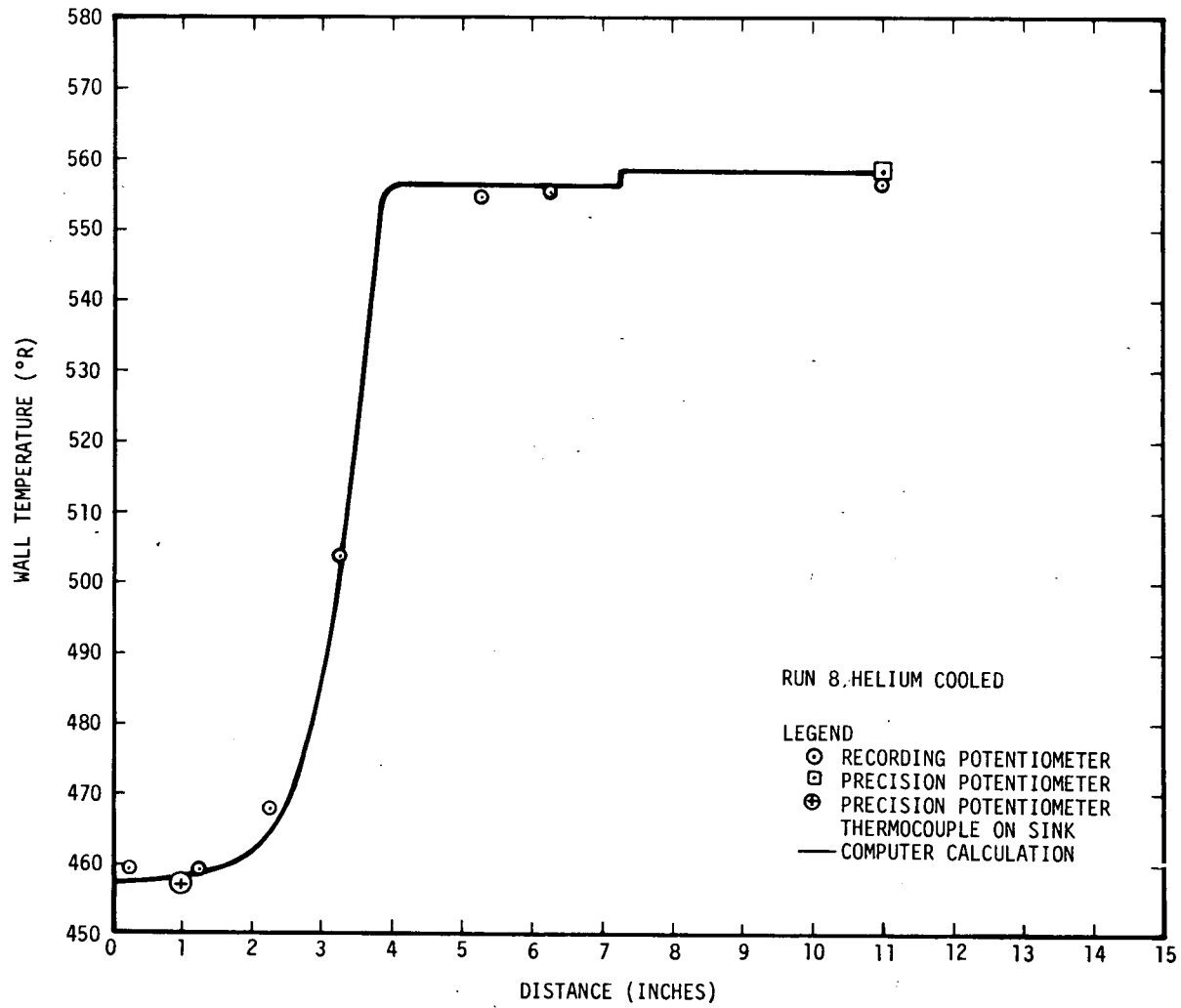


FIGURE 3-7. Temperature Profile for High Sink Conductance

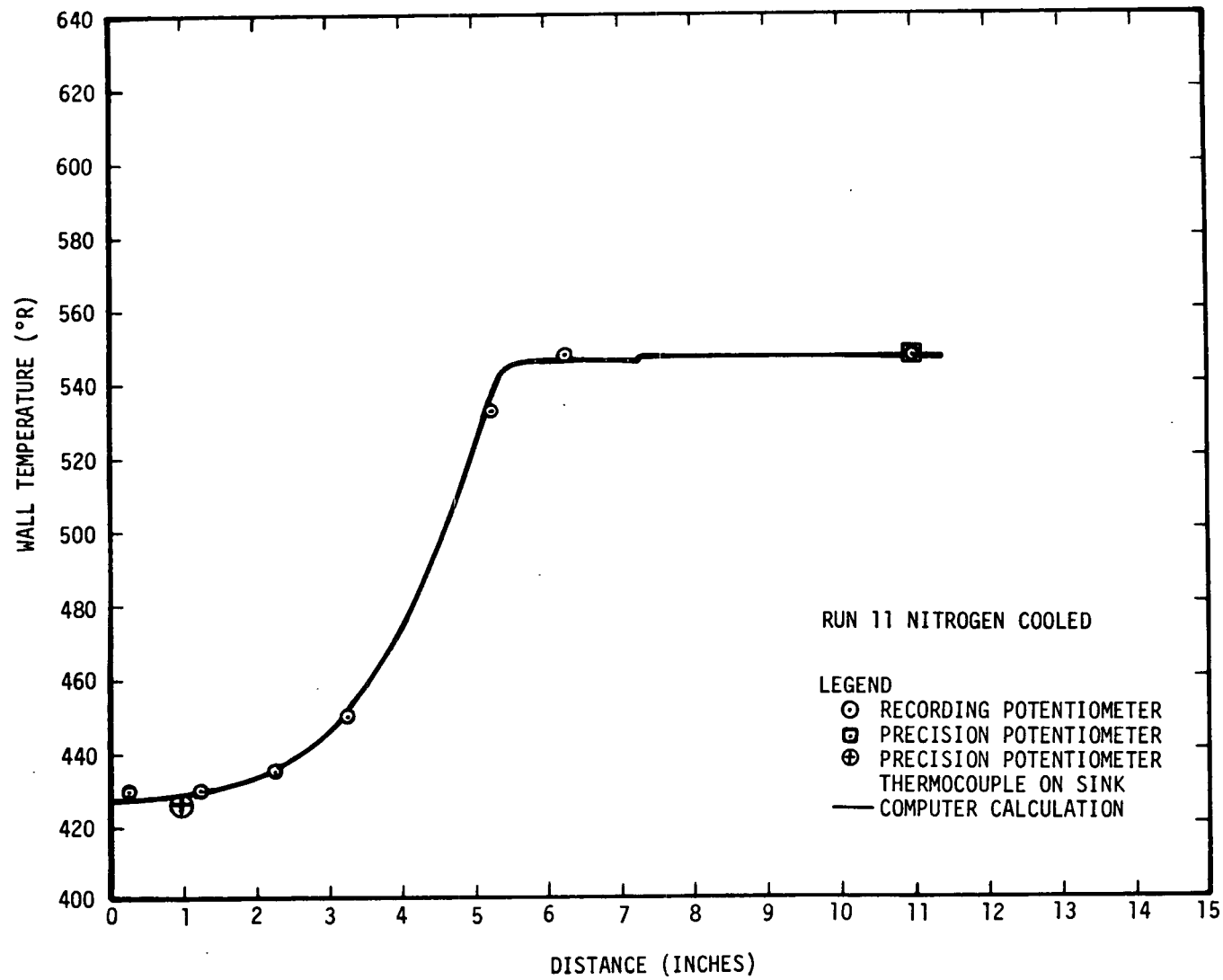


FIGURE 3-8. Temperature Profile for Low Sink Conductance

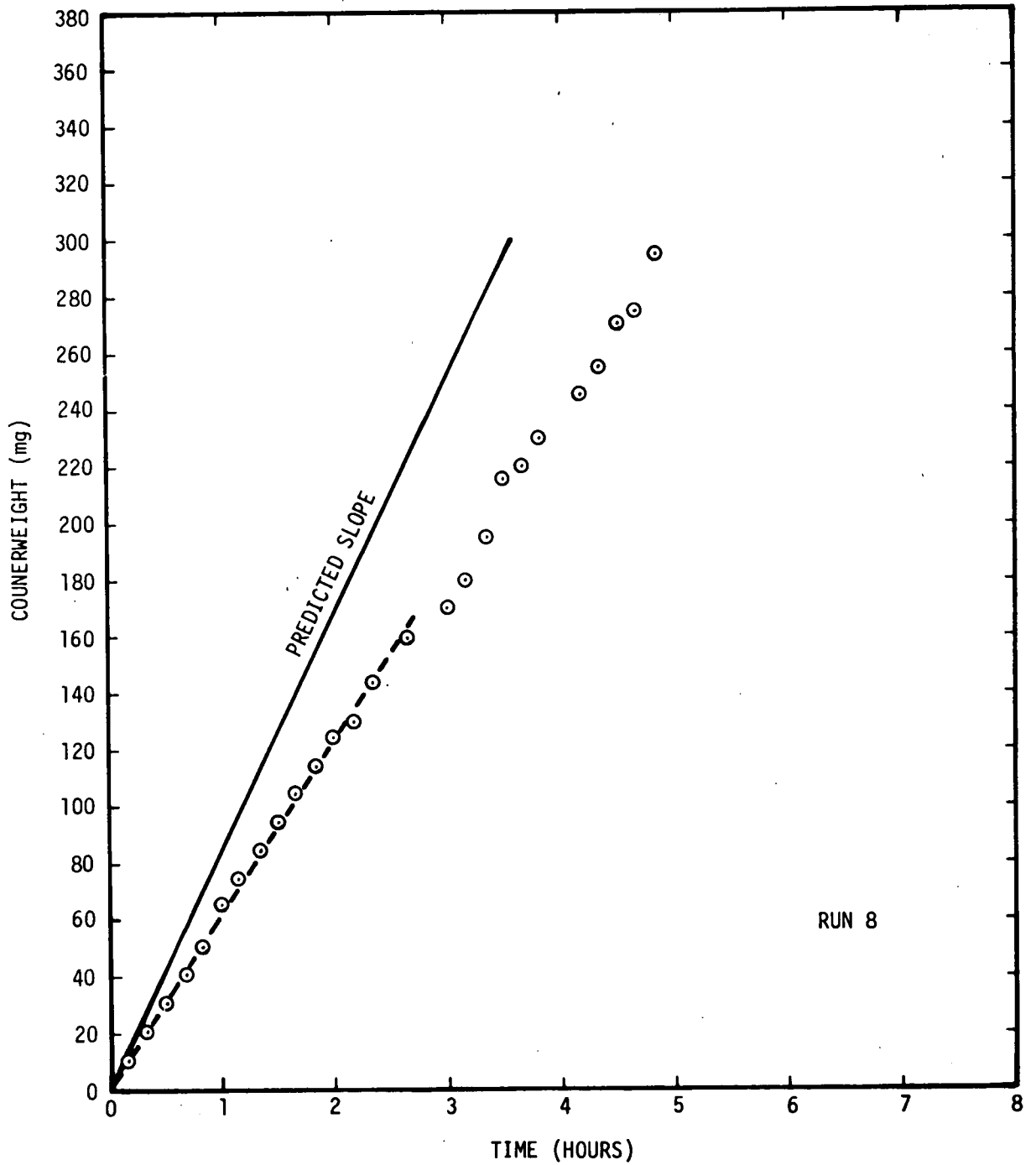


FIGURE 3-9. Balance Weight Versus Time During Diffusion Freezeout

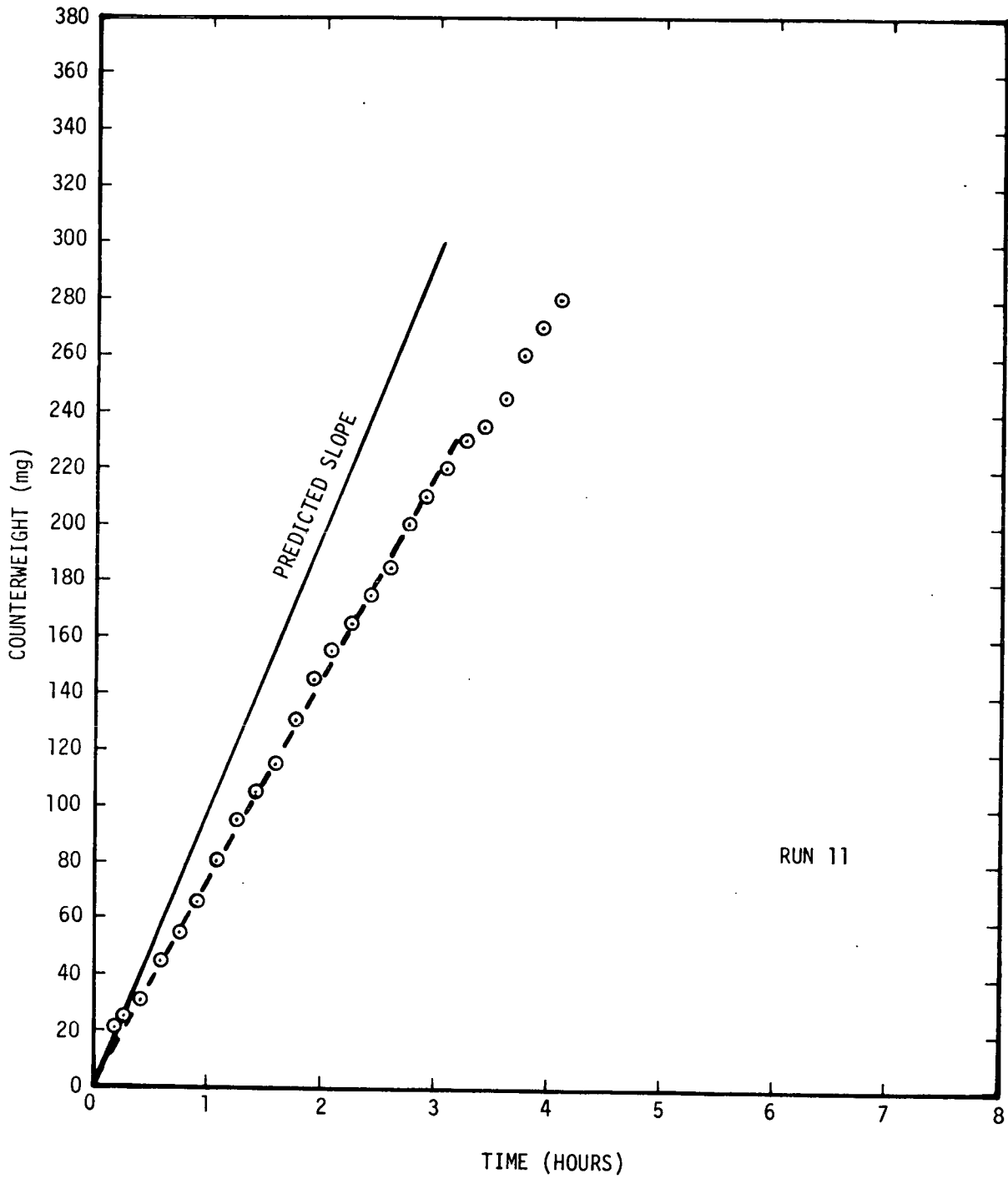


FIGURE 3-10. Balance Weight Versus Time During Diffusion Freezeout

so. It was this line which was used to fix the  $m_B$  values shown in Table 3-2.

Table 3-3 shows the freezeout rates converted from raw balance readings to true mass movement rates using the lever arm distances in Table 3-2. The distance  $z_B - z_K$  was an experimentally measured quantity and the distance  $z_R - z_C$  was a computed quantity as explained in the previous section. The next section discusses the fact that the true values of  $z_R - z_C$  cannot differ much from the calculated ones so that the  $m_{RC}$  measured values can stand as experimental results independent of the computer program validity.

### 3.3 Discussion

A clearly evident pattern in the data is that the diffusion freezeout rate increases with increasing condenser-to-sink conductance (helium vs. nitrogen in the gas gap). For example, runs 5 and 6 were made at similar evaporator and sink temperatures, and helium cooling yielded a freezeout rate more than twice that with nitrogen.

Another pattern which stands out is that a lower sink temperature yields a higher freezeout rate when the condenser coupling is fixed. For example, runs 7 and 11 for nitrogen cooling, and runs 8, 9 and 10 for helium cooling may be compared. However, it is important to note that in Table 3-2 lower sink temperatures are generally accompanied by lower evaporator temperatures for a given condenser coupling. This was a consequence of an attempt to set the evaporator temperature (through the power setting) such that the freezing point was located approximately mid-way along the condenser. Thus, the relationship between the freezeout rate and the sink temperature is partially obscured by the accompanying variations in  $T_E$ .

If one examines Fick's law for diffusion, the trends evident in the data are readily comprehended. The vapor diffusion flux in the gas blocked region of the heat pipe is given by:

$$J = -c D \frac{dx}{dz} \quad (3-3)$$

TABLE 3-3

COMPARISON OF MEASURED AND PREDICTED  
DIFFUSION FREEZEOUT RATES

(SEE TABLE 3-2 FOR EXPERIMENTAL CONDITIONS)

RUN	$\dot{m}_{RC}$ , MEAS.	$\dot{m}_{RC}$ , PRED.
	mg/hr	mg/hr
5	53	68.0
6	19	29.5
7	21	31.1
8	45	56.7
9	270	272
10	92	99.8
11	56	72.6

where:

- J - molar diffusion flux of vapor
- c - molar density
- $\mathcal{D}$  - diffusivity of vapor-gas pair
- x - mole fraction of vapor

At the freezing point, Eq. (3-3) can be written:

$$J = -c\mathcal{D} \left. \frac{dx}{dT} \right|_{T = T_F} \cdot \left. \frac{dT}{dz} \right|_{z = z_F} \quad (3-4)$$

As mentioned previously, although axial conduction and axial mass diffusion are coupled phenomena in the vapor-gas front region, the conduction effect dominates the shape of the axial temperature profile. Thus, an appropriate expression for the axial temperature gradient can be obtained by treating the condenser as a long fin, for which the temperature gradient at  $z_F$  is given by:

$$\left. \frac{dT}{dz} \right|_{z = z_F} = (T_F - T_S) \sqrt{\frac{hP}{\Sigma KA}} \quad (3-5)$$

where:

- h - condenser-to-sink coefficient of heat transfer
- P - pipe perimeter (circumference)
- $\Sigma KA$  - sum of the axial conductivity area products for the wall, wick and fluid

Furthermore, from the Clausius-Clapeyron relation:

$$x = \exp \left[ - \frac{\lambda}{RT_E} \left( \frac{T_E}{T} - 1 \right) \right] \quad (3-6)$$

and,

$$\left. \frac{dx}{dT} \right|_{T = T_F} = \frac{\lambda}{RT_F^2} \exp \left[ - \frac{\lambda}{RT_E} \left( \frac{T_E}{T_F} - 1 \right) \right] \quad (3-7)$$

where:

- $\lambda$  - latent heat of vaporization
- $T_E$  - evaporator vapor temperature
- $R$  - universal gas constant

Substituting Eqs. (3-5) and (3-7) into (3-4) yields the following approximate expression for the diffusion freezeout rate:

$$J = \frac{-c_D \lambda (T_F - T_S)}{RT_F^2} \cdot \exp \left[ - \frac{\lambda}{RT_F} \left( 1 - \frac{T_F}{T_E} \right) \right] \cdot \sqrt{\frac{hP}{\Sigma kA}} \quad (3-8)$$

From this expression one sees that a large  $h$  on the condenser does indeed lead to a high diffusion freezeout rate, as does a low sink temperature,  $T_S$ . The freezeout rate is also sensitive to  $T_E$ , particularly as  $T_E$  approaches  $T_F$ . A small drop in  $T_E$  then causes a large increase in diffusion freezeout. Note that the  $c_D$  product is insensitive to pressure and hence  $T_E$ . Finally, the equation shows that the freezeout rate can be reduced by increasing the axial conductance of the pipe.

It should also be noted that a convection vapor flux augments the diffusion flux,  $J$ , in an operating heat pipe, and this fact is accounted

for in the computer program. Thus, the above arguments apply only when the convection flux is small compared with that by diffusion. Nevertheless, the tendency for high  $h$ , low  $T_S$ , low  $T_E$  and low  $k$  to favor high freezeout rates would still prevail.

### 3.3.1 Comparison of Predicted and Measured Results

A number of uncertainties acted to make the agreement between experiment and theory imperfect. In the experiment itself friction and/or torques caused by the leads and flexible seal made the effective sensitivity of the system approximately 4 mg, although the balance itself was sensitive to 0.01 mg. This was established with the pipe inoperative by placing weights on the end of the condenser to simulate the movement of mass within the pipe, and then adding mass to the balance until the pipe recovered its original position. The mass of the condenser weights determined this way agreed to within 4 mg with that determined by weighing them on the balance directly.

As another check on systematic weighing errors, experiments were performed on two sets of knife edges, located at different positions along the pipe. Consistent results were obtained for both cases.

Other experimental uncertainties were introduced by lack of absolute constancy in sink temperature and through temperature measurement errors (even though a precision potentiometer was used to measure  $T_E$  and  $T_S$ ). There was also some uncertainty in the inert gas composition, nominally 53% Ne and 47%  $N_2$ , which makes the diffusivity  $D$  somewhat uncertain. Also, although radiation coupling in the frozen condenser was a small part of the total, particularly in the helium cooled runs, some question about the value of the emissivity on the brass inside wall of the cooling jacket existed. Further, the alignment of the pipe in the condenser cooling jacket affected the condenser coupling, since any eccentricity increases  $h$ .

The lengths  $z_K$  and  $z_B$  were of course known with high precision; ( $z_B - z_K$ ) was measured to within 0.1 percent. But the lengths  $z_R$  and

$z_C$  were more uncertain. Does the excess fluid reservoir desaturate uniformly as postulated, or does it desaturate from the evaporator end? The location of  $z_C$  at first thought may seem highly uncertain, but actually it is not much more so than  $z_R$ . The freezing point location,  $z_F$ , was known experimentally within 0.1 inches or so, and  $z_C$  is located very nearby independent of the computer results. The vapor pressure drops so rapidly with wall temperature that all of the vapor is condensed and frozen within a few inside diameters of the freezing point. The computer predicts  $z_F - z_C \approx 0.2$  inches for helium coupling and 0.6 inches for nitrogen coupling of the condenser to the sink.

Taking into account all of these experimental uncertainties, it is estimated that the experimental diffusion freezeout rates reported in Table 3-3 are accurate to within  $\pm 5\%$ , but that the experimental conditions under which the measurements were taken combine to yield a  $\pm 15\%$  uncertainty in the predictions.

In several cases, however, the discrepancy between measured and predicted freezeout rates exceeds fifteen percent. Furthermore, there seems to be a systematic variation in the ratio of measured to predicted values from 0.64 at low freezeout rates to 0.99 at high rates. This is probably due to several approximations in the analytical model itself, which tend to make its predicted freezeout rates conservative (too high). Chief among these is the neglect of radial resistance to vapor diffusion in the one-dimensional model of the vapor/gas dynamics. Recent analytical work by Rohani and Tien [10] suggests that a one-dimensional model is quite good for cases in which the vapor-gas front is sharp and axial diffusion rates are high, but less so when the front is spread out and diffusion rates are low. In the latter case, radial resistance to diffusion is significant so that a one-dimensional solution would tend to over predict freezeout rates. This is consistent with the experimental data.

In view of the approximations in the program and the experimental uncertainties, the 64 to 99 percent agreement between measured and predicted freezeout rates seems reasonable and suggests that the analytical

model upon which the program is based adequately describes the phenomena involved.

### 3.3.2 Design Implications

The application of gas-loaded heat pipes in spacecraft thermal control often requires that they operate with sub-freezing sink temperatures. Under such conditions it is necessary that the heat pipe engineer consider the diffusion freezeout phenomenon in designing the pipe.

Diffusion freezeout does not preclude the successful operation of gas-loaded heat pipes. However, it is necessary to assure that the freezeout rate is not so high that the evaporator fluid inventory be depleted to the point of failure before the frozen fluid is recovered. This occurs when the vapor-gas front moves further out in the condenser in response to a change in heat load or sink conditions, causing the previously frozen fluid to be thawed and re-circulated through the wick system. Thawing will, of course, also occur if the application involves cyclic sink conditions which rise above the freezing point. In that case, providing an excess fluid reservoir as was done in the experimental heat pipe prolongs the pipes ability to operate during a cold cycle.

The diffusion freezeout rate is a function of many variables including the working fluid, the non-condensable gas, the condenser-to-sink conductance, the axial conductance of the pipe (and radiator), the evaporator temperature, the sink temperature, and the pipe diameter. Because many of these same variables also influence other aspects of the heat pipe design (e.g., heat transfer capacity, overall pipe conductance, control sensitivity), it is generally necessary to perform a series of trade-offs to achieve a design meeting all requirements.

The experimental results reported in this paper suggest that the TRW Gaspipe Program adequately predicts diffusion freezeout rates for design purposes. Since it was previously shown that the program also correctly predicts temperature profiles and heat transfer characteristics, the authors recommend it for use in designing gas loaded heat pipes.

#### 4.0 GAS-AIDED START-UP FROM THE FROZEN STATE

There exists a potential problem in starting heat pipes from a frozen condition in that the evaporator can become depleted of working fluid before the rest of the heat pipe is thawed, resulting in a temperature overshoot and perhaps a failure to start. Under many circumstances this failure mode can be obviated by the inclusion of an appropriate quantity of non-condensable gas in the pipe. This results in a progressive, rather than uniform, start-up of the heat pipe which eliminates the need to thaw the entire pipe before fluid can return to the evaporator.

From the heat pipe designer's point of view one must know (1) under what circumstances this start-up scheme will work, and (2) how much gas should be put into the heat pipe. In an attempt to answer these questions, an analysis of gas-aided start-up has been performed. A somewhat simplified, but conservative, model was used for which it was possible to achieve a closed form solution to the problem. It is felt that, when verified experimentally, this solution will provide a satisfactory engineering design criterion for most situations.

#### 4.1 Assumptions and Simplifications in the Model

##### A Conservative Thawing Criterion:

Freezing stops passage of fluid through the wick. It is difficult to establish an accurate criterion for when a wick is so blocked. In an ordinary screen wick, how deeply must the thawing wave penetrate for liquid to be wicked? It would appear that partial wicking capability would be recovered in a multilayered wick as soon as a single layer thawed. In a single layer wick, however, it is not clear at what point partial wicking would be restored. It is conservative to assume that raising the pipe wall temperature to the freezing point is necessary, since the heating occurs via conduction through the wick. This criterion is conservative in the sense that it would lead to overdesign of evaporator liquid capacity.

### Axial Diffusion:

As discussed in the last section, axial diffusion is generally small for heat pipes of interest in spacecraft thermal control and contributes little to axial heat transfer. In such cases it is a reasonable approximation to assume a sharp front (step change in mole fraction) between the region which is gas blocked and that which is at the evaporator temperature.

### Axial Conduction:

Before the evaporator temperature reaches the boiling point; that is, before the saturation temperature becomes that corresponding to a vapor pressure equal to the total pressure in the condenser ( $P_{\text{vapor}} + P_{\text{gas}}$ ), mass transfer occurs by diffusion at only a low rate. During this time axial conduction acts to preheat the pipe to some degree. The section of the pipe immediately adjacent to the evaporator becomes heated so that the subcooling is much reduced. When the "boiling point" is reached, this portion of the condenser becomes exposed to vapor at the boiling point and collects condensed and perhaps frozen fluid. However, due to the preheating by axial conduction and the heating from contact with the vapor, this portion rapidly thaws and returns liquid to the evaporator, due to the capillary pumping head generated when the evaporator liquid is partly depleted. Subsequent condensation on this portion of the condenser supplies heat which by virtue of axial conduction preheats the next section of condenser. During this time, however, the condensate is returned to the evaporator from the thawed region.

In view of the preheating phenomenon caused by axial conduction, it would be conservative to neglect axial conduction. This hypothesis is put forward only for uniform pipes; a region of low axial conduction followed by one of high axial conduction as from a connecting conduit to the condenser presents some difficulties for qualitative arguments of the type used to advance this hypothesis. In any event the case of zero axial conduction is clearly a limiting case of interest.

With these assumptions, the proposed model is a variation of the "flat front" theory for steady-state operation of gas-loaded heat pipes. Both axial conduction and axial diffusion have been neglected. However, in the steady-state case the axial position of the "front" is the same at all radial locations; i.e., the vapor core, wick and wall. In the case at hand, the position of the front in the vapor core precedes that in the wick and wall during start-up.

#### 4.2 Formulation of Equations

The length of condenser exposed to the vapor temperature  $T_i$  of any given time  $t$  is  $L(t)$ . Neglecting the energy stored in the vapor and assuming that the condenser wall is virtually isothermal in the radial direction, because of wick-limited heat transfer, permits  $L(t)$  to be simply related to the evaporator power  $\dot{Q}$ .

$$\dot{Q} = \int_0^{L(t)} P_i h_i (T_i - T(z,t)) dz \quad (4-1)$$

A segment of condenser wall at location  $z$  first becomes exposed to  $T_i$  when

$$z = L(t_0) \quad (4-2)$$

During the subsequent time this segment of wall heats according to

$$\rho C_p A_c \frac{dT}{dt} = h_i P_i (T_i - T) - h_o P_o (T - T_s), \quad t > t_0(z) \quad (4-3)$$

$$(T = T_o, \quad t < t_0(z))$$

We define

$$T_\infty = \frac{h_i P_i T_i + h_o P_o T_s}{h_i P_i + h_o P_o} \quad (4-4)$$

and

$$\tau = \rho C_p A_c / (h_i P_i + h_o P_o) \quad (4-5)$$

Then the solution to Eq. (4-3) for constant  $T_i$  is

$$\frac{T_\infty - T(z,t)}{T_\infty - T_o} = e^{-[t-t_o(z)]/\tau} \quad (4-6)$$

The interface temperature  $T_i$  is constant, if the condenser pressure remains essentially constant during a time interval of a few  $\tau$ 's.

From Eq. (4-6) it is possible to find at once the time to thaw, that is, the time for  $T(z,t)$  to reach the freezing point  $T_F$  from the subcooled condition  $T_o$

$$\frac{T_\infty - T_F}{T_\infty - T_o} = e^{-t_{\text{thaw}}/\tau} \quad (4-7)$$

$$t_{\text{thaw}} = \tau \ln \frac{T_\infty - T_o}{T_\infty - T_F}$$

At  $t = 0$  Eq. (4-1) gives the initial value of  $L_o$ , the length of the domain for which  $t_o = 0$ .

$$\dot{Q} = P_i h_i L_o (T_i - T_o) \quad (4-8)$$

$$L_o = \frac{\dot{Q}}{P_i h_i (T_i - T_o)}$$

For  $L_o$  to be short it is necessary for  $T_i$  to be not too close to  $T_o$ . Therefore, enough gas must be present to have a pressure in the pipe volume somewhat greater than that of the vapor pressure at the freezing point.

During an initial time period from  $t = 0$  to  $t = t_{\text{thaw}}$ , under our wick performance criterion, no liquid may be returned to the evaporator. During this time the liquid level in the wick retreats an amount  $\delta_0$ .

$$\delta_0 \phi A_{\text{ev}} \rho_f \lambda = \dot{Q} t_{\text{thaw}} \quad (4-9)$$

$$\delta_0 = \frac{\dot{Q}}{\phi A_{\text{ev}} \rho_f \lambda} \tau \ln \frac{T_\infty - T_0}{T_\infty - T_F}$$

When the time  $t_{\text{thaw}}$  is reached, liquid in the amount of  $\delta_1$  is returned. This liquid multiplied by the latent heat is equal to the integral of the heat transfer through the wick of length  $L_0$  during the time to reach  $t_{\text{thaw}}$ .

$$\delta_1 A_{\text{ev}} \rho_f \lambda = h_i P_i L_0 \int_0^{t_{\text{thaw}}} (T_i - T) dt \quad (4-10)$$

$$\delta_1 = \frac{\dot{Q} \tau \ln \frac{T_\infty - T_0}{T_\infty - T_F}}{A_{\text{ev}} \rho_f \lambda} \left\{ \frac{T_i - T_\infty}{T_i - T_0} + \frac{T_F - T_0}{T_i - T_0} \left( \frac{1}{\ln \frac{T_\infty - T_0}{T_\infty - T_F}} \right) \right\}$$

The ratio of  $\delta_1$  to  $\delta_0$  is the fraction of liquid returned after the initial thaw.

$$f_1 = \frac{\delta_1}{\delta_0} = \frac{T_i - T_\infty}{T_i - T_0} + \frac{T_F - T_0}{T_i - T_0} \left( \frac{1}{\ln \frac{T_\infty - T_0}{T_\infty - T_F}} \right) \quad (4-11)$$

At time equal zero a heating wave proceeds down the tube according to Eqs. (4-1) and (4-6). The initial velocity  $V_0$  of this wave can be obtained by differentiating Eq. (4-1) with respect to  $t$ .

$$0 = P_i h_i (T_i - T_0) V_0 - P_i h_i L_0 (T_\infty - T_0) \frac{1}{\tau} \quad (4-12)$$

$$V_0 = \frac{T_\infty - T_0}{T_i - T_0} \frac{L_0}{\tau}$$

After time  $t_{thaw}$  passes, the thawing wave starts traveling down the tube at exactly the same velocity as the heating wave which preceded it. Since the velocity of the heating wave decreases monotonically with time, in a uniform tube, the velocity of the thawing wave is always greater and is thus always catching up. Thus the amount of working fluid returned to the evaporator increases monotonically after the initial waiting period  $t_{thaw}$ . This initial period is the critical one.

#### 4.3 Discussion

Since it appears that the initial thawing period is the critical one, this analysis, which deals only with the start of the thawing process, should yield the appropriate criteria for successful frozen start-ups.

To use this model in the design of heat pipes, one is concerned principally with Eqs. (4-4), (4-5) and (4-9). For an hypothesized heat pipe and start-up environment, values for the internal wick conductance per unit length ( $h_i P_i$ ), the external pipe conductance per unit length ( $h_o P_o$ ), and the sink temperature ( $T_s$ ) are known. From Eq. (4-4) it is then possible to calculate values of  $T_\infty$  for assumed values of  $T_i$  greater than the freezing point of the working fluid ( $T_F$ ).  $T_i$  is the temperature at which the vapor front begins to move out of the evaporator.

The hypothesized heat pipe also yields values for the thermal mass per unit length of condenser ( $\rho C_p A_c$ ), which includes wick, fluid, wall, fins, etc. Thus, everything is known from which to calculate the time constant  $\tau$  with Eq. (4-5).

Eq. (4-9) is then used to calculate the maximum liquid recession into the evaporator wick prior to liquid return ( $\delta_0$ ) for a given start-up input power ( $\dot{Q}$ ). The other parameters; initial temperature ( $T_0$ ), freezing point ( $T_F$ ), evaporator wick area ( $A_{ev}$ ), fluid density ( $\rho_f$ ), latent heat of vaporization ( $\lambda$ ), and wick porosity ( $\phi$ ) are all known quantities.

The criterion for a successful start is that the initial liquid return to the evaporator occurs before the evaporator wick depletion ( $\delta_0$ ) becomes excessive. The allowable recession, of course, is dependent on the nature of the wick, and requires some engineering judgement. For homogeneous wicks it appears as though total depletion is permissible. However, in the case of an annular artery,  $\delta_0$  must not exceed the artery wall thickness.

The procedure outlined will yield the minimum value of  $T_i$  necessary to achieve a successful start. This is then used to establish the required non-condensable gas inventory:

$$\mathcal{M} = \frac{[P_v(T_i) - P_v(T_0)] V_{ad + cond}}{R_u T_0} \quad (4-13)$$

Clearly there exists a minimum gas inventory for successful start-up. Raising  $\mathcal{M}$  increases  $T_i$  and lowers  $\delta_0$ . Thus, values of  $\mathcal{M}$  in excess of the minimum provide a factor of safety. The magnitude of this factor of safety, however, must be traded off against larger steady-state condenser blockage which accompanies higher gas inventories. The length of the steady-state gas blocked region and the possibility of a long-term diffusion freezeout problem ( $T_s$  is below  $T_F$  for frozen start-up conditions) can be determined with the TRW Gaspipeline Program [9].

These equations have not yet been studied in great detail parametrically. However, it appears that from an engineering point of view, the initial thaw process in frozen start-ups can generally be handled through the inclusion of an appropriate quantity of non-condensable gas. On the other hand, a long period with the evaporator shut-down and maintained at a temperature above  $T_o$  but below  $T_{fp}$  will cause loss of fluid by diffusion. This mode of drying out the evaporator must also be examined.

## 5.0 TRANSIENT BEHAVIOR OF HOT RESERVOIR HEAT PIPES: THE TRANPIPE PROGRAM

Gas diffusion plays an important role in the behavior of hot reservoir variable conductance heat pipes subjected to cyclic or other temporal changes in heat load or sink conditions [2, 3, 4]. Overdriving a pipe by imposing so large a heat load or evaporator temperature that vapor enters the reservoir gives rise to diffusion-dominated transient behavior. One example is when a non-wicked hot reservoir pipe is overdriven so that vapor diffuses into (and gas out of) the reservoir with the result that the evaporator temperature rises slowly with time following the initial transient. A second and more important example is when an overdriven pipe has the heat load reduced to a value which is within its normal control range. Unfortunately, instead of the pipe immediately returning to a proper low value of evaporator temperature, it continues to hold a high evaporator temperature and returns to normal operation only slowly as the vapor in the reservoir diffuses out. Another important example is when changes occur in the effective sink temperature. Once again, the pipe responds slowly to such changes as vapor and gas diffuse into or out of the non-wicked reservoir.

Because hot reservoir heat pipes generally offer better control than cold reservoir systems [2, 3], it is important that we fully understand them and have the analytical tools available to adequately predict their performance. This section presents an analytical model for hot reservoir heat pipes leading to such a computational tool - the TRW Transient Gaspipe Program (TRANPIPE).

### 5.1 Analytical Model

The analytical model employed to predict diffusion dominated transient heat pipe performance is defined by the following list of features:

1. A prescribed source heat load  $\dot{Q}(t)$ .

2. A lumped thermal capacity for the source,  $C_{so} = (MC_p)_{so}$ .
3. A lumped thermal capacity evaporator of length  $L_{ev}$  connected thermally to the source by thermal conductance  $\pi D_o L_{ev} h_{ev}$ .
4. An adiabatic section of length  $L_{ad}$ .
5. A finned, radiating and convecting, and axially conducting condenser of length  $L_c$ .
6. An unwicked gas reservoir with lumped volume  $V_{res}$  connected to the end of the condenser by a tube of inside diameter  $D_{dif}$  and a length  $L_{dif}$ . The reservoir is assumed to be at the evaporator temperature  $T_{ev}$ .

### 5.1.1 Thermostatics

The heat stored within the system is taken to be composed of the following items:

1. Source heat storage:

$$Q_{so} = (MC_p)_{so} T_{so} = C_{so} T_{so} \quad (5-1)$$

2. Evaporator heat storage:

$$Q_{ev} = (MC_p)_{ev} T_{ev} = C_{ev} T_{ev} \quad (5-2)$$

3. Adiabatic section heat storage:

$$Q_{ad} = (MC_p)_{ad} T_v = C_{ad} T_v \quad (5-3)$$

4. Heat stored in condenser:

$$Q_c = (MC_p)_c \left\{ \frac{L_b}{L_c} (1-\eta_b) T_b + \left[ 1 - \frac{L_b}{L_c} (1-\eta_b) \right] T_v \right\} \quad (5-4)$$

Note that we neglect the heat stored in the vapor in the pipe, on the one hand, but overstate the heat stored in the condenser, on the other hand, because most of the heat capacity of the condenser is effective at a temperature below  $T_v$  due to wick resistance. The quantity  $\eta_b$  is the fraction of the blocked condenser which is nevertheless hot, because of axial conduction. If there were no axial conduction, we would have  $\eta_b = 0$ .

The gas stored within the system is taken to be as follows:

1. When the pipe is overdriven ( $L_b = 0$ ) all the gas is contained in the reservoir

$$\mathcal{M}_{\text{gas}} = \frac{x_{\text{res}} P_{\text{sat}}(T_v) V_{\text{res}}}{R_u T_{\text{res}}} \quad (5-5)$$

2. When the pipe is gas controlled, both the reservoir and blocked portion of the condenser contain gas

$$\mathcal{M}_{\text{gas}} = A_v L_b (1 - \eta_b) \frac{P_{\text{sat}}(T_v) - P_{\text{sat}}(T_b)}{R_u T_b} + \mathcal{M}_{\text{gas, res}} \quad (5-6)$$

where the approximation is made that  $\eta_b$  applies to both temperature and mass concentration profiles.

The mole fraction of non-condensable at the end of the reservoir is

$$x_{\text{end}} = \frac{P_{\text{sat}}(T_v) - P_{\text{sat}}(T_{\text{end}})}{P_{\text{sat}}(T_v)} \quad (5-7)$$

The temperature distribution along the condenser is assumed to be such that

$$\eta_b = \frac{\tanh \beta}{\beta} \quad (5-8)$$

$$T_{\text{end}} = T_b + \frac{T_v - T_b}{\cosh \beta} \quad (5-9)$$

$$\beta^2 = \frac{(4\epsilon\sigma T_v^3 + h_f)\eta_f P_f L_b^2}{\sum KA} \quad (5-10)$$

The reader will recognize that these results are taken from the classical one-dimensional fin of constant cross-sectional area and perimeter by linearizing the radiation and introducing an equivalent radiation heat transfer coefficient  $h_r = 4\epsilon\sigma T_v^3$ .

### 5.1.2 Thermodynamics

Under dynamic conditions the heat flow rates are as follows:

1. Heat flow into and out of source: The power load  $\dot{Q}_{so}$  imposed upon the source is stored and transmitted to the evaporator.

$$\dot{Q}_{so} = \frac{dQ_{so}}{dt} + UA (T_{so} - T_v) \quad (5-11)$$

2. Heat flow from evaporator to pipe: The heat from the source is stored within the pipe and lost from the unblocked portion of the condenser.

$$UA (T_{so} - T_v) = \frac{dQ_{\text{pipe}}}{dt} + \eta_f P_f \left[ L_c - L_b (1 - \eta_b) \right] \cdot \left[ \epsilon (\sigma T_w^4 - \sigma T_s^4) + h_f (T_w - T_s) \right] \quad (5-12)$$

where:

$$Q_{\text{pipe}} = Q_{ev} + Q_{ad} + Q_c \quad (5-13)$$

The total mole transfer rate of gas and vapor into the reservoir is as follows:

$$\dot{m}_{\text{tot}} = A_{\text{diff}} cv^* = \frac{d}{dt} \left( \frac{P_{\text{sat}}(T_v) V_{\text{res}}}{R_u T_{\text{res}}} \right) \quad (5-14)$$

That for the gas by diffusion and convection into the reservoir is

$$\dot{m}_{\text{gas, res}} = \dot{m}_{\text{tot}} \left[ x_{\text{end}} + (x_{\text{end}} - x_{\text{res}}) \frac{e^{-L^*_{\text{diff}}}}{1 - e^{-L^*_{\text{diff}}}} \right] \quad (5-15)$$

$cv^* > 0$

If convection occurs out of the reservoir into the pipe as when the pipe temperature is falling,

$$\dot{m}_{\text{gas, res}} = - \left| A_{\text{diff}} cv^* \right| \left[ x_{\text{res}} + (x_{\text{res}} - x_{\text{end}}) \frac{e^{-L^*_{\text{diff}}}}{1 - e^{-L^*_{\text{diff}}}} \right] \quad (5-16)$$

$cv^* < 0$

The quantity  $L^*_{\text{diff}}$  is a measure of the strength of the convection relative to that of diffusion from the classical solution for flow in a Stefan tube

$$L^*_{\text{diff}} = \frac{|\dot{m}_{\text{tot}}| L_{\text{diff}}}{c \mathcal{O} A_{\text{diff}}} \quad (5-17)$$

When  $L^*_{\text{diff}}$  is very large, convection completely dominates the mass transfer into or out of the reservoir, and, when it is small, diffusion alone prevails.

### 5.1.3 Numerical Solution

Given a set of parameters describing the state of the system at time  $t_1$ ,

$$T_{\text{so}}^{(1)}, T_v^{(1)}, T_b^{(1)}, \dot{m}_{\text{gas, res}}^{(1)}$$

we employ a system of equations giving the change in this state which occurs during the time from  $t_1$  to  $t_2 = t_1 + \Delta t$ ,

$$\Delta T_{so} = T_{so}^{(2)} - T_{so}^{(1)}$$

$$\Delta T_v = T_v^{(2)} - T_v^{(1)}$$

$$\Delta T_b = T_b^{(2)} - T_b^{(1)}$$

$$\Delta \mathcal{M}_{\text{gas, res}} = \mathcal{M}_{\text{gas, res}}^{(2)} - \mathcal{M}_{\text{gas, res}}^{(1)}$$

The system of equations is then used by marching forward a step in time, finding the new state parameters, and taking another step, etc. The system of equations employed must be compatible with the thermodynamics and thermodynamics in the limit as the time step  $\Delta t$  approaches zero.

#### 5.1.4 Change of Non-Condensable in the Reservoir

If the pipe is gas controlled, that is,  $\mathcal{M}_{\text{gas}} > \mathcal{M}_{\text{gas, res}}$  so that the condenser contains some gas too, we find first the mass flow into or out of the reservoir. The total amount of gas and vapor within the reservoir is

$$\mathcal{M}_{\text{tot}} = \frac{P_{\text{sat}}(T_v) V_{\text{res}}}{R_u T_{\text{res}}} = \frac{P_{\text{sat}}(T_v) V_{\text{res}}}{R_u T_v}$$

when  $T_{\text{res}} = T_v$ . The flow rate is then

$$\dot{\mathcal{M}}_{\text{tot}} = \frac{d\mathcal{M}_{\text{tot}}}{dt} = \frac{V_{\text{res}}}{R_u} \left\{ \frac{1}{T_v} \frac{dP_v}{dT_v} - \frac{P_v}{T_v^2} \right\} \frac{dT_v}{dt}$$

For a vapor pressure law of the form

$$P_v = \exp \left\{ - \left[ A + \frac{B}{T_v} + \frac{C}{T_v^2} \right] \right\} \quad (5-18)$$

we find

$$\frac{dP_v}{dT_v} = \exp \left\{ - \left[ A + \frac{B}{T_v} + \frac{C}{T_v^2} \right] \right\} \left[ + \frac{B}{T_v^2} + \frac{2C}{T_v^3} \right]$$

$$\frac{dP_v}{dT_v} = \frac{P_v}{T_v^2} \left[ B + \frac{2C}{T_v} \right]$$

Substituting, we obtain

$$\dot{m}_{\text{tot}} = B_v (T_v) \frac{dT_v}{dt} \quad (5-19)$$

where

$$B_v (T_v) = \frac{P_{\text{sat}} (T_v) V_{\text{res}}}{R_u T_v^2} \left\{ \frac{B}{T_v} + \frac{2C}{T_v^2} - 1 \right\} \quad (5-20)$$

Depending upon whether  $\dot{m}_{\text{tot}}$  is positive or negative, we use Eq. (5-15) or (5-16) to find  $\dot{m}_{\text{gas, res}}$ . If  $\dot{m}_{\text{tot}}$  is positive and  $\dot{m}_{\text{gas, res}} < \dot{m}_{\text{gas}}$ , then we can write

$$\dot{m}_{\text{gas, res}}^{(2)} - \dot{m}_{\text{gas, res}}^{(1)} = + B_v (T_v) F_{\text{pos}} \frac{dT_v}{dt} \Delta t \quad (5-21)$$

where

$$F_{\text{pos}} = X_{\text{end}} + (X_{\text{end}} - X_{\text{res}}) \frac{e^{-L^*} \text{diff}}{1 - e^{-L^*} \text{diff}} \quad (5-22)$$

If  $\dot{m}_{\text{tot}}$  is negative and  $\dot{m}_{\text{gas, res}} \leq \dot{m}_{\text{gas}}$ , then we write

$$\dot{m}_{\text{gas, res}}^{(2)} - \dot{m}_{\text{gas, res}}^{(1)} = - B_v (T_v) F_{\text{neg}} \frac{dT_v}{dt} \Delta t \quad (5-23)$$

where

$$F_{\text{neg}} = X_{\text{res}} + (X_{\text{res}} - X_{\text{end}}) \frac{e^{-L^* \text{diff}}}{1 - e^{-L^* \text{diff}}} \quad (5-24)$$

If  $\mathcal{M}_{\text{gas, res}} > \mathcal{M}_{\text{gas}}$ , a situation physically impossible, then we correct  $\mathcal{M}_{\text{gas, res}}$  to  $\mathcal{M}_{\text{gas}}$

$$\mathcal{M}_{\text{gas, res}}^{(2)} - \mathcal{M}_{\text{gas, res}}^{(1)} = \mathcal{M}_{\text{gas}} - \mathcal{M}_{\text{gas, res}}^{(1)} \quad (5-25)$$

### 5.1.5 Vapor and Source Temperature Changes

Two operating conditions must be distinguished, the gas controlled condition,  $\mathcal{M}_{\text{gas, res}} < \mathcal{M}_{\text{gas}}$ , and the overdriven condition

$\mathcal{M}_{\text{gas, res}} \geq \mathcal{M}_{\text{gas}}$ . In the overdriven condition,  $L_b = 0$ , and Eqs. (5-12) and (5-13) and (5-1) through (5-4) give

$$UA (T_{\text{so}} - T_v) = C_{\text{pipe}} \frac{dT_v}{dt} + \eta_f P_f L_c \left[ \epsilon (\sigma T_w^4 - \sigma T_s^4) + h_f (T_w - T_s) \right] \quad (5-26)$$

where

$$C_{\text{pipe}} = (MC_p)_{\text{ev}} + (MC_p)_{\text{ad}} + (MC_p)_c$$

Here the resistance of the wick in causing the condenser to operate below  $T_v$  has been neglected in accounting for  $dQ_c/dt = \dot{Q}_c$ . But, the resistance of the wick may have a significant effect on the heat loss term, so  $T_w$  was written in that term instead of  $T_v$ . Let the wick resistance be defined

$$R = \frac{\ln \frac{D_i}{D_i - 2\delta_{\text{wick}}}}{2\pi L_c K_{\text{wick}}} \quad (5-27)$$

and, linearizing the radiation so that the combined effect of radiation and convection can be treated, let

$$S = \eta PL_c (4\epsilon\sigma T_v^3 + h_f) \quad (5-28)$$

denote a surface thermal conductance and

$$T_c = \frac{\epsilon\sigma T_s^4 + h_f T_s + 3\epsilon\sigma T_v^4}{4\epsilon\sigma T_v^3 + h_f} \quad (5-29)$$

an effective cooling temperature.

Then the equations for  $dT_v/dt$  and  $dT_{so}/dt$  are

$$UA (T_{so} - T_v) = C_{pipe} \frac{dT_v}{dt} + \frac{S}{1+RS} (T_v - T_c) \quad (5-30)$$

$$\dot{Q}_{so} = C_{so} \frac{dT_{so}}{dt} + UA (T_{so} - T_v) \quad (5-31)$$

When these are solved simultaneously for constant  $\dot{Q}_{so}$  and  $T_c$  subject to initial conditions  $T_v = T_v^{(1)}$  and  $T_{so} = T_{so}^{(1)}$  when  $\Delta t = 0$ , the result for  $T_v^{(2)} - T_v^{(1)}$  is

$$T_v^{(2)} - T_v^{(1)} = C_1 (1 - e^{-m_1 \Delta t}) + C_2 (1 - e^{-m_2 \Delta t}) \quad (5-32)$$

where

$$m_1 = \left[ \frac{1 + \sqrt{1-\gamma}}{2} \right] \left[ \frac{\tau_{tot}}{\tau_{pipe} \tau_{so}} \right] \quad (5-33)$$

$$m_2 = \left[ \frac{1 - \sqrt{1-\gamma}}{2} \right] \left[ \frac{\tau_{tot}}{\tau_{pipe} \tau_{so}} \right] \quad (5-34)$$

and

$$\tau_{\text{tot}} = \tau_{\text{so}} + (C_{\text{pipe}} + C_{\text{so}}) / S_{\text{fp}} \quad (5-35)$$

$$\gamma = \frac{4\tau_{\text{pipe}} \tau_{\text{so}}}{\tau_{\text{tot}}^2} \quad (5-36)$$

$$\tau_{\text{so}} = C_{\text{so}} / UA \quad (5-37)$$

$$\tau_{\text{pipe}} = C_{\text{pipe}} / S_{\text{fp}} \quad (5-38)$$

$$S_{\text{fp}} = S / (1 + RS) \quad (5-39)$$

$$C_1 = (Q_{\text{so}} / S_{\text{fp}}) - (T_v - T_c) - C_2 \quad (5-40)$$

$$C_2 = (\phi_1 + \phi_2 - \phi_3) / (m_1 - m_2) \quad (5-41)$$

$$\phi_1 = Q_{\text{so}} m_1 / S_{\text{fp}} \quad (5-42)$$

$$\phi_2 = (T_v - T_c) \left[ \frac{C_{\text{so}}}{C_{\text{pipe}} \tau_{\text{so}}} + \frac{1}{\tau_{\text{pipe}}} - m_1 \right] \quad (5-43)$$

$$\phi_3 = (T_{\text{so}} - T_c) \left[ \frac{C_{\text{so}}}{C_{\text{pipe}} \tau_{\text{so}}} \right] \quad (5-44)$$

The symbol  $\tau$  is used to denote a time constant (hr or sec) and  $C$  a thermal capacity (Btu/°R or joule/°K).

For the source temperature

$$T_{so}^{(2)} - T_{so}^{(1)} = (1 + R_{srp} - R_1) C_1 (1 - e^{-m_1 \Delta t}) + (1 + R_{srp} - R_2) C_2 (1 - e^{-m_2 \Delta t}) \quad (5-45)$$

where the ratios are

$$R_{srp} = S_{fp}/UA \quad (5-46)$$

$$R_1 = C_{pipe} m_1/UA \quad (5-47)$$

$$R_2 = C_{pipe} m_2/UA \quad (5-48)$$

In the gas controlled condition,  $\dot{m}_{gas, res} < \dot{m}_{gas}$ , the effect of a blocked portion of pipe on the heat losses and heat contents must be accounted for. In this case Eq. (5-11) and (5-12) give

$$UA (T_{so} - T_v) = \frac{dQ_{pipe}}{dt} + \eta_f P_f L_c \left[ 1 - \frac{L_b}{L_c} (1 - \eta_b) \right] \cdot \left[ \epsilon (\sigma T_w^4 - \sigma T_s^4) + h_p (T_w - T_s) \right], \quad (5-49)$$

and Eqs. (5-2) through (5-4) together with Eq. (5-13) give

$$\frac{dQ_{pipe}}{dt} = C_{pipe} \frac{dT_v}{dt} - C_c \frac{d}{dt} \left[ \frac{L_b}{L_c} (1 - \eta_b) (T_v - T_b) \right] \quad (5-50)$$

As before, we introduce R, S, and  $T_c$ , Eqs. (5-27) - (5-29)

$$UA (T_{so} - T_v) = C_{pipe} \frac{dT_v}{dt} - C_c \frac{d}{dt} \left[ \frac{L_b}{L_c} (1 - \eta_b) (T_v - T_b) \right] + \frac{S}{1+RS} \left[ 1 - \frac{L_b}{L_c} (1 - \eta_b) \right] (T_v - T_c) \quad (5-51)$$

Differentiating Eq. (5-6) gives

$$\frac{d\dot{m}_{\text{gas, res}}}{dt} = -A_v L_c \frac{d}{dt} \left[ \frac{L_b}{L_c} (1-\eta_b) \frac{P_{\text{sat}}(T_v) - P_{\text{sat}}(T_b)}{R_u T_b} \right] \quad (5-52)$$

Consistent with our assumption of similar temperature and mass concentration profiles which allowed us to employ the same  $\eta_b$  in Eq. (5-6) as was used in Eq. (5-4), we approximate Eq. (5-52)

$$\frac{d\dot{m}_{\text{gas, res}}}{dt} \doteq - \left( \frac{A_v L_c}{R_u T_b} \right) \left( \frac{P_{\text{sat}}(T_v) - P_{\text{sat}}(T_b)}{T_v - T_b} \right) \frac{d}{dt} \left[ \frac{L_b}{L_c} (1-\eta_b) (T_v - T_b) \right]$$

$$\frac{d}{dt} \left[ \frac{L_b}{L_c} (1-\eta_b) (T_v - T_b) \right] \doteq - \frac{\dot{m}_{\text{gas, res}}}{\dot{m}_{\text{fp}}} (T_v - T_b) \quad (5-53)$$

where

$$\dot{m}_{\text{fp}} = A_v L_c \frac{P_{\text{sat}}(T_v) - P_{\text{sat}}(T_b)}{R_u T_b} \quad (5-54)$$

Eq. (5-51) then becomes

$$UA (T_{\text{so}} - T_v) = C_{\text{pipe}} \frac{dT_v}{dt} + C_c (T_v - T_b) \frac{\dot{m}_{\text{gas, res}}}{\dot{m}_{\text{fp}}} + \frac{S}{1+RS} \left[ 1 - \frac{L_b}{L_c} (1-\eta_b) \right] (T_v - T_b) \quad (5-55)$$

Introducing Eqs. (5-15), (5-16), (5-19), (5-22), and (5-24) we obtain

$$UA (T_{\text{so}} - T_v) = C_{\text{pipe}} \frac{dT_v}{dt} + C_c (T_v - T_b) \frac{B_v}{\dot{m}_{\text{fp}}} F \frac{dT_v}{dt} + \frac{S}{1+RS} \left[ 1 - \frac{L_b}{L_c} (1-\eta_b) \right] (T_v - T_b) \quad (5-56)$$

For purposes of numerical calculation the term  $C_c (T_v - T_b) B_v F / \mathcal{M}_{fp}$  may be regarded as constant. In that case we regard Eq. (5-56) as identical in form with Eq. (5-30) with blocked pipe quantities

$$C_{bp} = C_{pipe} + C_c \frac{(T_v - T_b) B_v F}{\mathcal{M}_{fp}} \quad (5-57)$$

$$S_{bp} = \frac{S}{1+RS} \left[ 1 - \frac{L_b}{L_c} (1 - \eta_b) \right] \quad (5-58)$$

replacing full pipe values of  $C_{pipe}$  and  $S_{fp}$  respectively. Thus Eqs. (5-32) through (5-48) can be taken over.

#### 5.1.6 Blocked Condenser Temperature Change

If the sink temperature varies, the temperature of the blocked portion of the pipe follows it subject to the time lag caused by its thermal capacity. Neglecting axial conduction in the blocked portion of the condenser, we can write that the rate of cooling of the blocked pipe is

$$- \frac{C_c}{L_c} \frac{dT_b}{dt} = \eta_f P_f \left[ \epsilon (\sigma T_b^4 - \sigma T_s^4) + h_f (T_b - T_s) \right] \quad (5-59)$$

An expression which reduces to Eq. (5-59) in the limit as  $\Delta t$  goes to zero is

$$T_b(2) - T_b(1) = (T_s - T_b) (1 - e^{-\Delta t / \tau_b}) \quad (5-60)$$

where the blocked pipe time constant is

$$\tau_b = C_c \left\{ \eta_f P_f L_c \left[ h_f t (T_b + T_s) (T_b^2 + T_s^2) \epsilon \sigma \right] \right\}^{-1} \quad (5-61)$$

### 5.1.7 Flow Chart

Figure 5-1 shows a flow chart for the main program. The main program calls subroutine INPT which reads in the input data. Then the source, vapor, and condenser temperatures are initialized as is the time and amount of gas in the reservoir. (The initial values of the temperatures are input data, and the reservoir is assumed to be at saturation conditions corresponding to the total pressure and condenser temperature). MAIN then calls DUTY to find the input operating conditions at the time of concern. It then calls DELTA repeatedly. Incremental values are added to the time, temperatures, and amount of gas in the reservoir.

The heart of the program is subroutine DELTA which is shown charted in Figures 5-2 and 5-3. For simplicity in programming this first diffusion-transient heat pipe program, axial conduction was assumed to have a small effect on the condenser heat loss and gas inventory. Accordingly,  $\eta_b$  was taken to be zero. However, Eq. (5-9) which includes the effect of axial conduction on the reservoir conditions, was retained.

### 5.1.8 Start-up

The preceding expressions apply after a gas front has been established, that is, after the evaporator has been swept clear of gas. If the pipe at time zero is in a gas-blocked condition so that the total pressure is greater than the vapor pressure in the evaporator, and some of the gas inventory is present in the evaporator, then it is necessary to make use of a special subroutine, START.

During the start-up period the evaporator and adiabatic section are assumed to be uniform in composition and temperature, and the heat loss from the evaporator is neglected until the evaporator and adiabatic section are swept clear of gas. Consistent with this neglect of vapor transport, the condenser is assumed to receive no heat input from the evaporator during the start-up period. This neglect leads to over-estimating the rate of evaporator temperature rise and the rate at

FIGURE 5-1  
FLOW CHART FOR MAIN PROGRAM

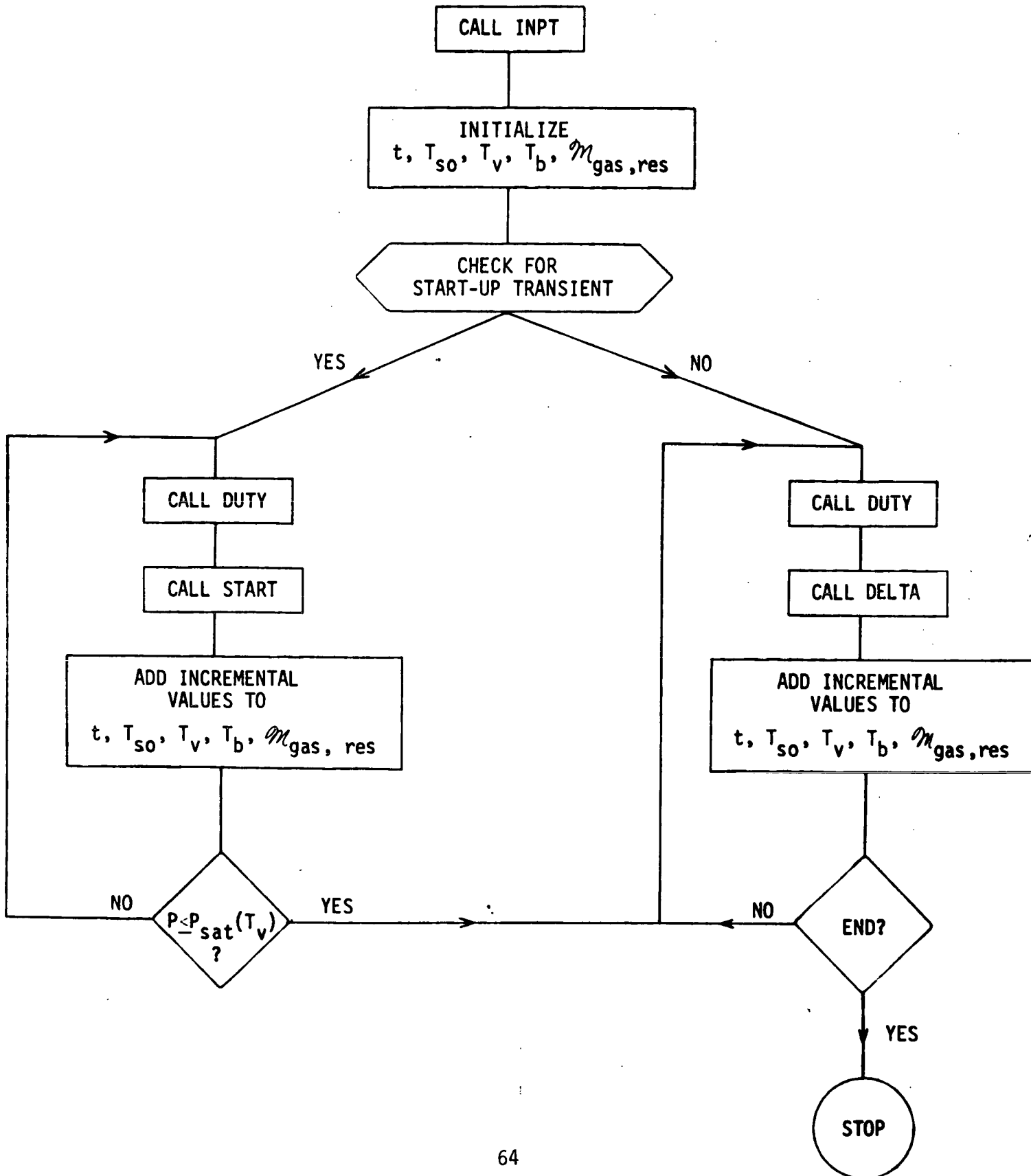


FIGURE 5-2  
FLOW CHART FOR SUBROUTINE DELTA

a)  $m_{\text{gas, res}} < m_{\text{gas}}$

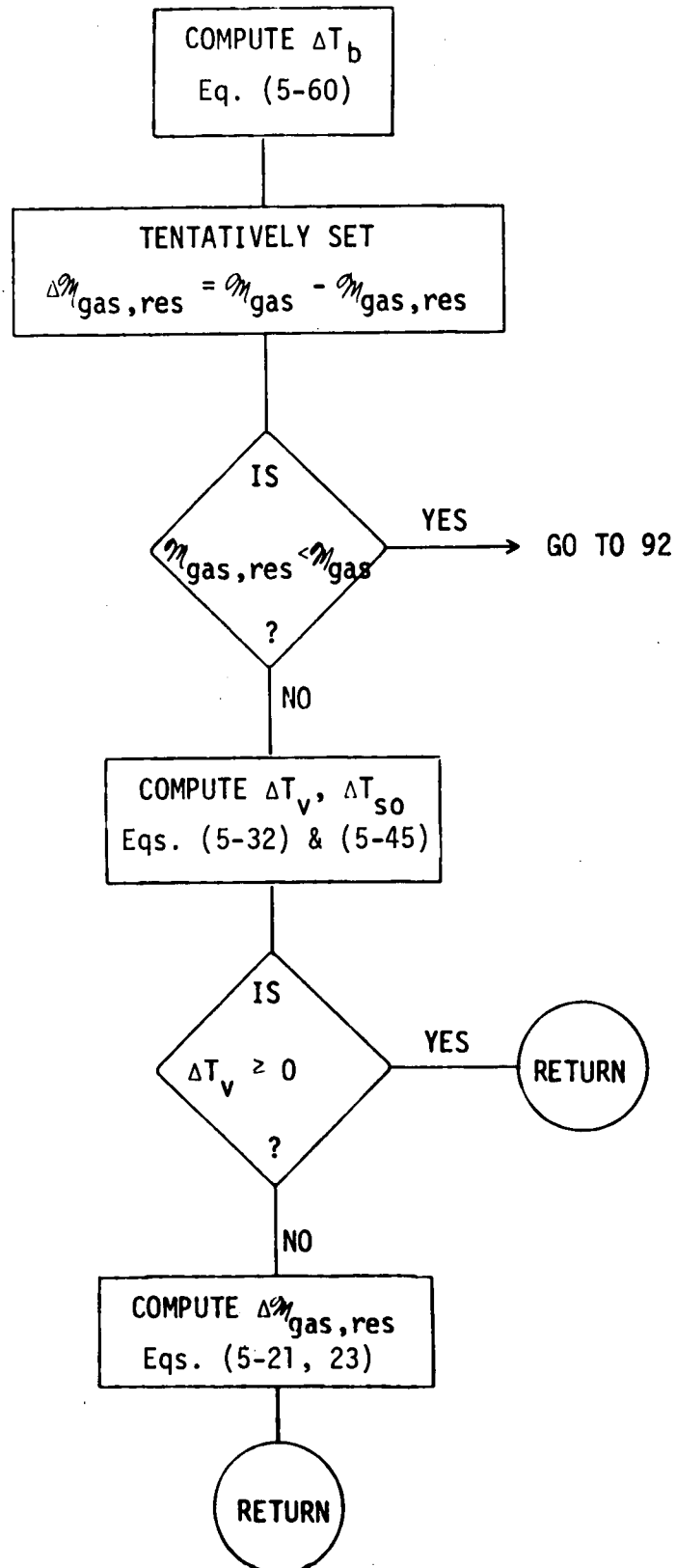
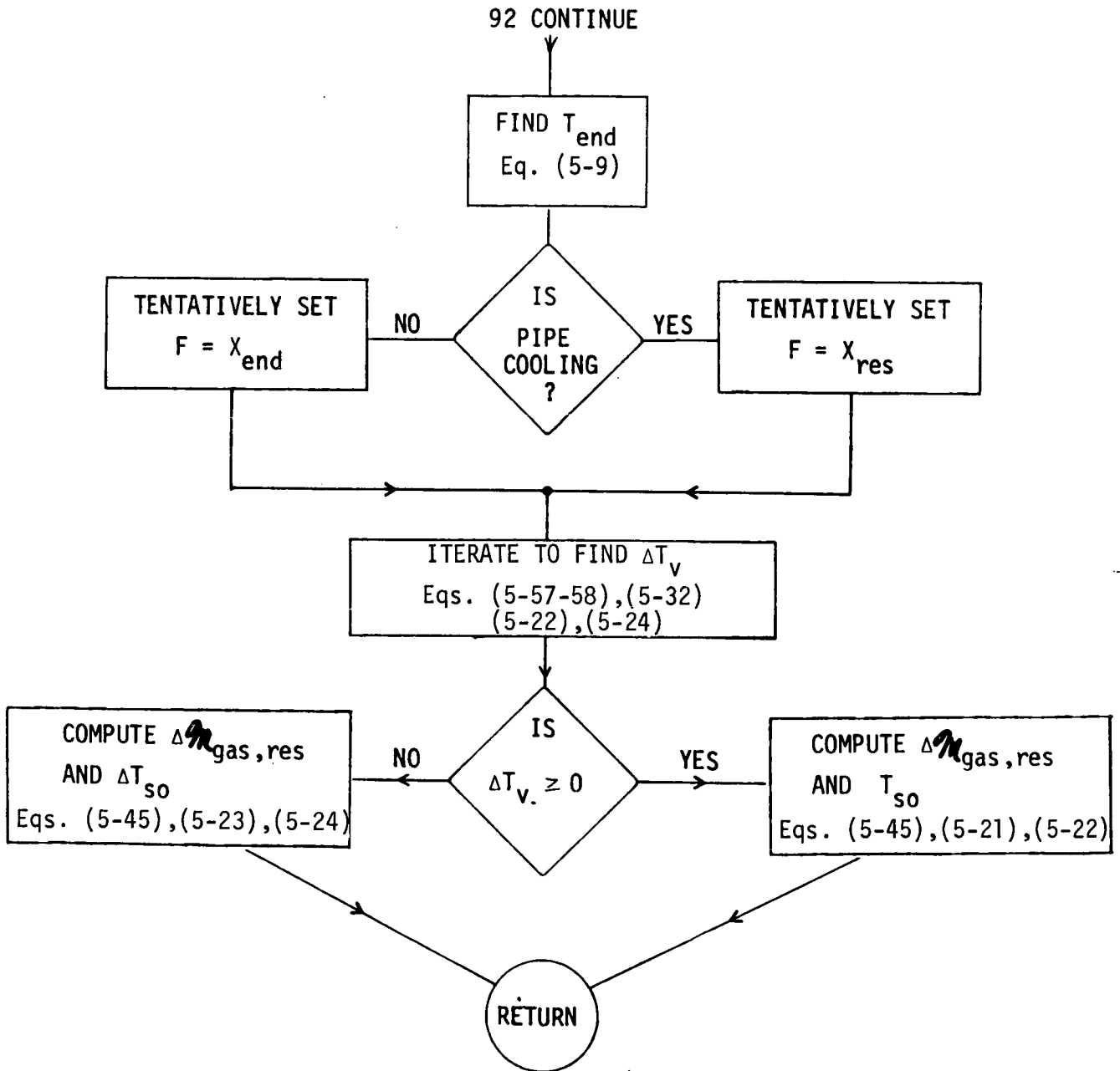


FIGURE 5-3  
FLOW CHART FOR SUBROUTINE DELTA

b)  $\dot{m}_{gas, res} \geq \dot{m}_{gas}$



which the condenser temperature falls. The governing equations for  $T_b$ ,  $T_v$ , and  $T_{so}$  are then Eqs. (5-59), (5-30), and (5-31) with  $S$  set equal to zero. The result for  $T_b$  is the same as before, Eq. (5-60). Eqs. (5-30) and (5-31) yield

$$T_{so}^{(2)} - T_{so}^{(1)} = \frac{Q_{so} \Delta t}{(C_{so} + C_{ev})} - C_1 (1 - e^{-m \Delta t}) \quad (5-62)$$

$$T_v^{(2)} - T_v^{(1)} = \frac{Q_{so} \Delta t}{(C_{so} + C_{ev})} + C_1 (1 - e^{-m \Delta t}) \frac{C_{so}}{C_{ev}} \quad (5-63)$$

where

$$\tau = \tau_{so} \frac{C_{ev}}{(C_{so} + C_{ev})} \quad (5-64)$$

$$C_1 = \frac{C_{ev}}{(C_{so} + C_{ev})} \left[ (T_{so} - T_v) - \frac{C_{ev}}{(C_{so} + C_{ev})} \frac{Q_{so}}{UA} \right] \quad (5-65)$$

$$m = \frac{C_{ev} + C_{so}}{C_{ev} \tau_{so}} \quad (5-66)$$

The capacity  $C_{ev}$  is that of the evaporator and adiabatic section. During this start-up transient the total pressure is controlled by the requirement that

$$\dot{m}_{gas} = \frac{(P_{tot} - P_{sat}(T_v)) V_{ev}}{R T_v} + \frac{(P_{tot} - P_{sat}(T_b)) V_c}{R T_b} + \dot{m}_{gas, res} \quad (5-67)$$

where  $V_{ev}$  is the volume of both the evaporator and adiabatic section. The time derivative is

$$0 = \frac{V_{ev}}{R} \left[ \frac{d}{dt} \left( \frac{P_{tot}}{T_v} \right) - \frac{d}{dt} \left( \frac{P_{sat}(T_v)}{T_v} \right) \right] + \frac{V_c}{R} \left[ \frac{d}{dt} \left( \frac{P_{tot}}{T_b} \right) - \frac{d}{dt} \left( \frac{P_{sat}(T_b)}{T_b} \right) \right] + \dot{m}_{gas, res} \quad (5-68)$$

The start-up transient is probably sufficiently fast so that diffusion could be neglected. Nevertheless, Eqs. (5-21)-(5-24) are used to calculate  $\dot{m}_{\text{gas, res}}$ . In order to do so it is necessary to find

$$\dot{m}_{\text{tot}} = \frac{d}{dt} \left( \frac{P_{\text{tot}} V_{\text{res}}}{R T_v} \right) \quad (5-69)$$

Eqs. (5-68) and (5-69) together with Eqs. (5-21)-(5-24) serve to establish  $dP_{\text{tot}}/dt$

$$\frac{dP_{\text{tot}}}{dt} = \frac{1}{\phi_p} \left[ \phi_v \frac{dT_v}{dt} + \phi_b \frac{dT_b}{dt} \right] \quad (5-70)$$

$$\phi_v = \frac{P_{\text{tot}} V_{\text{tot}}}{R T_v^2} + \frac{V_{\text{ev}}}{V_{\text{res}}} B_v \quad (5-71)$$

$$\phi_b = \frac{P_{\text{tot}} V_c}{R T_b^2} + \frac{P_{\text{sat}}(T_b) V_c}{R_u T_b^2} \left[ \frac{B}{T_b} + \frac{2C}{T_b^2} - 1 \right] \quad (5-72)$$

$$\phi_p = \frac{V_{\text{tot}}}{R T_v} + \frac{V_c}{R T_b} \quad (5-73)$$

$$V_{\text{tot}} = V_{\text{ev}} + F V_{\text{res}} \quad (5-74)$$

where F is given by Eq. (5-22) or (5-24).

When  $P_{\text{tot}}$  falls to  $P_{\text{sat}}(T_v)$  (or  $P_{\text{sat}}(T_v)$  rises to  $P_{\text{tot}}$ ) the program exits from subroutine START and operates in the normal fashion described by Eqs. (5-1) to (5-61).

## 5.2 Discussion

A test case was run for methanol in a 0.4375 inch O.D. pipe. It was found that a time increment smaller than 0.1 minutes was necessary

for numerical stability. Since the program was operational, and the program schedule was tight, no revisions were made. However, in retrospect the approach taken was somewhat inefficient for the reason that a small change in  $T_v$  produces a large change in  $L_b$  when the pipe is gas controlled, and this large change in  $L_b$  drastically changes  $dT_v/dt$ . A more efficient approach might be to expand the quantity

$$\left[ 1 - \frac{L_b}{L_c} (1 - \eta_b) \right]$$

appearing in Eq. (5-58) about  $T_v = T_{v0}$  and to treat the first order term

$$\left( \frac{\partial}{\partial T_v} \left[ 1 - \frac{L_b}{L_c} (1 - \eta_b) \right] \right)_{T_v = T_{v0}} (T_v - T_{v0})$$

as the quantity which varies with  $T_v$  during time interval  $\Delta t$ , while the term  $(T_v - T_c)$  is regarded as constant at the value  $T_{v0} - T_c$  during the interval. In this way new forms of Eqs. (5-32) and (5-45) can be derived and their stability considerably improved.

## 6.0 TRANSIENT BEHAVIOR OF HOT RESERVOIR HEAT PIPES: EXPERIMENTS

A developmental hot reservoir variable conductance heat pipe was fabricated for the purpose of testing the TRW Transient Gaspipe Program (TRANPIPE) and to examine an hypothesized design approach to achieve rapid recovery from liquid in the reservoir. A number of experiments were performed to measure transient performance as a function of reservoir feedtube geometry, evaporator thermal mass, condenser to sink thermal coupling and working fluid gas pairs. These measurements were compared with the analytical predictions for verification of the model.

In addition, the test unit was utilized to study the characteristics of hot reservoir heat pipes and make improvements, if possible. For this reason the test profile was quite severe; e.g., sudden high power start-up, severely overdriving, introduction of liquid into the gas reservoir, etc. It should be clear, then, that the results presented in this study are not intended to show the virtues of this type heat pipe but, to the contrary, are intended to explore the troublesome areas.

### 6.1 Test Apparatus

The test apparatus consists of the experimental hot reservoir heat pipe and the associated instrumentation, coolant supply, etc.

#### 6.1.1 Heat Pipe

An assembly drawing of the experimental heat pipe is shown in Figure 6-1. The heat pipe has a single zone condenser with very low radial wick resistance. The wick structure consists of circumferential grooves cut in the stainless steel tube and an axial homogeneous metal

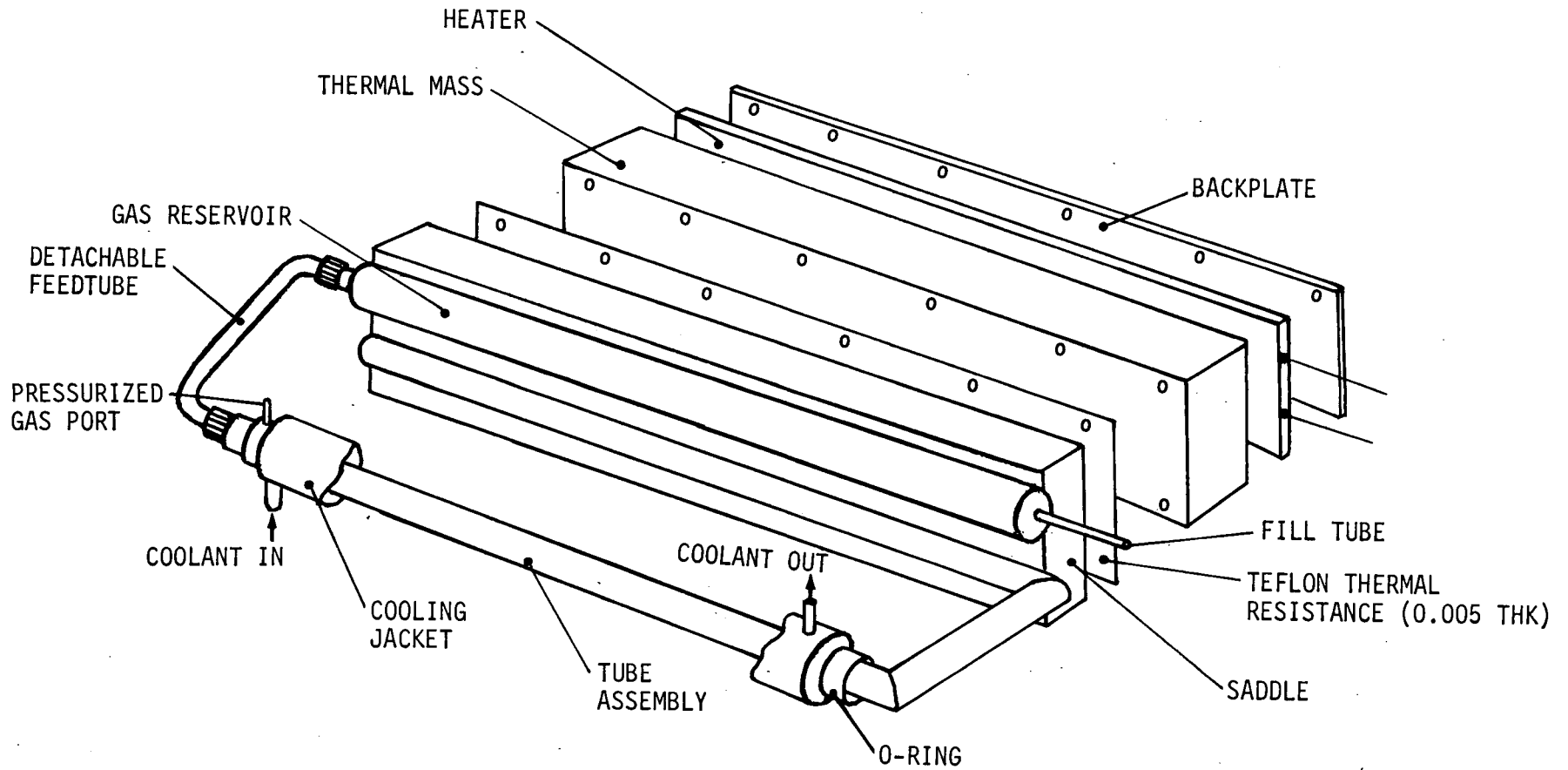


FIGURE 6-1. Schematic Drawing of Experimental Apparatus For Hot Reservoir Heat Pipe Transient Studies

felt wick diametrically located.

The approach taken was to construct a flexible laboratory type hot reservoir heat pipe, which could be easily modified in order to test various configurations. Provision was made for attaching metal blocks to simulate the thermal mass associated with most cooling applications. Swagelok\* fittings were utilized to allow testing with different feed-tubes. A thermal resistance could be imposed by the insertion of thin sheets of teflon between the heat source and the saddle. The external condenser resistance was obtained by providing a thin gas filled annular gap of 0.083 inches between the condenser wall and cooling jacket. Heat transfer across this gap is primarily by conduction and radiation. (Convection effects have been found to be quite small in such a thin gap.) This external resistance was varied by using different types of gas in the gap. Helium, for example, has a thermal conductivity on the order of six times greater than air.

The sizing of the various elements was accomplished with the aid of the transient computer program itself. Using methanol as the working fluid, nitrogen as the control gas and a 3/8 inch diameter feedtube between the gas reservoir and condenser, the program predicted a diffusion-influenced transient recovery time on the order of three to four hours. Substitution of a 1/4 inch diameter feedtube would exhibit recovery times approximately twice as long as those with the 3/8 inch tube. Similarly, substitution of helium as the control gas in place of nitrogen would yield substantially more rapid diffusion transients. (The diffusion coefficient for helium/methanol is on the order of four times greater than nitrogen/methanol.) In addition, it was found in the preliminary analysis that the temperature transients were relatively insensitive to the thermal mass once a reasonable amount was applied. For this reason, tests would be run without an external thermal mass, and then repeated with a substantial mass attached to the evaporator. Details of the apparatus are indicated on the working drawings shown in Appendix A.

---

\*Trademark, Crawford Fitting Company

The gas reservoir is mounted in a special aluminum saddle outside of and parallel to the evaporator. As shown in cross section in Figure A-4, the saddle is constructed such that the reservoir is mounted very close to the heat input surface, but there is a substantial thickness of aluminum between the evaporator and the heat input zone. It was hypothesized that this approach would allow the reservoir to operate at a temperature equal to or slightly above the evaporator; in this mode the heat pipe could reverse itself with the gas reservoir acting as the evaporator leading to rapid recovery from liquid in the reservoir. In addition, a single layer of fine mesh screen was installed inside the reservoir to assure uniform liquid distribution over the hottest parts of the internal surface until depletion of the liquid. This wick was not continuous with the heat pipe wick; i.e., there was no wick in the feedtube.

Some thought was given to the feedtube entrance design. At first a simple baffle or splash guard was considered, but this would trap liquid and block the feedtube in a low gravity environment. Therefore, for purposes of this experiment the feedtube was simply capped off, and forty 0.033 in. diameter holes were drilled within the last 1/4 inch length (Figure A-1). These holes are large enough to prevent a significant capillary head due to liquid "bridging." A more elaborate approach was considered beyond the scope of this program, but it is felt that further consideration should be given to the problem.

The fill tube was mounted at the end of the reservoir in order to insert known quantities of liquid in the reservoir and observe the subsequent recovery. The heat pipe and reservoir were soldered in the saddle by first copper striking and nickel plating the mating surfaces. A coat of black paint (CAT-A-LAC Flat Black 463-3-8) was applied to the outside condenser surface and the inside surface of the cooling jacket to provide a known emissivity ( $\sim 0.86$ ) across the annular gas gap.

Two noteworthy problems were encountered during fabrication of the test assembly. First, because of the differential expansion of aluminum and stainless steel the saddle warped slightly on cooling during soldering. This could possibly be improved on future units by better clamping. Second, it was extremely difficult to bend the feedtubes within the

specified tolerances. Thus, there is some misalignment in the completed assembly. These discrepancies have relatively little influence, of course, on the thermal performance.

A photograph of the completed test unit is shown in Figure 6-2.

### 6.1.2 Test Setup

A schematic diagram of the test setup is shown in Figure 6-4. Figure 6-3 is a photograph showing the experimental heat pipe in the test installation.

Heat input was provided by an Electrofilm 5 watt/in<sup>2</sup> strip heater (Part #112000-212) bonded to the saddle with RTV. This heater was 2 in. wide by 12 in. long by 0.045 in. thick; it should not exceed 450°F in temperature. After completion of Run 1 (see procedure) the heater was removed from the saddle and attached to the thermal mass.

Two Haake\* constant temperature circulators were used with appropriate valves, Figure 6-4, to provide step changes in sink temperature. The heat sink was either liquid nitrogen or a pumped refrigeration loop. The liquid nitrogen was simply vented to ambient through the cooling coils of the constant temperature controllers. Pressurized helium or nitrogen was connected to the annular condenser gas gap port. A very small over-pressure was maintained during the testing. The slight bleed flow associated with leakage around the thermocouple wires, "O-rings", etc., was shown to have a negligible effect on the overall heat transfer.

A total of twelve copper-constantan thermocouples were attached to the heat pipe, saddle and thermal mass for continuous readout on a 12-point temperature recorder. The thermocouple locations are indicated in Figure 6-5. Additional thermocouples (3A and 13A) were attached to the adiabatic section and the cooling jacket for checkout with a potentiometer.

The test apparatus was well insulated throughout the testing. Rubber, refrigeration type insulation was used on the condenser cooling jacket and coolant lines. Ceramic fiber insulation was used on the remainder

---

\*Haake Instruments, Inc.

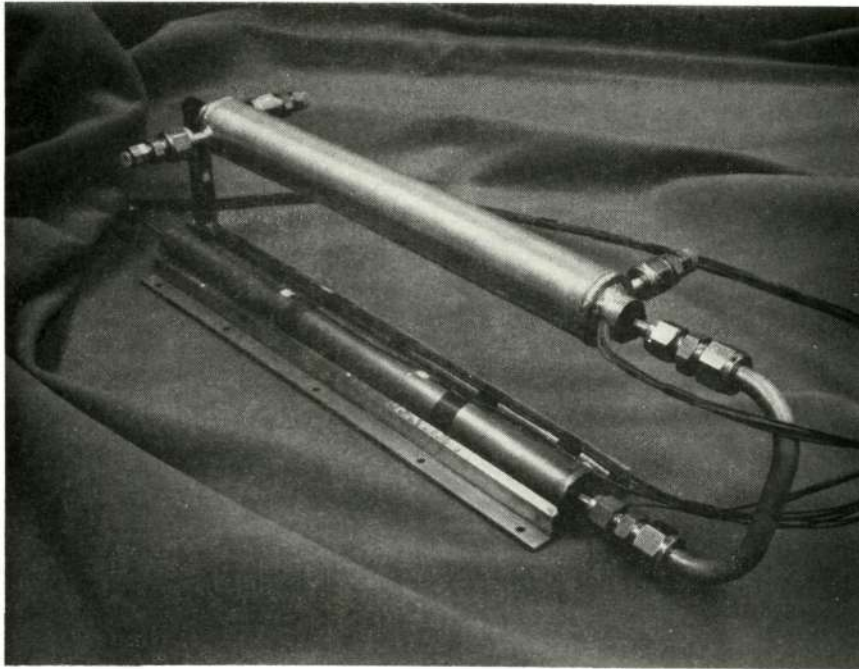


FIGURE 6-2. Experimental Hot Reservoir Heat Pipe

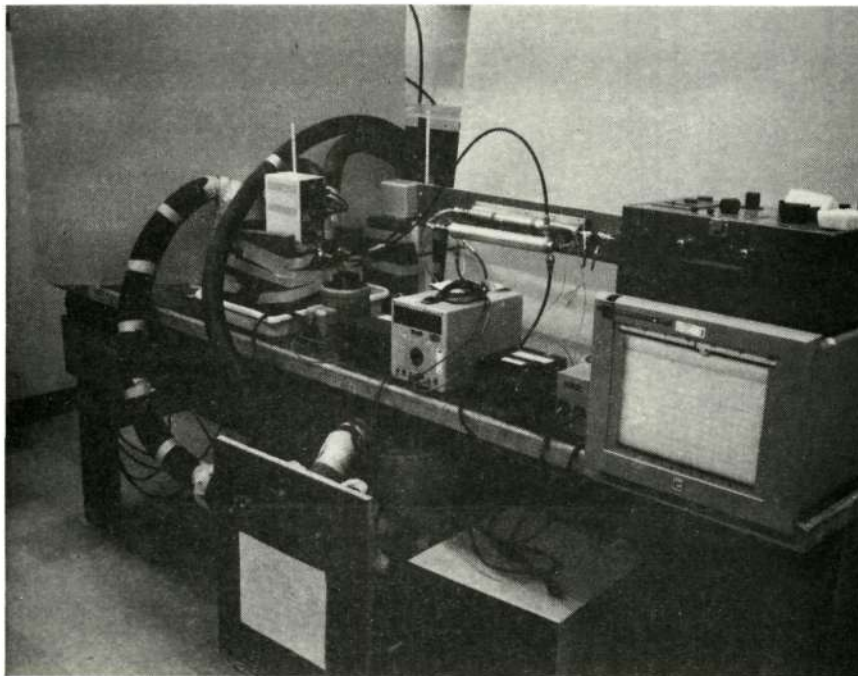


FIGURE 6-3. Test Installation

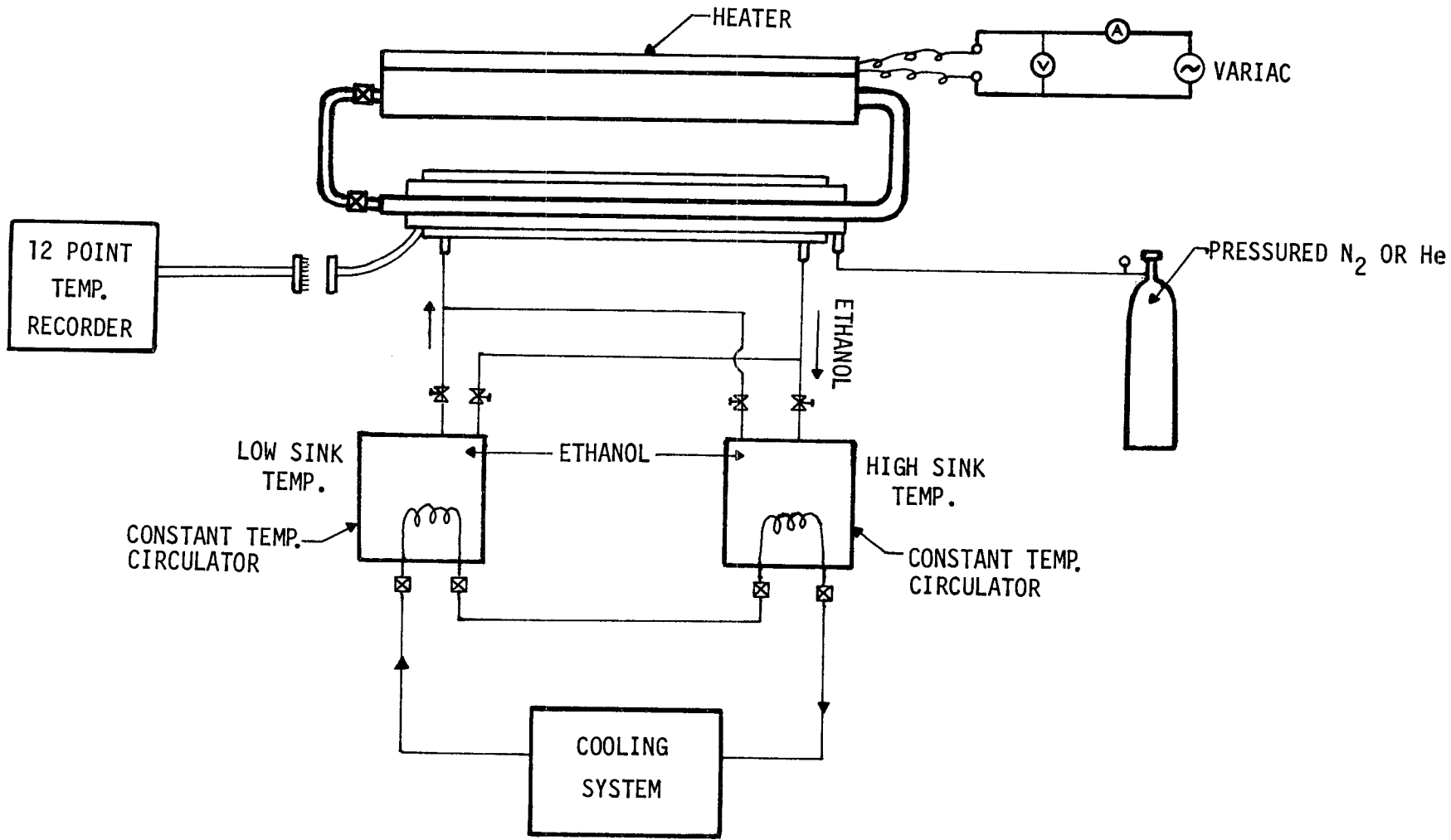
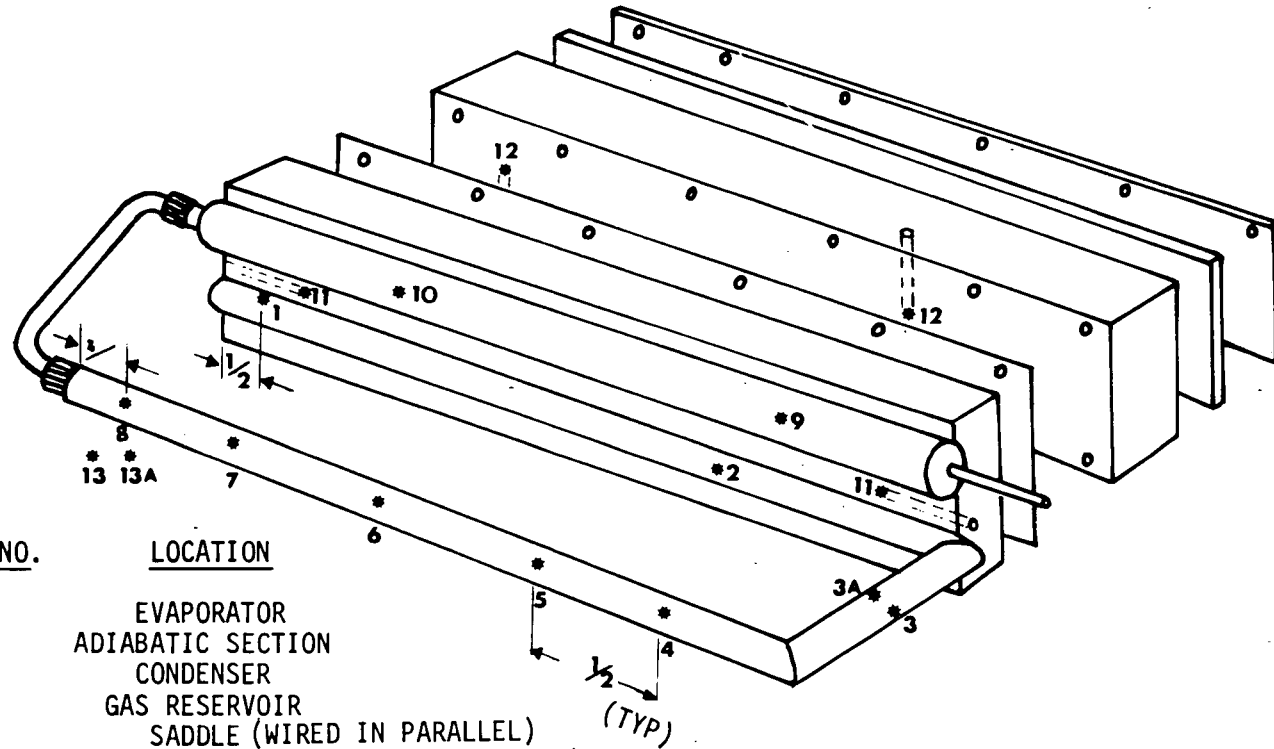


FIGURE 6-4. Schematic Diagram of Test Setup



<u>THERMOCOUPLE NO.</u>	<u>LOCATION</u>
1 & 2	EVAPORATOR
3	ADIABATIC SECTION
4 - 8	CONDENSER
9 & 10	GAS RESERVOIR
11	SADDLE (WIRED IN PARALLEL)
12	THERMAL MASS (WIRED IN PARALLEL)
13	COOLING JACKET

FIGURE 6-5. Thermocouple Locations

of the unit. This is a high temperature type insulation, but also has a relatively low thermal conductivity at room temperature. In addition, the tests were designed to operate near ambient temperature to minimize the losses. An empirical insulation conductance of 0.26 Btu/hr-°F was used in the data reduction. This coefficient was obtained by operating the coolant at the same temperature as the heat source and measuring the corresponding heat input.

## 6.2 Procedure

This section outlines the test plan for the experimental heat pipe. For clarity, the details of the actual testing are not included here, but are given with the test results.

Prior to testing, the heat pipe was filled with nitrogen as the control gas and methanol as the working fluid. The nitrogen was put in first at a pressure of 1.70 to 1.85 psia at room temperature, which corresponds to approximately  $2.2 \times 10^{-6}$  to  $2.4 \times 10^{-6}$  lb-moles. Then the pipe was filled with  $25.0 \pm 0.5$  cc methanol at room temperature. Because the fill tube was located on the gas reservoir, as previously explained, it was necessary to perform an initial startup prior to formal testing in order to purge liquid from the reservoir after each reprocessing. In addition to this, it was necessary to maintain a small amount of heat on the fill tube throughout the testing to prevent condensation in the fill tube. This was accomplished with a heater wire wrapped around the fill tube. The apparatus was tilted slightly to prevent the accumulation of excess liquid at the feedtube entrance.

The test plan was broken into three parts:

- Startup with Liquid in the Gas Reservoir
- Temperature Control Range and Operating Limits
- Transient Performance Runs

An important question to be answered during the initial startup was whether or not the pipe would operate in reverse when liquid was present in the gas reservoir. This would enable the reservoir to purge itself of liquid much more rapidly than by diffusion only. Next, the operating limits were experimentally verified.

The transient performance runs consisted of startup, overdriving and a change in sink temperature within the control range, as indicated in Figure 6-6. (The magnitude of the power levels and sink temperatures were experimentally determined as previously stated). Although an estimated time scale is shown, no subsequent changes in power or temperature settings were made until steady-state conditions were reached.

Several variations of the experimental device were utilized to investigate the transient response characteristics. The sequence of testing is outlined in Table 6-1. Each test run was compared with the transient gas pipe program predictions.

### 6.3 Results

In addition to verification of the analysis, a primary purpose of the program was to study the performance of hot reservoir heat pipes and make improvements, if possible. For this reason, the test unit was subjected to quite severe test conditions; e.g., sudden high power startup, severely overdriving, etc.

One troublesome aspect of hot reservoir heat pipes is the problem of liquid in the gas reservoir. Startup measurements were made for situations wherein known quantities of liquid were purposefully introduced into the reservoir, and the system allowed to equilibrate with and without auxiliary heater power. Although these experiments were actually performed after completion of the formal transient testing, the results are included in the following section on startup.

The calibration results, necessary for the transient test profile, are presented next. Finally the transient test results are given for comparison with analysis.

#### 6.3.1 Startup (Liquid in the Reservoir)

During the initial startup it was observed that the gas reservoir operated at essentially the same temperature as the evaporator. As anticipated, the vapor pressure of liquid present in the gas reservoir displaced the noncondensable gas into the condenser resulting in a significant temperature overshoot. However, it was not clear whether the

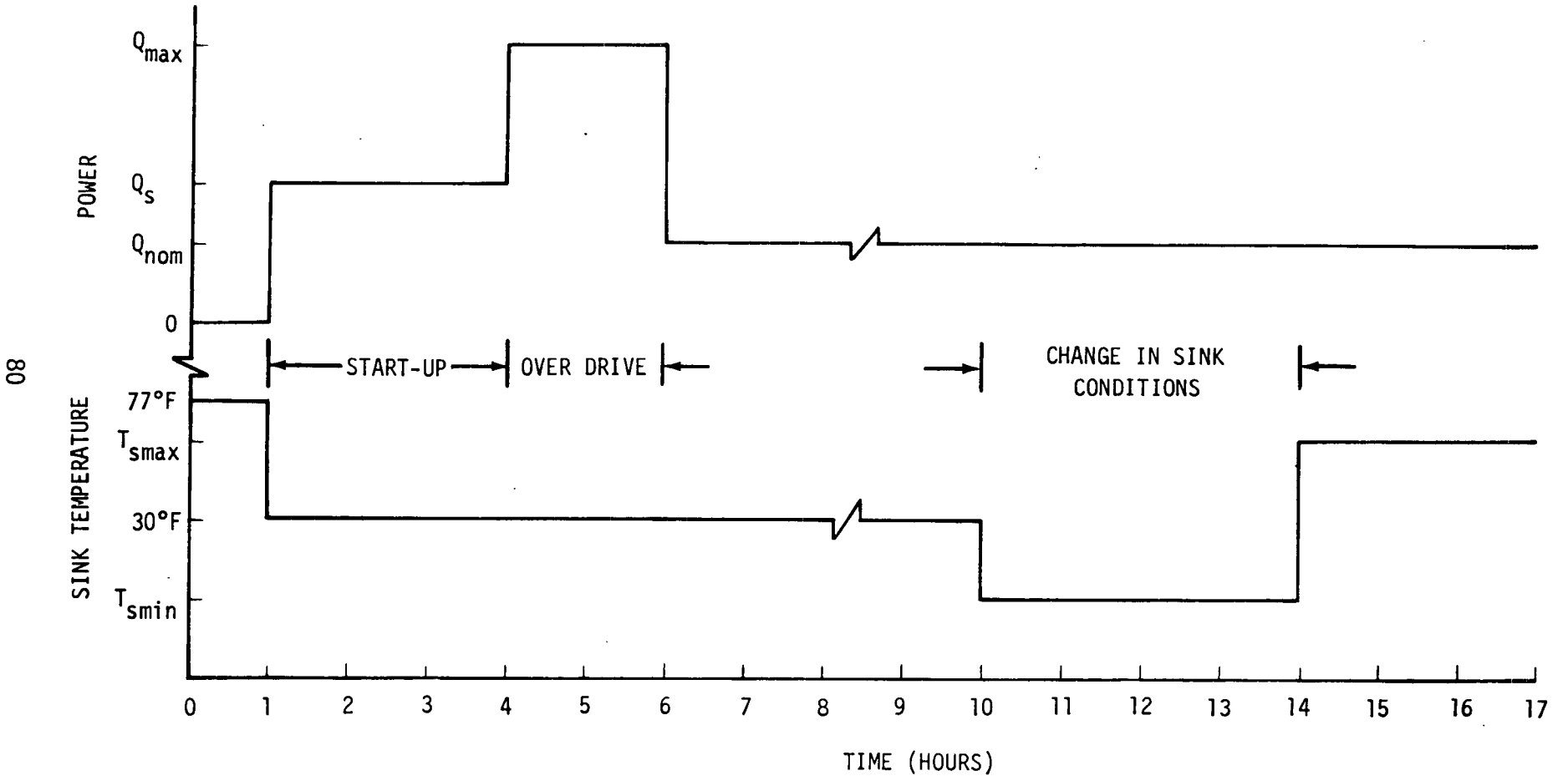


FIGURE 6-6. Input Power and Sink Temperature Test Profile

80

TABLE 6-1

## TEST SCHEDULE - TRANPIPE

<u>RUN NO.</u>	<u>GAS LOAD</u>	<u>CONDENSER COUPLING</u>	<u>THERMAL MASS (LB)*</u>	<u>FEEDTUBE DIA. (IN.)</u>
1	Nitrogen	Helium	None	0.375
2	Nitrogen	Helium	3.3	0.375
3**	Nitrogen	Nitrogen	3.3	0.375
4***	Nitrogen	Helium	3.3	0.375
Reprocess for helium gas load.				
5	Helium	Helium	3.3	0.375
Reprocess for 0.25 in. diameter feedtube.				
6	Nitrogen	Helium	3.3	0.25

---

\* Aluminum block

\*\* Startup and overdrive only

\*\*\* Insert known quantity of liquid in gas reservoir -  
startup only

liquid was removed from the reservoir by reversed heat pipe action or diffusion of the vapor through gas in the feedtube.

Because of these observations, further experiments (in addition to the formal procedure outlined in the previous section) were conducted to study the behavior during startup. These experiments consisted of introducing known quantities of liquid into the reservoir and subjecting the test unit to a step change in power and sink temperature. The test set-up was modified as follows for this purpose:

- 3cc methanol underfill
- graduated burette attached to fill tube (with valves and vacuum line)
- auxiliary heater placed on the gas reservoir

The purpose of the initial underfill was to allow several runs (fluid additions) without reprocessing. This heat pipe is not particularly sensitive to underfill because a simple homogeneous wick is utilized without arteries and because of the high axial conductance of the aluminum saddle.

The auxiliary heater was used only to determine whether the saddle design was valid or not by the application of small amounts of power (< 2 or 3 watts) to make up for insulation losses, etc. That is, even though the reservoir was mounted close to the heat input surface relative to the evaporator as previously discussed, there was some concern that the larger exposed surface of the reservoir might result in greater heat loss, causing it to run cool.

The heat pipe configuration for the startup experiments corresponds to Run 4, Table 6-1. The nitrogen gas load was approximately the same for each run ( $2.2$  to  $2.4 \times 10^{-6}$  lb-moles). Each startup run was conducted with a step change in evaporator heat input from 0 to 25 watts with a simultaneous change in sink temperature from room temperature to approximately 30°F. These conditions correspond to a steady-state full-on condenser.

The results shown in Figure 6-7 correspond to the test conditions given in Table 6-2. A startup without liquid in the reservoir is also

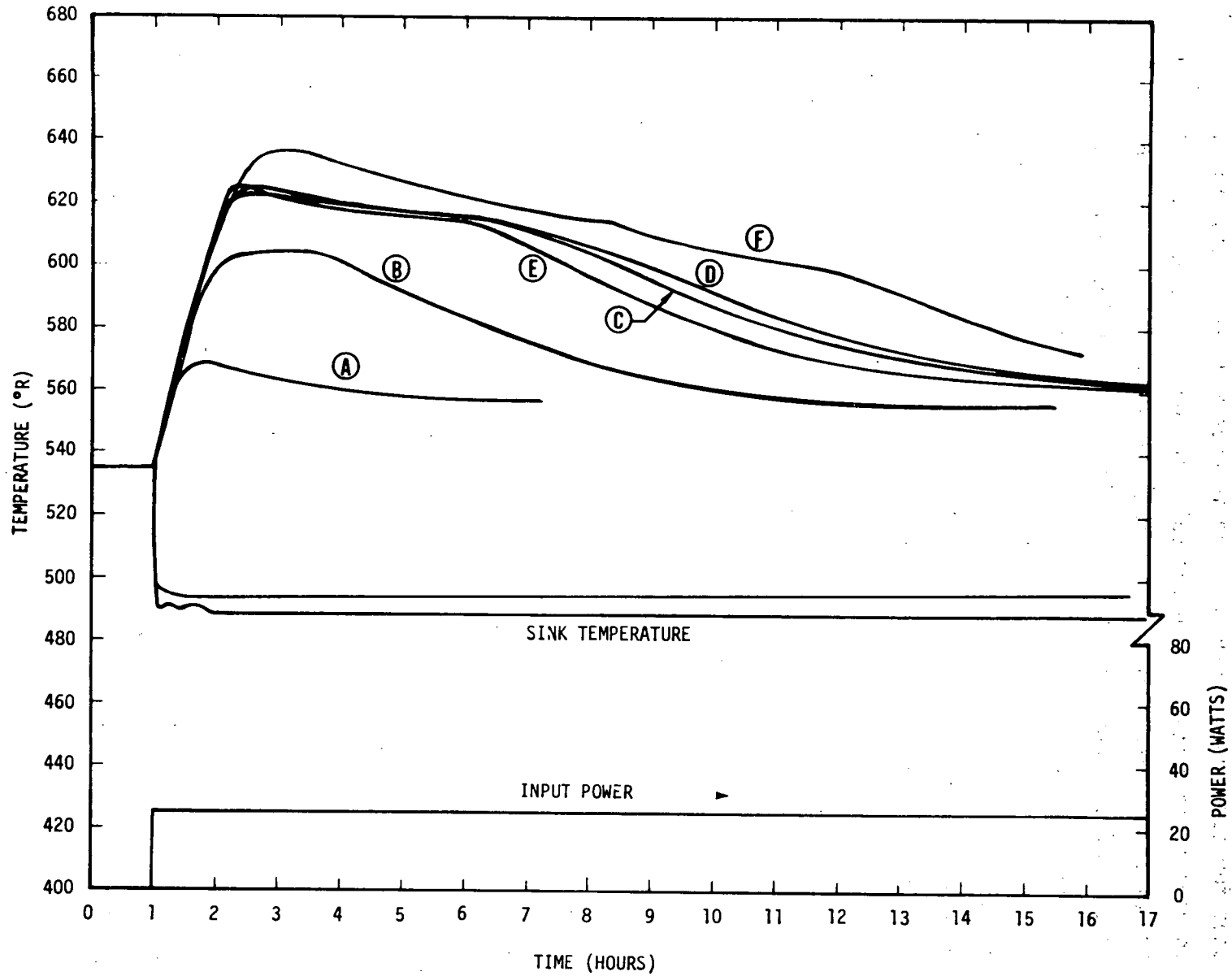


FIGURE 6-7. Experimental Results for Start-up with Liquid in the Reservoir

included for comparison (curve A). An interesting result was that for liquid amounts in excess of a given value (between 0.5cc and 1.0cc for this configuration) the temperature overshoot and recovery time is essentially independent of the amount in the reservoir. This implies that, indeed, liquid must be purged from the reservoir primarily by heat pipe action, for diffusion of vapor through gas in the feedtube would be highly time dependent for various amounts. Moreover, the application of heat to the gas reservoir (curve E) did not significantly affect the overshoot or recovery time. However, the results indicate an initial plateau which causes a longer recovery time than would be expected. It was thought that this plateau was caused by droplets condensing along the feedtube itself or perhaps blockage of the holes at the feedtube entrance with liquid as it is purged from the reservoir.

For this reason the apparatus was modified again by wrapping a heater wire around the feedtube and placing a thermocouple on the feedtube bend at the condenser end. This thermocouple replaced  $\bar{\epsilon}$  #6 for printout, Figure 6-5, so that the feedtube temperature could be monitored during the test. The temperature was maintained 10°F to 20°F below the gas reservoir. It was observed that the application of feedtube heat did not improve the recovery time, but in fact caused a greater overshoot in temperature, and a much longer recovery time (curve F). This result yields further evidence that some of the holes in the feedtube entrance (Figure A-1) might have been blocked with liquid. Although heating may have prevented condensation along the feedtube it would also increase the vapor pressure of working fluid at the condenser entrance leading to the observed performance.

A discussion of these results is given in the conclusion of the report. It is apparent that further developmental work is required in the areas of the feedtube and feedtube entrance design.

TABLE 6-2  
STARTUP WITH LIQUID IN THE RESERVOIR

<u>CURVE (Figure 4-1)</u>	<u>AMOUNT OF LIQUID (cc)</u>	<u>COMMENTS</u>
A	None	-
B	0.25	Run 4
C	1.0	-
D	2.0	-
E	2.0	With reservoir heat ( $\sim 2.2$ watts)
F	1.0	With feedtube heat

### 6.3.2 Temperature Control Range and Operating Limits

Before the transient performance tests could be run, it was first necessary to experimentally establish the minimum and maximum sink temperatures and power levels indicated on the test profile in Figure 6-6. The heat pipe configuration corresponds to Run 1 of the procedure, Table 6-1 for these tests.

#### 6.3.2.1 Full-On Power ( $Q_s$ )

With a coolant temperature of 30°F the heater power was slowly increased in increments of 5 watts until the vapor-gas front was positioned between thermocouples #7 and 8 (Figure 6-5) at the end of the condenser. When the front was at this location thermocouple #8 was approximately 10°F above the sink temperature with a vapor temperature of 86°F indicating that the condenser was full-on but not overdriven. The corresponding power at this full-on condition was 25 watts. This power was used for startup in the transient testing.

#### 6.3.2.2 Maximum Power ( $Q_{max}$ )

In order to determine the maximum power for overdriving without

wick failure or excessive temperature rise the power was increased in increments of 5 watts beyond the full-on value previously recorded. The power was increased up to 50 watts with a vapor temperature of 127°F and an overall temperature drop between the evaporator and condenser of 9°F. On close examination it was seen that the wick may have started to dry out at 25 watts, but there was no "burn-out" because of the high axial conductance of the aluminum saddle. Thus, the maximum power for overdriving was set at 50 watts.

#### 6.3.2.3 Nominal Power ( $Q_{nom}$ )

It was found that the power could be reduced to less than 1 watt before the condenser was fully shut-off. Therefore the nominal power was taken at 12 watts, which is essentially the average of the full-on and minimum power. This placed the vapor-gas front approximately in the middle of the condenser with a 30°F sink temperature.

#### 6.3.2.4 Maximum Sink Temperature ( $T_{smax}$ )

The maximum sink temperature which could be attained without significantly exceeding the set point temperature at the nominal power of 12 watts was on the order of 50°F. At 56°F, for example, the operating temperature (vapor temperature) had increased to 96°F.

#### 6.3.2.5 Minimum Sink Temperature ( $T_{smin}$ )

With a heat input of 12 watts the sink temperature was slowly decreased in 5°F increments until a temperature of -20°F was reached. A lower minimum temperature would cause difficulty in the testing, and the vapor pressure of the methanol is already negligible (0.07 psia) at this temperature. The heat pipe operating temperature was 82°F at this condition.

#### 6.3.3 Transient Performance

Once the operating limits were established the test unit was subjected to the transient test profile given in Figure 6-6 for the various

configurations listed in Table 6-1. Concurrent with the collection of data, predictive runs were made with the TRANPIPE computer program.

#### 6.3.3.1 Run 1

The calculated and experimental results of Run No. 1 are shown in Figure 6-8. The results suggest that the analytical model is valid. Based on this run, it can be said that it takes about 5 to 6 minutes of CDC 6500 computer time to model a 24 hour real time transient test.

#### 6.3.3.2 Run 2

Figure 6-9 shows the results for the same conditions as in Figure 6-8, but a substantial thermal mass of 3.3 lb. aluminum was added to the saddle. This represents a more realistic case in that most cooling applications involve thermal mass and a thermal resistance between the heat source and heat pipe evaporator. Although a thin teflon sheet was originally intended for this resistance, a 70% to 90% copper/silicone slurry was actually used. The thermal conductance of this mixture was approximately 13.1 Btu/hr-°F.

The primary effect of the increased thermal source mass was a slower temperature response to step changes in input power, as expected.

#### 6.3.3.3 Run 3

With nitrogen in the gas gap it was possible to put in only 6 watts heater power without overdriving the pipe in contrast with 25 watts with helium (Figure 6-10). Similarly, the input power for overdriving was reduced to 17 watts for this test. It was not possible to correctly predict this run without a modification of the computer program to include a heat transfer conductance to account for insulation losses to the surroundings. The reason for this is that the input power levels were so low that the insulation losses were an appreciable percentage of the total input. After modification of the program, Run Nos. 1 and 2 were recalculated to include the insulation loss. These latter results are the ones shown in Figures 6-8 and 6-9.

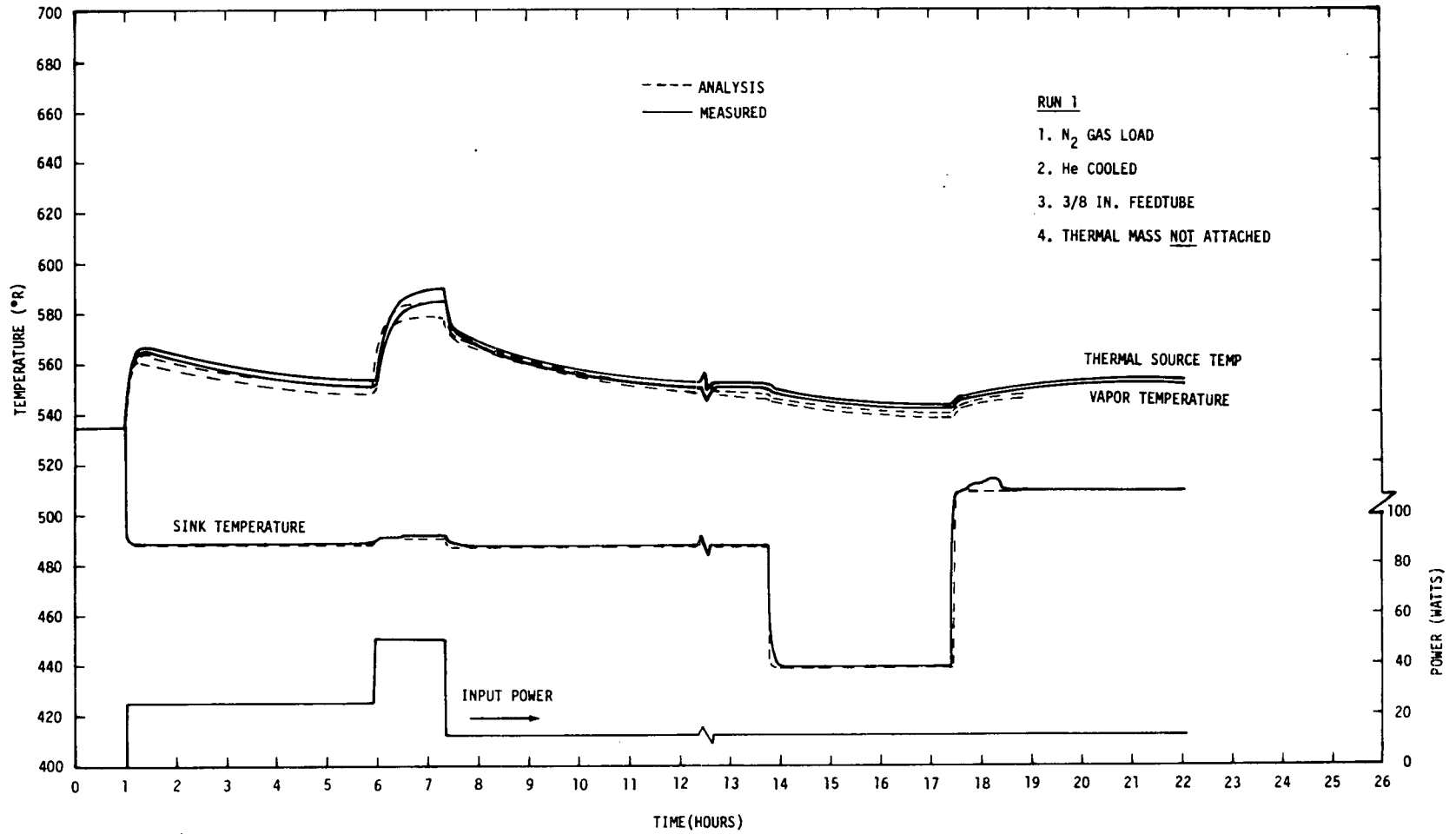


FIGURE 6-8. Transient Performance (Without Thermal Mass)

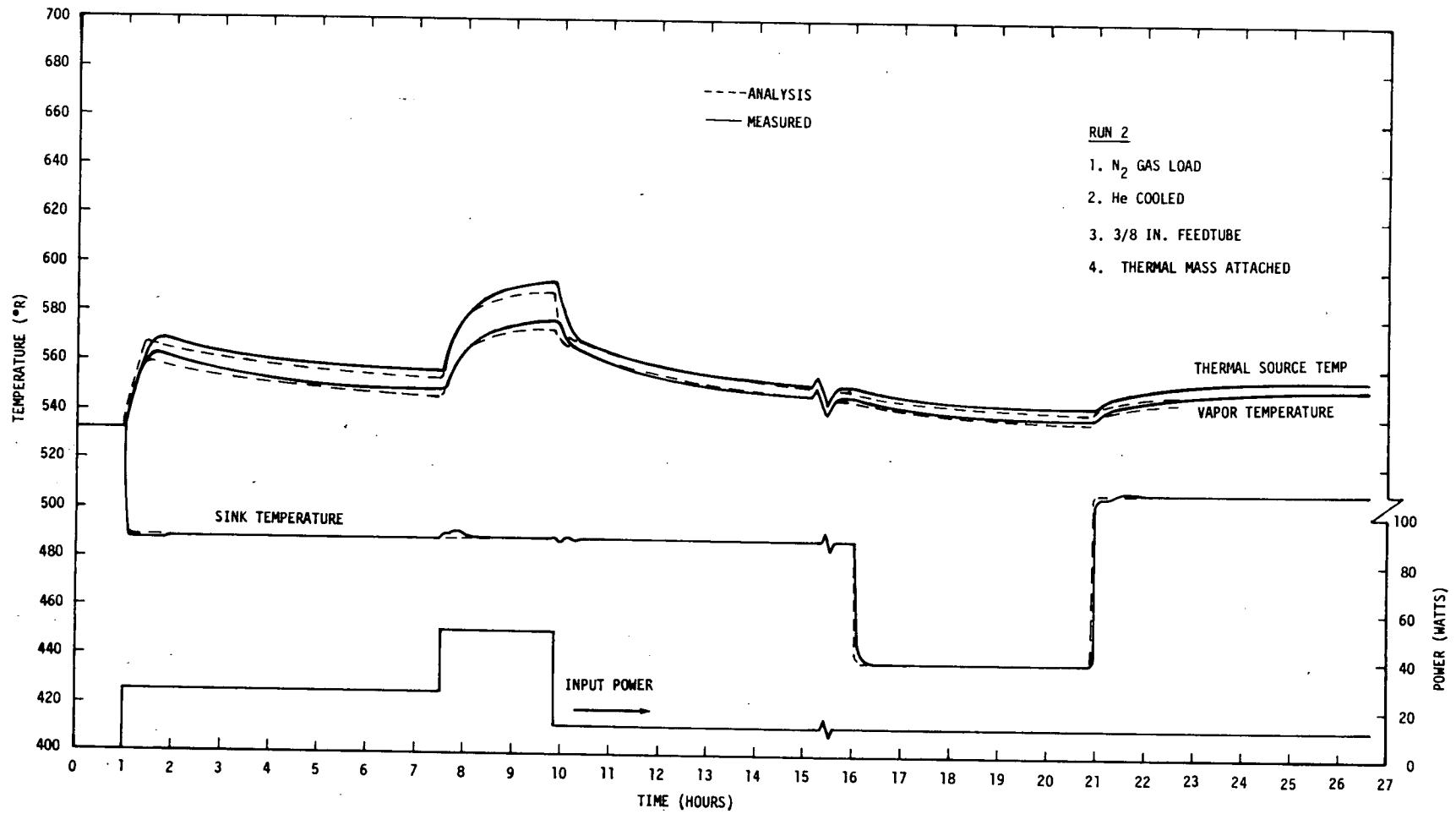


FIGURE 6-9. Transient Performance (With Thermal Mass Attached)

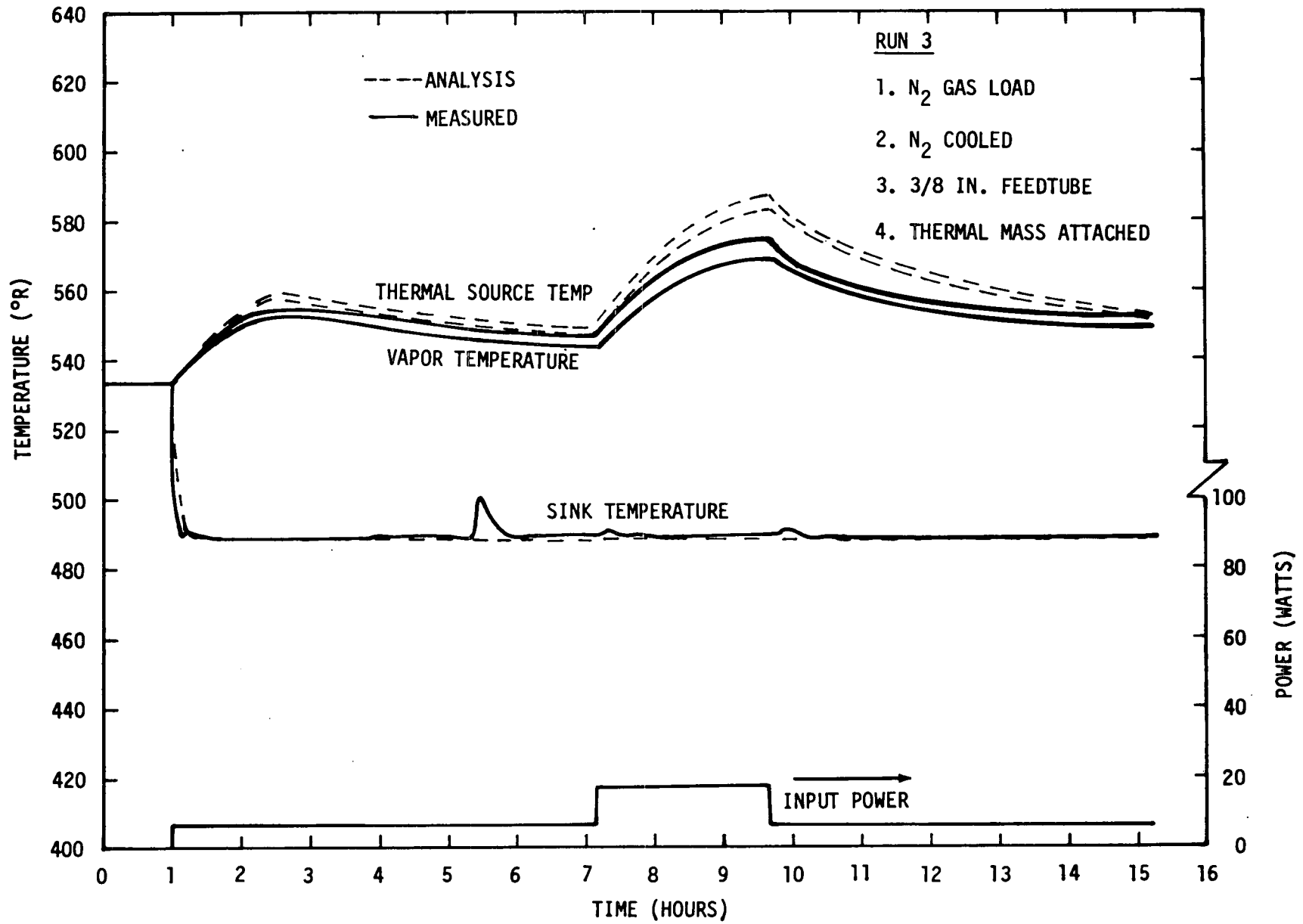


FIGURE 6-10. Transient Performance (Nitrogen Cooled)

#### 6.3.3.4 Run 4

Run No. 4 is included in the preceding section on startup with liquid in the reservoir.

#### 6.3.3.5 Run 5

After reprocessing the test apparatus with helium as the control gas, Run No. 5 of the test schedule was performed. The observed diffusion recovery times due to startup, overdriving and changes in sink temperature were a factor of two or three faster than with nitrogen as the control gas (Figure 6-11). This is expected because the diffusion coefficient for helium is on the order of four times greater than nitrogen. It is interesting to note that whereas the calculated recovery time for nitrogen is slightly longer than experimental, the computed values for helium are in the opposite direction. This shows that the model is essentially correct, but there may be some uncertainty in the diffusion coefficients.

#### 6.3.3.6 Run 6

Next the 3/8 inch OD feedtube was removed and replaced with the 1/4 inch OD feedtube. The pipe was reprocessed with nitrogen and extremely slow recovery times were observed as shown in Figure 6-12. In fact, it was decided to terminate the test after completion of the startup and overdrive because of the long times involved. By simply ratioing the equivalent feedtube lengths and diameters, one would expect a factor of 1.7 increase in recovery time.

### 6.4 Conclusions and Recommendations

The experimental results suggest that the analytical model forming the basis for the computer program (TRANPIPE) is sufficient for engineering design purposes. However, it was necessary to include a heat transfer conductance to account for insulation losses or heat leak to the surroundings. The need for this modification became apparent in Run 3 when nitrogen was used in the condenser gas gap in place of helium. Since the input power levels in Run 3 were quite low the insulation losses were an appreciable percentage of the total input.

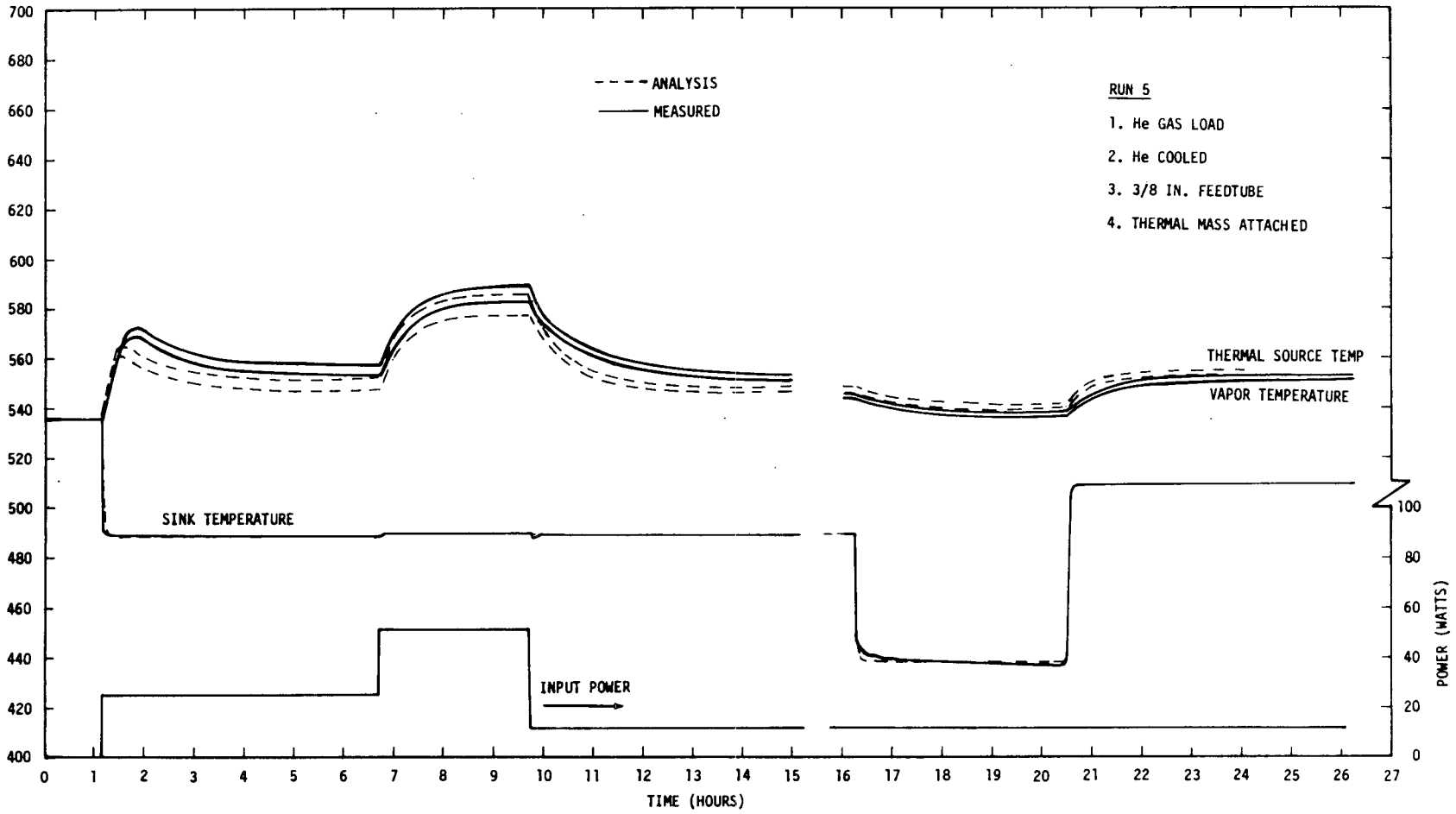


FIGURE 6-11. Transient Performance (Helium Control Gas)

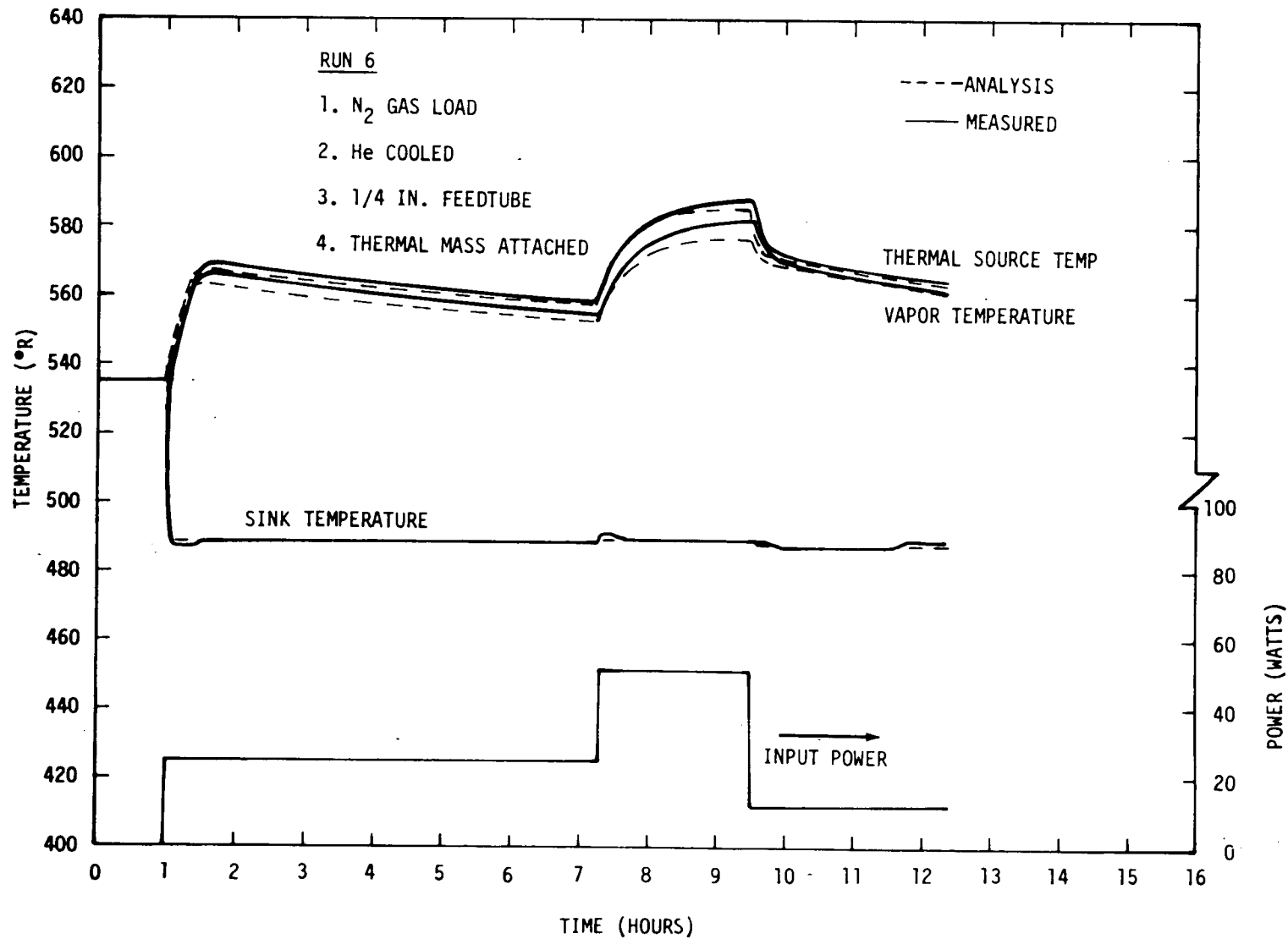


FIGURE 6-12. Transient Performance (1/4 Inch Feedtube)

Two interrelated problem areas emerge from the test program that are associated with hot reservoir heat pipes:

- prevention of liquid in the reservoir
- rapid recovery and minimum temperature overshoot due to liquid in the reservoir

Prevention of liquid from entering the gas reservoir is difficult, for a solution that works in 1-G such as baffles or a check valve, is apt to trap liquid and not work in a low gravity environment. Similarly, a 0-G solution may not prevent liquid from entering the reservoir in ground handling. Several thoughts pertaining to an appropriate feedtube design have been identified. A high thermal conductivity material which enters the condenser through an insulated end cap, for example, would help prevent condensation inside the feedtube. Since the feedtube is warm, the end could be covered with a coarse mesh wick that would trap droplets due to vibration or shock and evaporate them from the outer surface. A bimetallic element might be arranged to close off the entrance when the heat pipe is nonoperational. These are, of course, preliminary thoughts and it was concluded that the development of such a device was beyond the scope of this program and would perhaps involve some 0-G testing.

However, a major part of the testing in this program was directed toward providing rapid recovery and minimum temperature overshoot if liquid does in fact enter the gas reservoir. It was verified that a rapid liquid removal rate could be achieved by placing the reservoir outside and parallel to the evaporator in a mounting saddle which allows it to run at a temperature equal to or hotter than the evaporator - "a hair-pin design." Moreover, when auxiliary heat was applied to the gas reservoir there was little improvement showing that the saddle design was valid. When a thermocouple was placed on the feedtube near the condenser end, it was observed that with liquid present in the reservoir a vapor gas front forms near the condenser entrance to rapidly purge the liquid by reversed heat pipe action rather than by diffusion through the feedtube. Referring to Figure 6-7, for start-up with liquid in the reservoir, it was concluded that all the liquid was removed from the reservoir within the first 1-1/4 hour regardless of the amount. However, there is an initial plateau in the recovery which is

probably caused by blockage of the holes at the feedtube entrance with liquid as it is purged from the reservoir.

It is suggested that further testing should include cutting off the feedtube entrance. This would involve removal of the heat pipe end cap and rewelding. Much could be learned by installing a glass feedtube. In addition to this, it is felt that the temperature overshoot due to liquid in the reservoir could be virtually eliminated by providing a place for the gas to go instead of completely blocking off the condenser. This could be accomplished by providing an auxiliary gas reservoir in the adiabatic section.

Additional analytical work might include modification of the current program to increase its efficiency. Also, a subroutine for liquid in the reservoir, with and without an auxiliary gas reservoir, would be desirable.

In summary, useful design information was obtained as a result of this program. It should be emphasized that additional work remains to be done. However, it can be said that the "hair-pin design" represents at least an order of magnitude improvement over an internal reservoir design in terms of rapid recovery from liquid in the reservoir. Also, it is easier to fabricate since an internal reservoir leads to a step change in pipe cross section in order to contain the reservoir.

## 7.0 REFERENCES

1. B. D. Marcus, "Theory and Design of Variable Conductance Heat Pipe: Hydrodynamics and Heat Transfer," Research Report No. 1, TRW Report No. 13111-6021-R0-00, April 1971.
2. B. D. Marcus, "Theory and Design of Variable Conductance Heat Pipes: Control Techniques," Research Report No. 2, TRW Report No. 13111-6027-R0-00, July 1971.
3. B. D. Marcus, "Theory and Design of Variable Conductance Heat Pipes," NASA CR-2018, April 1972.
4. B. D. Marcus and G. L. Fleischman, "Steady-State and Transient Performance of Hot Reservoir Gas-Controlled Heat Pipes," ASME Paper No. 70-HT/SpT-11, 1970.
5. D. K. Edwards and B. D. Marcus, "Heat and Mass Transfer in the Vicinity of the Vapor-Gas Front in a Gas Loaded Heat Pipe," ASME Jour. of Heat Transfer, Vol, 94, Ser. C, No. 2, pp 155-162, 1972.
6. J. P. Kirkpatrick and B. D. Marcus, "A Variable Conductance Heat Pipe Flight Experiment," AIAA Paper No. 71-411, AIAA 6th Thermophysics Conf., 1971.
7. J. P. Kirkpatrick and B. D. Marcus, "A Variable Conductance Heat Pipe/Radiator for the Lunar Surface Magnetometer," AIAA Paper No. 72-271, AIAA 7th Thermophysics Conf., 1972.
8. B. D. Marcus, "Ames Heat Pipe Experiment (AHPE) Experiment Description Document," NASA CR-114413, January 1972.
9. D. K. Edwards, G. L. Fleischman and B. D. Marcus, "User's Manual for the TRW Gaspipes Program," NASA CR-114306, April 1971.
10. A. R. Rohani and C. L. Tien, "Steady Two-Dimensional Heat and Mass Transfer in the Vapor-Gas Region of a Gas-Loaded Heat Pipe," ASME Paper No. 72-WA/HT-34, 1972.

## 8.0 NOMENCLATURE

A	-	Area
$A_c$	-	Cross sectional area
C	-	Thermal capacity
$C_p$	-	Specific heat
D	-	Diameter
$\mathcal{D}$	-	Diffusivity
J	-	Molar diffusion flux
K	-	Thermal conductivity
L	-	Length
M	-	Mass
$m$	-	Molar inventory
$\dot{m}$	-	Mole transfer rate
P	-	Pressure; Perimeter
Q	-	Thermal energy
$\dot{Q}$	-	Heat transfer rate
R	-	Wick resistance (thermal); Universal Gas Constant
$R_u$	-	Universal gas constant
S	-	Surface thermal conductance
T	-	Temperature

$T_c$	-	Effective cooling temperature
$U$	-	Overall coefficient of heat transfer
$V$	-	Volume; Velocity
$X$	-	Mole fraction
$c$	-	Molar density
$h$	-	Coefficient of heat transfer
$h_f$	-	Convective coefficient of heat transfer
$k$	-	Thermal conductivity
$\dot{m}_B$	-	Rate of mass addition to balance
$\dot{m}_{RC}$	-	Diffusion freezeout rate
$\dot{m}_V$	-	Axial vapor mass transfer rate
$q''$	-	Heat flux
$t$	-	Time
$v^*$	-	Velocity
$x$	-	Mole fraction
$z$	-	Axial Position; Distance
$\delta_0$	-	Liquid recession in wick

$\delta_{\text{wick}}$	-	Wick thickness
$e$	-	Emissivity
$\eta_b$	-	Effectiveness (axial)
$\eta_f$	-	Fin effectiveness (transverse)
$\phi$	-	Wick porosity
$\lambda$	-	Latent heat of vaporization
$\rho$	-	Density
$\tau$	-	Time constant

Subscripts (except when defined otherwise):

$ad$	-	Adiabatic Section
$b$	-	Gas blocked
$bp$	-	Blocked pipe
$B$	-	Analytical balance
$c, \text{ cond}$	-	Condenser
$C$	-	Center of mass
$dif$	-	Diffusion (gas feed) tube
$ev, E$	-	Evaporator
$end$	-	Reservoir feed tube - condenser interface
$f$	-	Fluid; Fin

F	-	Freezing point
gas	-	Gas
i	-	Interface
K	-	Knife Edges
meas	-	Measured
o	-	External, Initial
pipe	-	Heat pipe
pred	-	Predicted
R, res	-	Reservoir
s, S	-	Sink
sat	-	Saturation
so	-	Source
thaw	-	Thaw
tot	-	Total
v	-	Vapor
w	-	Wall
wick	-	Wick

Note: In addition to the nomenclature tabulated here, numerous intermediate, reference and non-dimensional variables have been defined and used in the analytical portion of the text.

9.0

APPENDIX A

DRAWINGS

EXPERIMENTAL HOT RESERVOIR HEAT PIPE

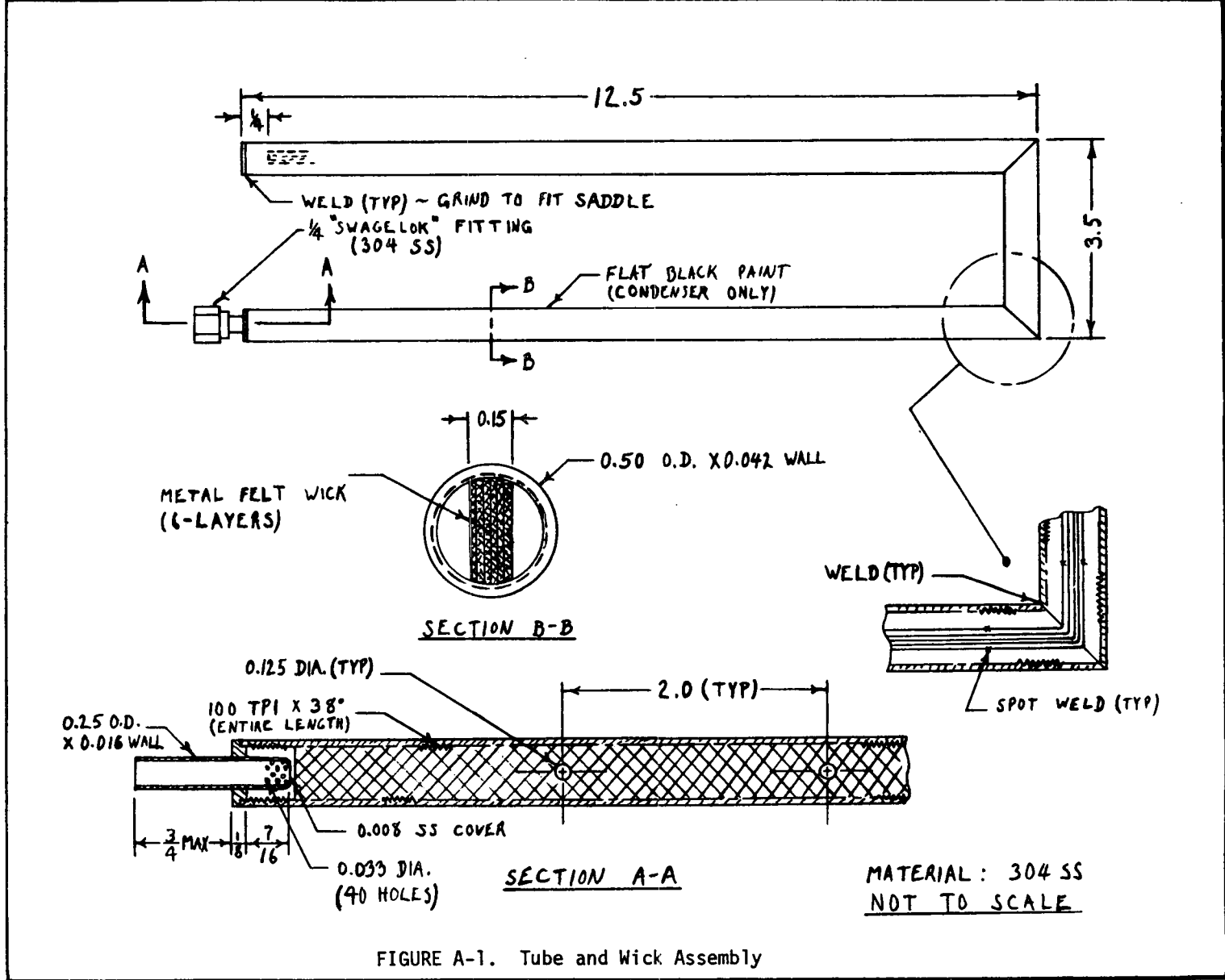
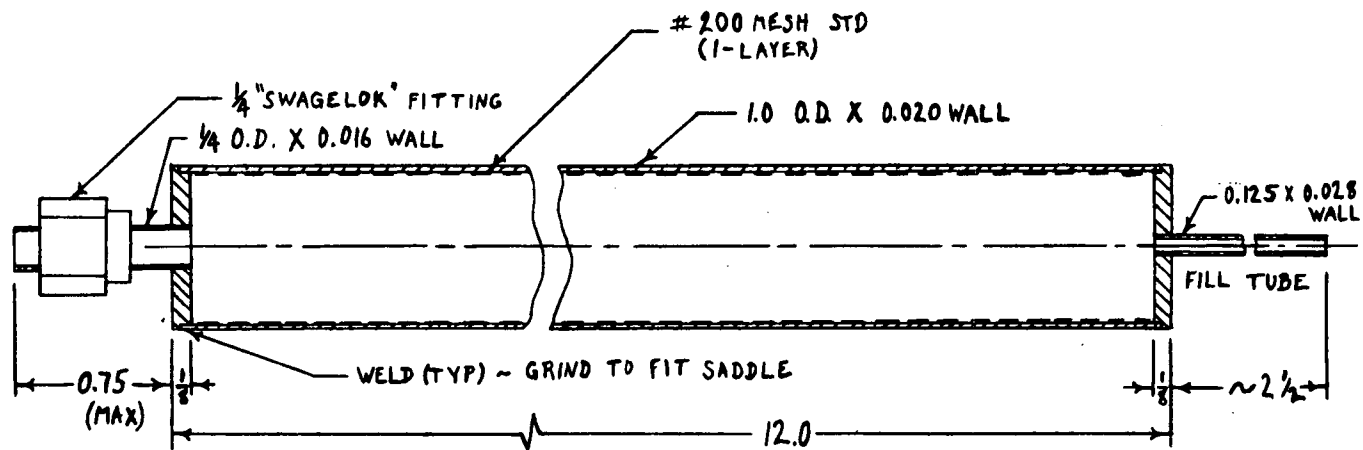


FIGURE A-1. Tube and Wick Assembly

SK

CHG LTR



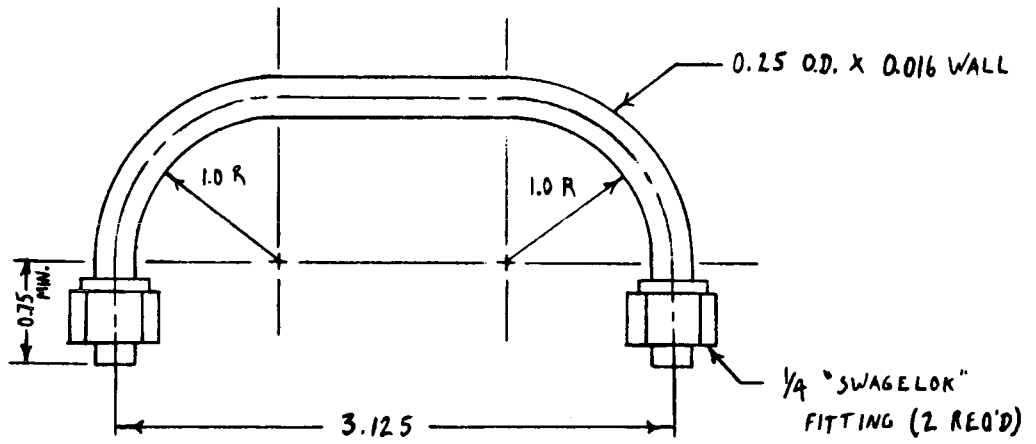
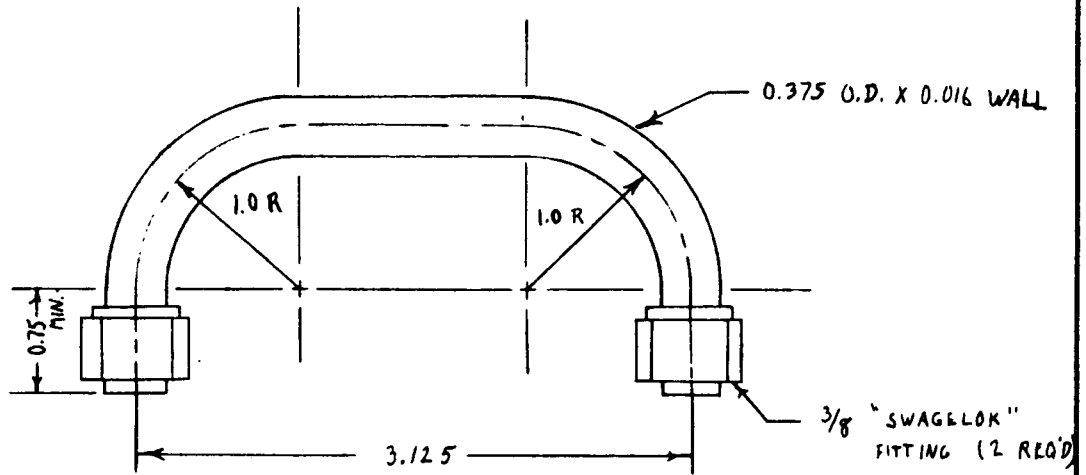
MATERIAL: 304 SS  
SCALE: 1" ~ 1"

FIGURE A-2. Gas Reservoir

103

13111-6046-RU-00

SK  
CMG LTR



ALL TOLERANCES  $\pm 0.01$   
MATERIAL: 304 SS (1 EACH)  
NOT TO SCALE

FIGURE A-3. Feedtube

SK

CHG LTR

MATERIAL: ALUMINUM  
NOT TO SCALE

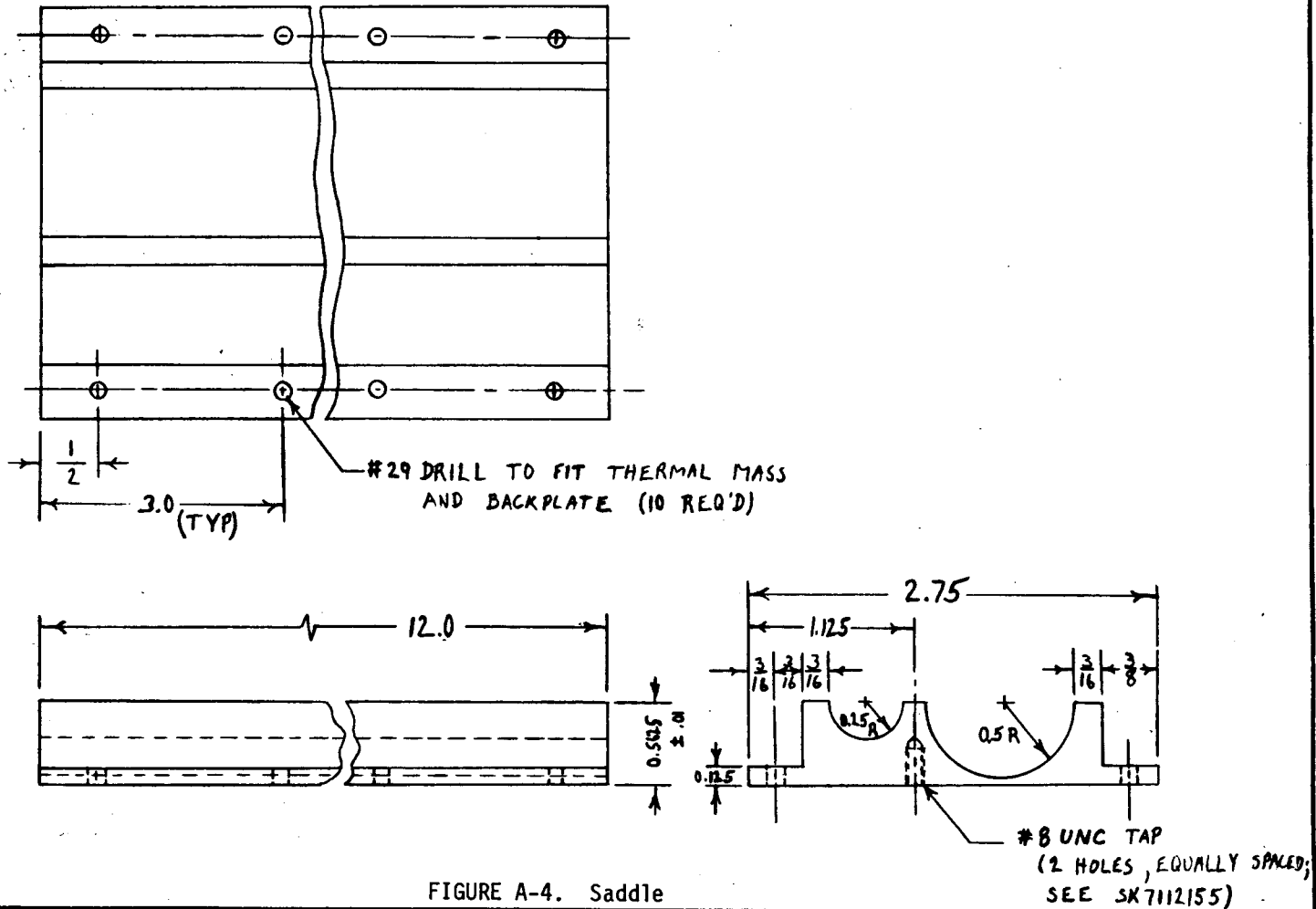


FIGURE A-4. Saddle

SK

CHG LTR

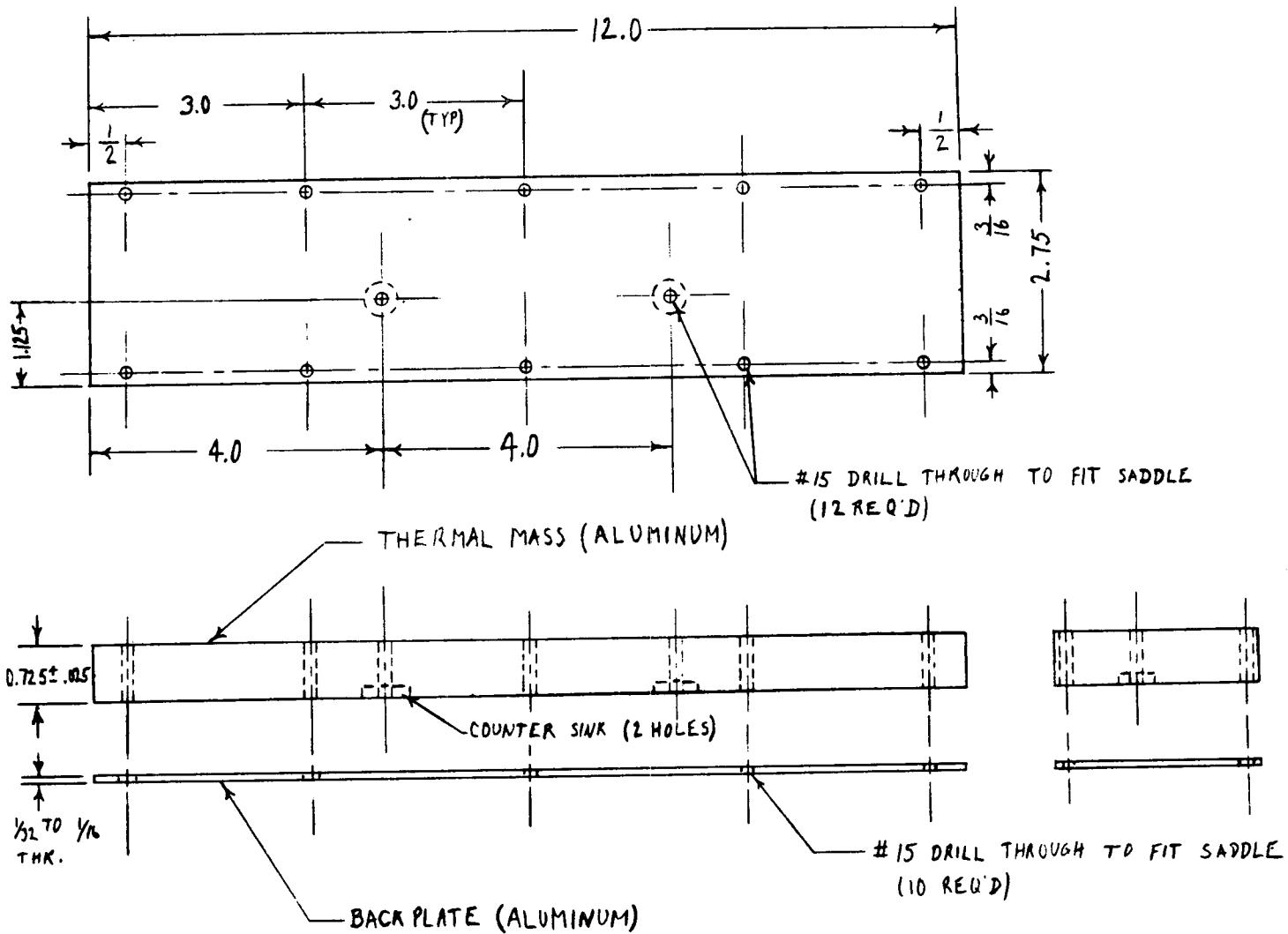
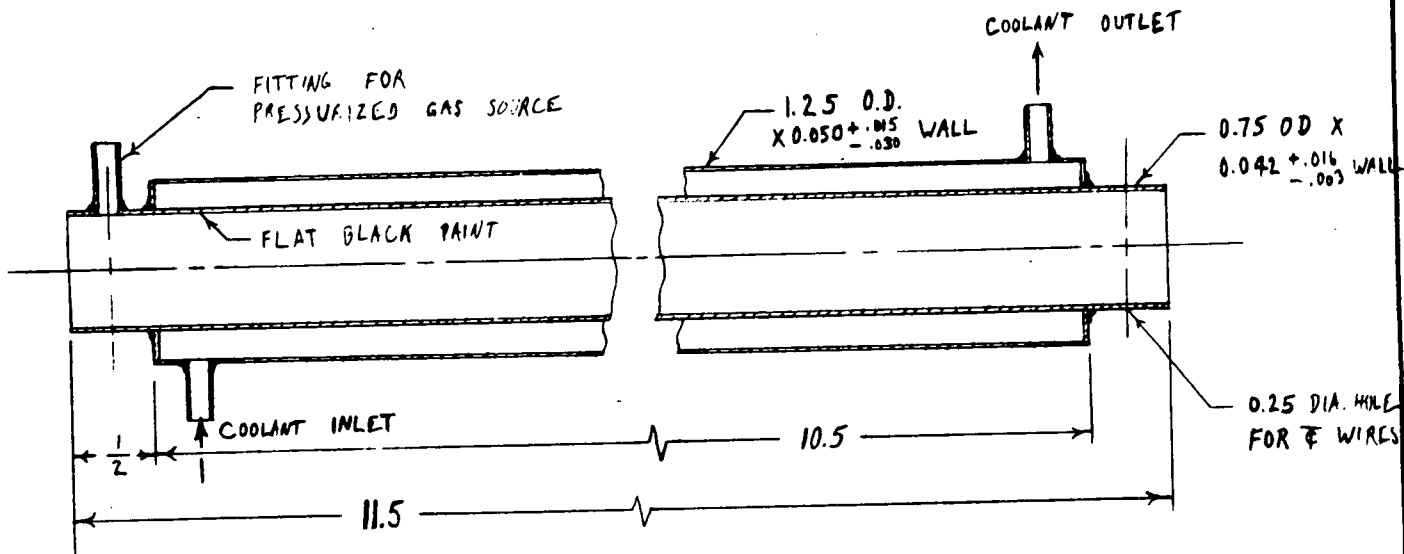


FIGURE A-5. Thermal Mass and Backplate

SK

CHG LTR



107

MATERIAL : ALUMINUM

NOT TO SCALE

FIGURE A-6. Cooling Jacket